Sodium Alanate Nanoparticles for Hydrogen Storage

Cornelis Peter Baldé

ISBN: 978-90-393-4747-8

Cover lay-out by Maatje van Eck, Loods103
Drukkerij Ponsen & Looijen bv, Wageningen

Sodium Alanate Nanoparticles for Hydrogen Storage

Waterstofopslag in nanodeeltjes
van Natriumalanaat

(met een samenvatting in het Nederlands)

Proefschrift

ter verkrijging van de graad van doctor aan de Universiteit Utrecht op gezag van de rector magnificus, prof. dr. J.C. Stoof, ingevolge het besluit van het college voor promoties in het openbaar te verdedigen op woensdag 12 maart 2008 des middags te 4:15 uur

door

Cornelis Peter Baldé

geboren op 6 juni 1980
te Rotterdam

Promotor: Prof. Dr. Ir. K.P. de Jong

Co-promotor: Dr. J.H. Bitter

Dit proefschrift werd (mede) mogelijk gemaakt met financiële steun van NWO/ACTS.

Verdraaid Interessant, maar gaat u verder ...
(vrij naar Wim T. Schippers)

Contents

1

General Introduction

Introduction

Hydrogen is a potential means to store and transport energy. Its chemical energy can be converted to electricity in a fuel cell where the hydrogen reacts with oxygen to form water. When the hydrogen is produced from a sustainable source, the process has zero emissions except for water and can be considered environmentally benign. The storage of hydrogen for vehicular applications requires the most stringent conditions in terms of volume, weight, operation temperature, hydrogen sorption rates, and safety.[1, 2] Until now, no hydrogen storage material has been discovered that fulfills all the criteria.

Several storage methods are considered, such as high pressure storage, cryogenic H_2, physisorbed H_2, or H_2 in metal-hydrides. Figure 1 shows the relative volume of various storage methods compared to the size of a car. High-pressure storage at 200 bar requires a large volume and is therefore undesirable. Cryogenic hydrogen storage increases the volumetric density, but the cryo-liquefaction process requires a substantial amount of energy and H_2 evaporates with ~1% per day from the tank.[3]

Moreover, the safety of liquefied and pressurized storage is questioned in case of a tank rupture.[2] Another option is to store hydrogen by physisorption in porous materials, *e.g.* carbon[4] or metal-organic frameworks.[5] This is typically demonstrated at 77 K due to the weak Van der Waals forces between the physisorbed hydrogen and the porous support material. The low temperature implies that storage of hydrogen is less suitable for automotive purposes.

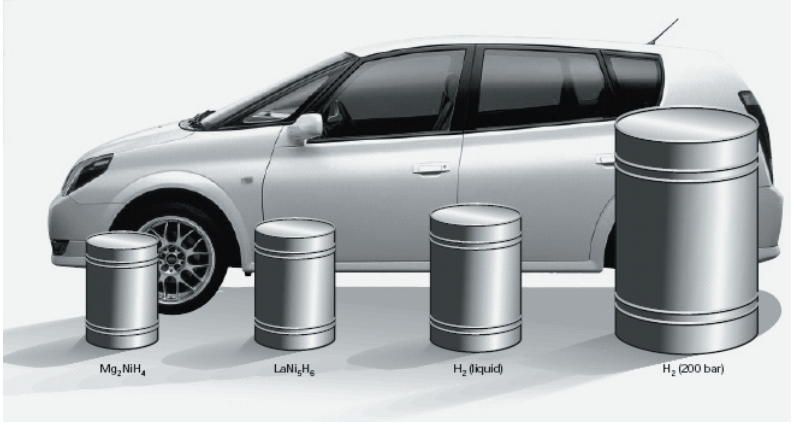

Figure 1 Volume of 4 kg hydrogen compacted in different ways, with size relative to the size of a car. Reproduced in courtesy from ref.[1]

An alternative is to store hydrogen in a metal hydride. This occupies a reasonable amount of space compared to a car as seen from the $MgNiH_4$ and $LaNi_5H_6$ containers in Figure 1.

The pioneering work of hydrogen storage using metal-hydrides dates from 1967[6] and led to the development of hydrogen storage tank prototypes for stationary and mobile applications in the decades after.[7] Unfortunately, the storage tanks were too heavy to be applied for vehicular applications, due to the use of heavy atoms (La, Ni, Fe, etc) to absorb the hydrogen. Thus, the hydrogen needs to be bonded to lighter materials.

Promising in that respect is hydrogen storage in light-weight complex metal hydrides. In the last years, Li, Na, Mg, Ca and K salts of AlH_4^-, NH_2^-, and BH_4^- (alanates, amides and boranes) have received most attention. However, for all (complex) metal hydrides kinetic barriers restrict dehydrogenation and rehydrogenation rates[8] and need to be reduced.

Of these potential hydrogen storage media, the structure and storage properties of sodium alanate ($NaAlH_4$) have received most attention in the last 10 years as can be concluded from several reviews.[8-11] This complex metal hydride can, for that reason, be considered as a model system to establish generally applicable conclusions for hydrogen storage materials.
$NaAlH_4$ can store up to 5.6 wt% H_2 via the reactions shown in Eq (1).

$$NaAlH_4 \leftrightarrow \tfrac{1}{3}\, Na_3AlH_6 + \tfrac{2}{3}\, Al + H_2 \leftrightarrow NaH + Al + 1\tfrac{1}{2}\, H_2 \qquad (1)$$

Thermodynamics predict that the equilibrium pressure of H_2 is 1 bar at 30 °C for $NaAlH_4$ and 110 °C for Na_3AlH_6. In 1997, a breakthrough has been achieved by Bogdanovic *et al.*, who discovered that admixing a Ti-precursor via a wet chemical procedure accelerated hydrogen desorption and absorption rates.[12] Later, ball milling of the Ti precursor with the $NaAlH_4$ has been identified to increase sorption rates even further.[13]

It has been elucidated in several studies that the mass transfer in the solid is the rate-limiting step for sorption in Ti-catalyzed $NaAlH_4$, due to the phase transitions (see Eq. 1).[14-16] The lower limit of the $NaAlH_4$ particle size is 150-200 nm when using ball milling[17] or in the micrometer size range for the wet-chemical preparation route.[18] This indicates that the mass transfer lengths of the solid are large during hydrogen extraction and uptake. Therefore, the absorption and desorption rates might be accelerated when the $NaAlH_4$ particles are further reduced in size. The preparation of particles smaller than 100 nm, however, cannot be achieved with the conventional techniques. Thus different preparation methods are required. For the proof of principle we dispersed $NaAlH_4$ on the surface of a support material.

The preparation of nanoparticles on porous materials can be adapted from the field of heterogeneous catalysis. A solution containing the metal precursor is impregnated to a porous support material until the pore volume is completely filled. Subsequent drying deposits the metal precursor on the support material. Several reports indicate that the particle size of the metal can be controlled to or adjusted within the nm range by adapting drying procedure, calcination treatments, or by using physical constrains of the support material.[19-22]

When the pore volume impregnation method is translated to deposit $NaAlH_4$ on a porous support, one has to consider that the alanate can react irreversibly to a variety of oxygen groups that might be present on the support. Thus, a support that contains a small concentration of oxygen is desired in order to prevent hydrogen losses. Our study focused therefore on the use of Carbon Nanofibers (CNF), as they can be prepared to contain small a concentration of oxygen.[23]

Scope of the thesis

The aim of this study is to relate structural properties of the Ti catalyst and/or the particle size of the $NaAlH_4$ to the hydrogen storage characteristics. In **chapter 2** we describe the synthesis of nanostructured $NaAlH_4$ on carbon nanofibers (CNF). The relevance of the drying step and $NaAlH_4$ loading are discussed for the particle size of $NaAlH_4$. A quantitative size-performance relationship of the particle size and the activation energy for hydrogen desorption is presented. The absorption properties of the nanostructured $NaAlH_4$ are compared to that of Ti-catalyzed bulk $NaAlH_4$. **Chapter 3** reports the preparation, structure and performance of $Ti(OBu)_4$ catalyzed nanostructured $NaAlH_4$ on CNF. The performance for hydrogen storage is related to the particle size of $NaAlH_4$ and to the local structure of the Ti. **Chapter 4** deals on the structure of the Ti in ball-milled $TiCl_3$-$NaAlH_4$ with X-ray diffraction, Ti K-edge extended X-ray absorption fine structure (EXAFS) and Ti K-edge X-ray absorption near edge structure (XANES). A structural representation of the Ti is proposed for the as-prepared material and the deactivation process of the Ti catalyst is discussed. **Chapter 5** reports the local structure investigation of ball-milled $Ti(OBu)_4$-$NaAlH_4$ as a function of temperature. The local structure of the Ti is compared to that of ball milled $TiCl_3$-$NaAlH_4$ and is linked to literature data on hydrogen desorption and absorption kinetics. **Chapter 6** describes the first Al K-edge XANES and EXAFS study of $NaAlH_4$. The XANES and EXAFS are discussed and compared to that of an oxidized $NaAlH_4$.

References

1. Schlapbach, L.; Züttel, A., *Nature* **2001,** 414, 353-358.
2. Schüth, F., *Nature* **2005,** 434, 712-713.
3. Ross, D. K., *Vacuum* **2006,** 80, 1084-1089.
4. Nijkamp, M. G.; Raaymakers, J. E. M. J.; van Dillen, A. J.; de Jong, K. P., *Appl. Phys. A: Mater. Sci. Process.* **2001,** 72, (5), 619-623.
5. Rosi, N. L.; Eckert, J.; Eddaoudi, M.; Vodak, D. T.; Kim, J.; O'Keeffe, M.; Yaghi, O. M., *Science* **2003,** 300 (5622), 1127-1129.
6. Reilly, J. J.; Wiswall, R. H., *Inorg. Chem.* **1967,** 6, 2220-2223.
7. Lynch, F. E., *J. Less Com. Metals* **1991,** 172-174, 943-958.
8. Orimo, S.; Nakamori, Y.; Eliseo, J. R.; Züttel, A.; Jensen, C. M., *Chem. Rev.* **2007,** 107, (10), 4111 - 4132.
9. Bogdanovic, B.; Eberle, U.; Felderhoff, M.; Schüth, F., *Scr. Mater.* **2007,** 56, 813–816.
10. Schüth, F.; Bogdanovic, B.; Felderhof, M., *Chem. Commun.* **2004,** 37, 2249-2258.
11. Grochala, W.; Edwards, P. P., *Chem. Rev.* **2004,** 104 (3), 1283-1315.
12. Bogdanovic, B.; Schwickardi, M., *J. Alloys Compd.* **1997,** 253-254, 1-9.
13. Jensen, C. M.; Zidan, R.; Mariels, N.; Hee, A.; Hagen, C., *Int. J. Hydrogen Energy* **1999,** 24, (5), 461-465.
14. Von Colbe, J. M. B.; Schmidt, W.; Felderhoff, M.; Bogdanovic, B.; Schüth, F., *Angew. Chem. Int. Ed.* **2006,** 45, (22), 3663-3665.
15. Kiyobayashi, T.; Srinivasan, S. S.; Sun, D.; Jensen, C. M., *J. Phys. Chem. A* **2003,** 107, 7671-7674.
16. Fichtner, M.; Canton, P.; Kirchner, O.; Leon, A., *J. Alloys Compd.* **2005,** 404–406, 732–737.
17. Brinks, H. W.; Hauback, B. C.; Srinivasan, S. S.; Jensen, C. M., *J. Phys. Chem. B* **2005,** 109, 15780-15785.
18. Bogdanovic, B.; Brand, R. A.; Marjanovic, A.; Schwickardi, M.; Tolle, J., *J. Alloys Compd.* **2000,** 302, 36-58.
19. Pan, X.; Fan, Z.; Chen, W.; Ding, Y.; Luo, H.; Bao, X., *Nature Mater.* **2007,** 6, 507-511.
20. Sietsma, J. R. A.; Meeldijk, J. D.; den Breejen, J. P.; Versluijs-Helder, M.; van Dillen, A. J.; de Jongh, P. E.; de Jong, K. P., *Angew. Chem. Int. Ed.* **2007,** 46, 4547-4549.
21. van Dillen, A. J.; Terörde, R. J. A. M.; Lensveld, D. J.; Geus, J. W.; de Jong, K. P., *J. Catal.* **2003,** 216, (1-2), 257-264.

22. Battiston, A. A.; Bitter, J. H.; de Groot, F. M. F.; Overweg, A. R.; Stephan, O.; van Bokhoven, J. A.; Kooyman, P. J.; van der Spek, C.; Vanko, G.; Koningsberger, D. C., *J. Catal.* **2003,** 213 251-271.

23. Toebes, M. L.; van Heeswijk, E. M. P.; Bitter, J. H.; van Dillen, A. J.; de Jong, K. P., *Carbon* **2004,** 42 (2), 307-315.

2

Sodium Alanate Nanoparticles - Linking Size to Hydrogen Storage Properties

Abstract

Important limitations in the application of light metal hydrides for hydrogen storage are slow kinetics and poor reversibility. To alleviate these problems doping and ball-milling are commonly applied, for $NaAlH_4$ leading to particle sizes down to 150 nm. By wet-chemical synthesis we have prepared carbon nanofiber-supported $NaAlH_4$ with particle size ranges of 1-10 μm, 19-30 nm and 2-10 nm. The hydrogen desorption temperatures and activation energies decreased from 186 °C and 116 kJ.mol^{-1} for the largest particles to 70 °C and 58 kJ.mol^{-1} for the smallest particles. In addition, decreasing particle sizes lowered the pressures needed for reloading. This reported size-performance correlation for $NaAlH_4$ may guide hydrogen storage research for a wide range of nanostructured light (metal) hydrides.

Introduction

Hydrogen storage materials need to fulfill strict requirements with respect to safety, capacity and kinetics for on-board application.[1] Lightweight metal hydrides are considered as storage media, but kinetic constraints limit their application. A promising approach to address this issue is to reduce the particle size of the metal hydride to the nanometer range, resulting in enhanced kinetics without the need of a catalyst.[2, 3] Nanoparticles often display modified behavior compared to bulk particles and are applied for instance in catalysis,[4, 5] chemical sensors,[6] or optics.[7, 8] Here, we focus on size effects of sodium alanate ($NaAlH_4$) particles. The structure and hydrogen storage properties of $NaAlH_4$ have been studied extensively over the last 10 years as can be concluded from several reviews.[9-12] This complex hydride can, therefore, be considered as a model system to arrive at more generally applicable conclusions on size effects for hydrogen storage materials.

Particle sizes of metal hydrides are usually decreased by ball milling, for $NaAlH_4$ preferably in the presence of a Ti-based catalyst.[13-15] However, with that method the particle size is difficult to control, the size-distribution is broad, and the smallest particle size achievable is typically 150 to 200 nm for $NaAlH_4$.[15] Therefore another preparation method is needed to study particles smaller than 150 nm. Nanoparticles are regularly synthesized by deposition of a metal precursor onto a support material in heterogeneous catalysis.[16, 17]

In the field of hydrogen storage, this approach has been demonstrated to facilitate H_2 desorption rates for $NaAlH_4$,[2] nanoscaffolded NH_3BH_3,[3, 18] and $LiBH_4$.[19, 20] However, the particle size of the hydrides used in those studies was not reported. Here, we present an extensive study using alternative preparation routes, characterization of the $NaAlH_4$ particle size and the effect of particle size on hydrogen storage properties. The $NaAlH_4$ particles were supported on Carbon Nanofibers (CNF). Particle sizes were determined using Scanning Electron Microscopy (SEM), Transmission Electron Microscopy (TEM) and quantitative Xray Photoelectron Spectroscopy (XPS). The hydrogen desorption properties of the samples were linked to the particle sizes and H_2 absorption characteristics were compared to those of ball milled $TiCl_3$-$NaAlH_4$.

Experimental

Fishbone CNF of 20-30 nm in diameter were grown from 5 wt% Ni/SiO_2 (425-850 μm SiO_2 particles) using H_2/CO as described by Van der Lee *et al.*[21] After CNF synthesis, SiO_2 was removed by refluxing the product in 1 M KOH. Subsequently, Ni was removed by refluxing the product in fresh concentrated HCl. After each refluxing step, the CNF were thoroughly washed with demi-water. Finally, the CNF were dried in inert atmosphere at 500 °C, and stored in a glovebox for further use. The CNF prepared in this way contained a low concentration (<0.02 $mmol.g^{-1}$) of oxygen-containing groups on the surface and had a specific surface area of 130 $m^2.g^{-1}$.[22]

All further sample handling was conducted under a dry and inert atmosphere using either Schlenk equipment or an N_2 filled glovebox with a circulation purifier. $NaAlH_4$ (90% Sigma Aldrich) was purified by dissolving it in dried THF followed by filtration to remove insoluble contaminants. The pure alanate was obtained as a white powder after evaporation of the THF under reduced pressure. It was stored in a glovebox and used within one day.

$NaAlH_4$ was deposited on CNF by pore volume (1 $ml.g^{-1}$) impregnation using dried THF as a solvent. Samples with $NaAlH_4$ loadings of 2 and 8 wt% were prepared by adapting the concentration of $NaAlH_4$ in the impregnation solution. Both samples were dried at reduced pressure (6 mbar) while heating from -40 to -15 °C over a period of 3 h; this is denoted as low temperature drying. In addition, a sample was prepared with a loading of 9 wt% which was dried at room temperature for 5 minutes at 6 mbar (denoted as room-temperature drying).

Temperature Programmed Desorption (TPD) of H_2 was performed using a Micromeritics AutoChem II 2920. 200 to 400 mg of sample was loaded in the reactor and heated, in 25 ml/min Ar flow while heating from -20 to 300 °C.

Reloading of the samples was performed in a high pressure magnetic suspension balance from Rubotherm.[23, 24] For "19-30 nm $NaAlH_4$", 250 mg sample was loaded in the balance. For ball milled $TiCl_3$-$NaAlH_4$ (prepared via procedure described by Haiduc *et al.*,[25] Ti/Al=0.05 at/at) 4 mg was loaded. Prior to the uptake measurement, the sample was desorbed at 0.1 bar H_2 pressure (99.999 % purity) at 250 °C. Next, the temperature was lowered to the absorption temperature (115 °C) and equilibrated for 1 hour. H_2 uptake was monitored by the weight increase of the sample during the subsequent pressure increase (1.38 $bar.min^{-1}$) to 100 bar H_2 pressure. Hydrogen uptake and desorption was determined after subtracting the weight changes of an empty sample holder and applying a buoyancy correction due to the volume of the sample.

For electron microscopy studies al samples were crushed by mortar and pestle in a glovebox. SEM studies were performed on an FEI XL30 FEG electron microscope equipped with an EDX detector. The crushed sample was fixed to a double-sided carbon tape and transported in an N_2 atmosphere to the microscope. Mounting the sample into the microscope involved brief (less than one minute) exposure to air. HR-TEM and STEM images were obtained using a Tecnai 20 (200 kV) equipped with an EDX and an HAADF detector. All samples were desorbed at 300 °C prior to analysis after which they were mounted to the sample holder. The specimens were passivated in air during transport to the microscope.

X-ray Photoelectron Spectroscopy (XPS) spectra were acquired from a Perkin Elmer (PHI) model 5580 spectrometer using Al K_α radiation. Samples were desorbed at 300 °C, passivated in ambient air, crushed and pressed on double-sided carbon tape. Shirley backgrounds were subtracted from the raw data to obtain the areas of the C_{1s}, Al_{2p} and Na_{1s} signals. The inelastic mean free path of photoelectrons generated in $NaAlH_4$ is very small, *i.e.,* 3.1 nm for C_{1s}, 2.6 nm for Al_{2p}, and 1.1 nm for Na_{1s}. Thus, the intensity ratio Al_{2p}/C_{1s}, and Na_{1s}/C_{1s} together with the loading and CNF specific surface area was used to calculate the dispersion of Na and Al on the CNF based on the model by Kuipers *et al*..[26, 27] Particle sizes obtained earlier for Co on CNF [4] with this model were in good agreement with TEM, EXAFS, and H_2 chemisorption results.

In-situ Powder X-ray Diffraction data were recorded on a Bruker-AXS D-8 diffractometer using $Co_{K\alpha 1,2}$ radiation. The sample was crushed, loaded in an Anton-Paar reaction chamber in the glovebox, closed and transported to the diffractometer. The reaction chamber was connected to a gas system and measurements were carried out in flowing N_2 with a ramp of 2 °C.min^{-1} to 250 °C.

Results and discussion

Preparation and structure of nano-$NaAlH_4$

The CNF support material used in this study consisted of entangled fibers with diameters between 20 to 30 nm resulting in a porous skein. Figure 1A displays a typical SEM micrograph of a CNF skein to illustrate its morphology. The CNF skeins were impregnated with a solution of $NaAlH_4$ in THF until the pore volume was completely filled. $NaAlH_4$ was deposited on the CNF by subsequent drying. The drying conditions (temperature) and $NaAlH_4$ loading determined the size of $NaAlH_4$ particles on the CNF. Drying at room temperature under reduced pressure of 9 wt% $NaAlH_4$ on CNF resulted in particles varying from 1 μm (Figure 1B) to 10 μm (Figure 1C) at the outer surface of the CNF skeins. This sample will be referred to as: "1-10 μm $NaAlH_4$".

A second sample with a comparable loading of 8 wt% $NaAlH_4$ was dried at low temperature (-40 °C to -15 °C). In that sample, SEM did not reveal the presence of large $NaAlH_4$ particles (Figure 1D). However, the fibers, shown in Figure 1D for a relatively porous part of the sample, had been thickened by $NaAlH_4$ deposition suggesting $NaAlH_4$ present on the individual fibers. A particle size could not be derived from SEM but required XRD, TEM and XPS of the sample after hydrogen desorption, *i.e.,* $NaAlH_4$ decomposed to Al and NaH.[28] Whether the particle size of the material after desorption represented the original particle size has been verified with XRD.

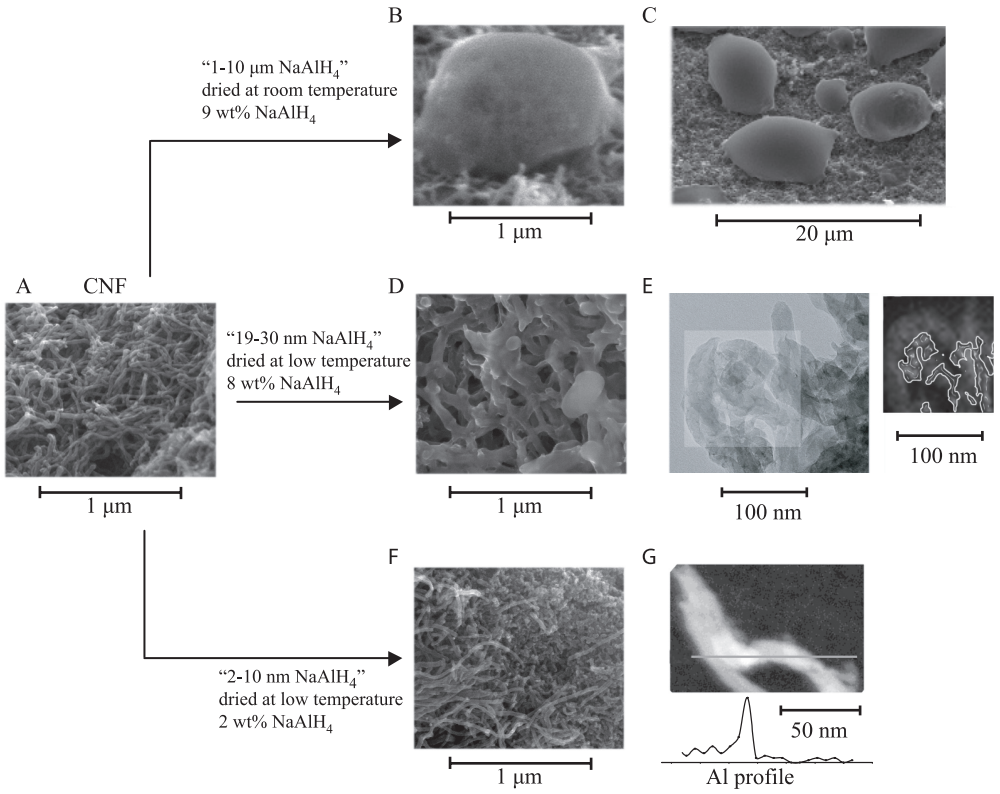

Figure 1. Overview of $NaAlH_4$/CNF samples. A) CNF skein prior to impregnation; B and C) SEM micrographs of "1-10 μm $NaAlH_4$"; D) SEM micrograph of "19-30 nm $NaAlH_4$"; E) TEM and an EDX elemental map of highlighted region (C in white and Al (shaded)) for "19-30 nm $NaAlH_4$" after desorption; F) SEM micrograph of "2-10 nm $NaAlH_4$"; G) TEM micrographs with Al profile of "2-10 nm $NaAlH_4$" after desorption.

Figure 2 shows a 2-dimensional plot of the XRD patterns of the 8 wt% $NaAlH_4$ as function of the desorption temperature. In the fresh material the diffractions of CNF, $NaAlH_4$, and Al were detected. During heating the intensity of the $NaAlH_4$ diffractions decreased and became zero above 150 °C. The disappearance of the $NaAlH_4$ diffractions was paralleled by an increase in the Al diffraction line. From the width of the $NaAlH_4$ and Al diffraction lines it was established that both the $NaAlH_4$ and Al particles were on average 22 nm. Therefore, the Al particle size obtained after decomposition by all techniques coincided with the original $NaAlH_4$ particle size.

Figure 1E shows a TEM micrograph of this sample after desorption together with the Al and C elemental maps of the highlighted region. The carbon map followed the structure of the fibers as expected. Al domains were detected on the fibers with sizes between 20 and 30 nm. The particle size of Al was additionally determined using quantitative XPS, which was based on the Al:C ratio of desorbed $NaAlH_4$ samples, specific surface area of the CNF and $NaAlH_4$ loading.[26, 27] The atomic Al:C and Na:C ratios are listed in Table 1. When the model was used assuming hemispherical particles, the Al particles size was calculated to be 19 nm (Table 1). The high atomic Na:C suggested that NaH was highly, possibly atomically, dispersed. The Al particle size is in agreement with the 20-30 nm particle size range obtained from TEM (Figure 1E), illustrating the suitability of the XPS model. The sample will be referred to as "19-30 nm $NaAlH_4$".

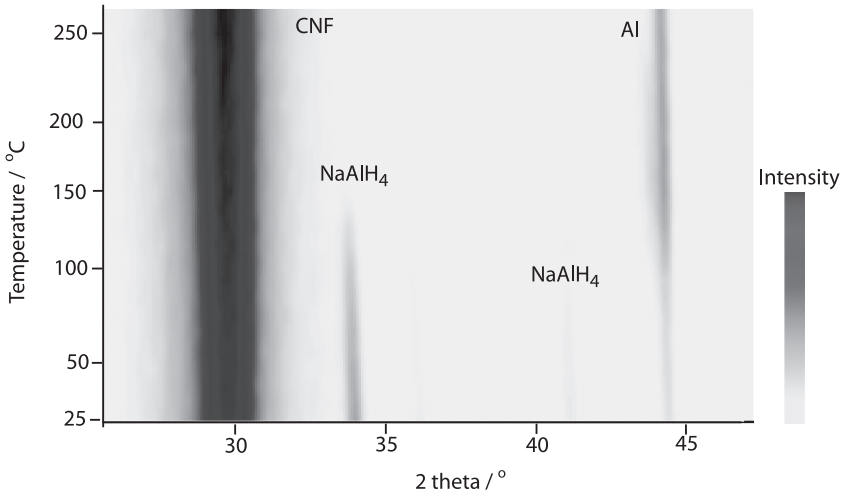

Figure 2. In-situ X-ray diffraction of "19-30 nm $NaAlH_4$" with heating ramp of 2 °C.min^{-1}.

Table 1. Atomic ratios and particle size obtained by XPS.

$NaAlH_4$ loading	Al:C (at / at)	Na:C (at / at)	Al (*d* / nm)
2 wt%	0.0055	0.032	2
8 wt%	0.0071	0.059	19

In the third sample, the fibers were impregnated with a lower concentration of $NaAlH_4$ in solution. The impregnated material was dried at low temperature, and the loading was 2 wt% $NaAlH_4$. SEM only detected the individual CNF fibers in this sample (Figure 1F), indicating that the $NaAlH_4$ particles were small. From STEM-EDX line scans over several single Al particles (one line scan is shown in Figure 1G) it was concluded that the upper limit of particle size was 10 nm. XPS shows that the atomic Al:C and Na:C ratios were significantly larger after normalization to the alanate loading for the 2wt% loaded sample, than for the 8 wt% loaded sample (Table 1). This indicates that the dispersion of Al and NaH was higher in the 2 wt% loaded sample than for the 8 wt% sample. When the same quantitative XPS model was applied, it was calculated thatthe 2 wt% loaded sample consisted of 2 nm Al particles. Such small Al particles could not be inferred from the EDX line scan shown in Figure 1G, as the spatial resolution was insufficient. Therefore, the combination of TEM and XPS provided a 2-10 nm particle size range, and the sample will be referred to as "2-10 nm $NaAlH_4$".

Influence of $NaAlH_4$ loading and drying

Thus, we have tuned the $NaAlH_4$ particle sizes in discrete ranges of 2-10 nm, 19-30 nm and 1-10 µm. A detailed discussion about the influence of the preparation parameters on the particle size can be found in the following part. During impregnation the pores of the CNF became completely filled with the $NaAlH_4$ solution. After impregnation the sample was dried during which the concentration of $NaAlH_4$ in the solution gradually increased eventually leading to precipitation of $NaAlH_4$. Precipitation initially takes place on anchoring sites, being either oxygen containing groups or defect sites on the carbon support. The precipitated particles can act as nucleation sites on which particles can grow, providing $NaAlH_4$ is present in the impregnation solution. As a consequence, the particle growth can be limited by using a lower concentration of $NaAlH_4$ in

solution. For that reason we prepared the sample with a lower concentration of $NaAlH_4$ resulting in 2 wt% $NaAlH_4$.

The importance of the drying procedure on particle size was shown for the preparation of nanoparticles in heterogeneous catalysis.[29, 30] In the current study, drying was performed in two ways denoted as low-temperature drying and room-temperature drying (see experimental). For the low-temperature drying, the cooling step to -40 °C might have resulted in over-saturation of the impregnation solution and consequently to precipitation of $NaAlH_4$ particles inside pores of the CNF skeins. In addition, the viscosity of the solvent increased at lower temperatures. This is favorable for a higher dispersion, since the viscous flow of $NaAlH_4$ with the evaporating solvent might be suppressed.[31]

In another sample, the impregnated skeins were dried at room temperature at 6 mbar pressure. This was detrimental for the dispersion of the $NaAlH_4$, as shown in Figure 1B and C. Boiling of the solvent possibly caused the formation of gas bubbles in the pores, which forced the $NaAlH_4$/THF solution to the surface of the CNF-skeins. After that, the THF evaporated further leaving μm-sized $NaAlH_4$ on the outer surface of the CNF skeins. The detrimental effect of room temperature drying was not observed in our previous study.[2] However, in that work the CNF were oxidized which resulted in ~0.2 $mmol.g^{-1}$ of oxygen-containing groups. The oxygen-containing groups might have functioned as anchoring sites. The CNF in the present work had not been oxidized and contained less than 0.02 $mmol.g^{-1}$ of oxygen-containing groups[22], *i.e.* a low amount of anchoring/nucleation sites. Therefore, for the non-oxidized CNF used in this study, the drying procedure was critical to prepare nano-sized particles of $NaAlH_4$.

Size-performance relationship

As described previously, we have tuned the $NaAlH_4$ particle sizes in discrete ranges of 2-10 nm, 19-30 nm and 1-10 μm. The effects of the particle size on H_2 desorption and absorption properties will be discussed in the next section. Figure 3 shows the H_2 desorption profiles for the three CNF-supported $NaAlH_4$ samples. The temperature at maximum desorption rate (T_{max}) was highest for "1-10 μm $NaAlH_4$" (186 °C) followed by "19-30 nm $NaAlH_4$" (164 °C) and lowest for "2-10 nm $NaAlH_4$" (70 °C). Thus, the smaller the particles, the lower the H_2 desorption temperature.

The activation energy for H_2 desorption was calculated using a Kissinger analysis that is based on the shifts in T_{max} with heating rates (β) of 0.5, 1, 2 and 5 $°C.min^{-1}$.[32] For that, $\ln(\beta/T_{max}^2)$ was plotted versus $1/T_{max}$ (see Figure 4). The slope of the curve represents $-E_{act}/R$ in which R is the gas constant. From the slope in Figure 4 was established that the E_{act} for H_2 desorption was 116 $kJ.mol^{-1}$ for "1-10 μm $NaAlH_4$", which is in good agreement with reported values for

uncatalyzed bulk $NaAlH_4$ (120 kJ.mol^{-1}).[33, 34] Thus, the 1-10 µm $NaAlH_4$ particles showed bulk-like H_2 desorption behavior. However, the sample desorbed a small amount of H_2 below 140 °C (Figure 3). This was probably H_2 desorption from a small fraction of the $NaAlH_4$ that was smaller in size (*vide infra*).

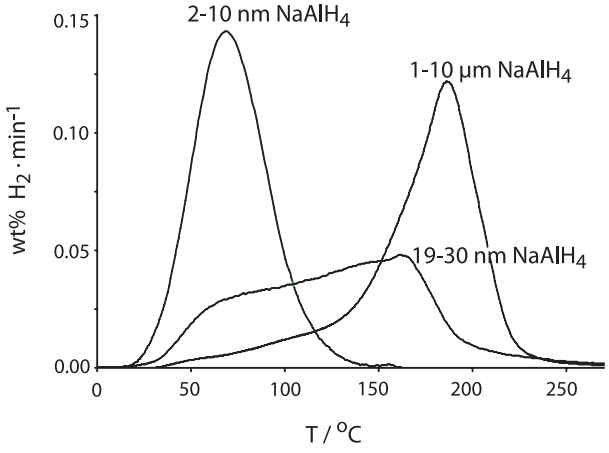

Figure 3. Temperature Programmed Desorption profiles of H_2 for $NaAlH_4$/CNF samples under Ar-atmosphere. Heating ramp 5 °C/min.

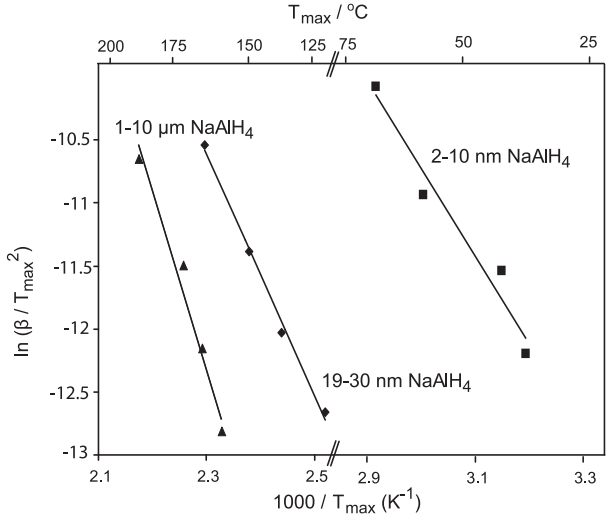

Figure 4. Kissinger plots, and temperature at maximum desorption rate (T_{max}) for $NaAlH_4$ samples.

The H_2 desorption from "19-30 nm $NaAlH_4$" proceeded from 25 to 250 °C. This indicates that a broad particle size distribution was present. Most likely, H_2 evolution from 25 to 100 °C came from a fraction of particles that had a similar size as for "2-10 nm $NaAlH_4$", since the desorption temperature coincided with that of "2-10 nm $NaAlH_4$" (Figure 3). The peak with T_{max} at 164 °C then reflects desorption from the larger (19-30 nm) $NaAlH_4$ particles. The activation energy for H_2 desorption from these particles was 80 kJ.mol^{-1} (Figure 4) a value comparable to that of Ti-catalyzed $NaAlH_4$.[33, 34] However in "19-30 nm $NaAlH_4$", no Ti was present as a catalyst. Thus, solely by reducing the particle size to the nanometer range, the activation energy decreased to the same value as ball milled $TiCl_3$-$NaAlH_4$.

The activation energy lowered to an unprecedented value of 58 kJ.mol^{-1} when the $NaAlH_4$ particle size was decreased to 2 - 10 nm. The relation between activation energies and particle size, *i.e.,* a size-performance relationship, is shown in Figure 5. This correlation opens the possibility to link experiment with theoretical calculations on metal hydride nanoclusters, since now the experimental available cluster size is in the same size range as those used in the theoretical studies.[35-38] But most importantly, the correlation is an advance that is applicable to other hydrogen storage materials as well.

A possible explanation for the reported particle size dependence for H_2 desorption can be found in the calculations performed by Vegge on the stability of the $NaAlH_4$ surfaces.[38] It appears that the (0 0 1) surface is the most stable and most abundant surface in $NaAlH_4$ particles from which it is difficult to desorb H_2. The relative abundance of this most stable surface is expected to decrease progressively by reducing the $NaAlH_4$ particle size, which might in turn lead to a decrease of the activation energy.

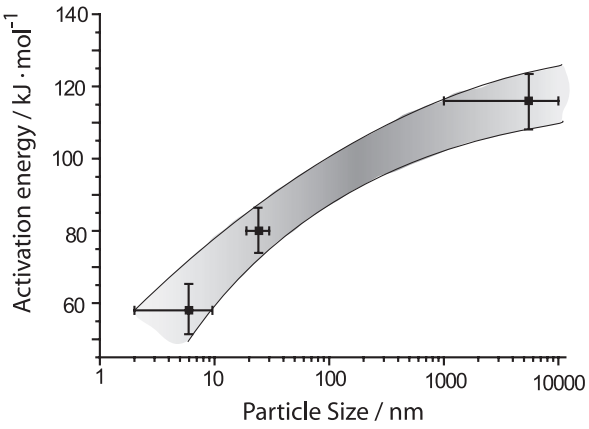

Figure 5 Relation between particle size and activation energy for hydrogen desorption from $NaAlH_4$/CNF. The spread in the particle size reflects the results from different characterization techniques, and the error-bars in activation energies were obtained from linear regression analysis.

The generally accepted target from the Department of Energy indicates that that an ideal automotive storage tank liberates H_2 from -30 to 85 °C. The often studied Ti-catalyzed $NaAlH_4$ has not met this target in a scale-up study.[39] However for "2-10 nm $NaAlH_4$", T_{max} ranged from 40 to 70 °C (Figures 3 and 4). These are, to the best of our knowledge, the lowest reported desorption temperatures for $NaAlH_4$, and indicate that the target is now within reach and nanosized $NaAlH_4$ has potential for application. The loading of the 2-10 nm $NaAlH_4$ particles in this paper was 2 wt% on the CNF and has to be increased for automotive applications. This might be achieved by encapsulation of the $NaAlH_4$ in nano-cavities rather than the here-reported deposition of $NaAlH_4$ on the convex surface of the nanofibers.

For application, reloading of the $NaAlH_4$ after H_2 extraction must be achieved at low H_2 pressure. We studied the uptake characteristic of "19-30 nm $NaAlH_4$" as a function of H_2 pressure at 115 °C (Figure 6). For reference, the pure support material (CNF) was included which did not absorb H_2 from 0.1 to 100 bar. The "19-30 nm $NaAlH_4$" started to absorb H_2 from a relatively low H_2 pressure of 20 bar. Please note that a typical catalyzed $NaAlH_4$ (ball milled $TiCl_3$-$NaAlH_4$) absorbed H_2 starting from 45 bar (Figure 6). It was also observed that the H_2 uptake from "19-30 nm $NaAlH_4$" was lower than the total hydrogen capacity (5.6 wt% H_2). A reason for the lower loading capacity might be that the sodium hydride and aluminum particles were physically separated at the CNF surface that hampered recombination of the NaH and Al to the $NaAlH_4$. The previously mentioned encapsulation, *i.e.* confining the $NaAlH_4$ in nanocavities, might overcome this as well.

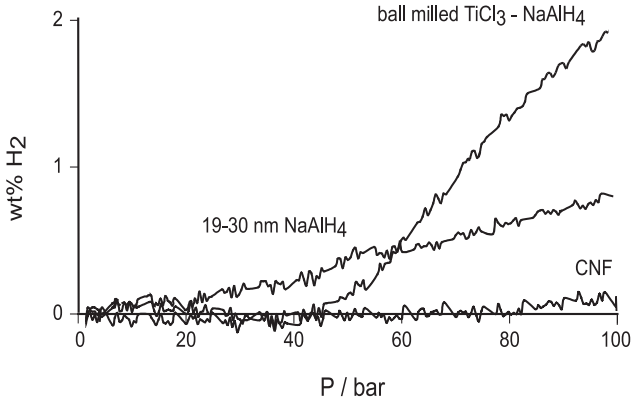

Figure 6 H_2 uptake for the 1st absorption step at 115 °C for 19-30 nm $NaAlH_4$ compared to the uptake from ball milled $TiCl_3$-$NaAlH_4$ and pure CNF. $\Delta P/\Delta t = 1.38$ bar.min^{-1}.

Conclusion

Summarizing, a quantitative relation is found between the activation energy for H_2 desorption and the particle size of $NaAlH_4$ varying from 116 kJ·mol^{-1} for 1-10 μm particles to 80 kJ.mol^{-1} for 19-30 nm particles, to 58 kJ.mol^{-1} for 2-10 nm particles, the latter being lower than for Ti-catalyzed $NaAlH_4$. For the 2-10 nm particles, the H_2 desorption temperature was below 70 °C, therewith meeting the target from the Department of Energy for H_2 release. Moreover, after desorption the nano-$NaAlH_4$ showed uptake under relatively low H_2 pressures (starting at 20 bar) which can lead to the development of safer, more economical and lighter storage tanks. The nanoparticles reported in this paper were non-catalyzed, and the improvement in activation energies, and absorption properties could be solely accounted by reducing the $NaAlH_4$ particle size. The size-performance relationship reported provides new avenues for other hydrides, such as other complex metal hydrides and amides, which contain a higher weight fraction of hydrogen.

Acknowledgements

Marjan Versluijs-Helder, Cor van der Spek, and Ad Mens are thanked for SEM, TEM and XPS measurements. Drs Bart Hereijgers is thanked for some of the sample. Dr. Petra de Jongh and Dr. Andy Beale are thanked for their input to the manuscript.

References

1. Schlapbach, L.; Züttel, A., *Nature* **2001,** 414, 353-358.
2. Baldé, C. P.; Hereijgers, B. P. C.; Bitter, J. H.; de Jong, K. P., *Angew. Chem. Int. Ed.* **2006,** 45, 3501-3503.
3. Gutowska, A.; Li, L.; Shin, Y.; Wang, C. M.; Li, X. S.; Linehan, J. C.; Smith, R. S.; Kay, B.D.; Schmid, B.; Shaw, W.; Gutowski, M.; Autrey, T., *Angew. Chem., Int. Ed.* **2005,** 44, 3578-3582.
4. Bezemer, G. L.; Bitter, J. H.; Kuipers, H. P. C. E.; Oosterbeek, H.; Holewijn, J. E.; Xu, X.; Kapteijn, F.; van Dillen, A. J.; de Jong, K. P., *J. Am. Chem. Soc.* **2006,** 128, 3956-3964.
5. Bell, A. T., *Science* **2003,** 299, 1688-1691.
6. Kong, J.; Franklin, N. R.; Zhou, C.; Chapline, M. G.; Peng, S.; Cho, K.; Dai, H., *Science* **2000,** 287, 622-625.

7. Xi, J.-Q.; Kim, J. K.; Schubert, E. F., *Nano Lett.* **2005,** 5, (7), 1385-1387.
8. Tong, L.; Lou, J.; R.Gattass, R.; He, S.; Chen, X.; Liu, L.; Mazur, E., *Nano Lett.* **2005,** 5 (2), 259-262.
9. Schüth, F.; Bogdanovic, B.; Felderhof, M., *Chem. Commun.* **2004,** 37, 2249-2258.
10. Grochala, W.; Edwards, P. P., *Chem. Rev.* **2004,** 104 (3), 1283-1315.
11. Orimo, S.; Nakamori, Y.; Eliseo, J. R.; Züttel, A.; Jensen, C. M., *Chem. Rev.* **2007,** 107, (10), 4111 - 4132.
12. Bogdanovic, B.; Eberle, U.; Felderhoff, M.; Schüth, F., *Scr. Mater.* **2007,** 56, 813–816.
13. Bogdanovic, B.; Felderhoff, M.; Pommerin, A.; Schüth, F.; Spielkamp, N., *Adv. Mater.* **2006,** 18, 1198-1201.
14. Fichtner, M.; Fuhr, O.; Kircher, O.; Rothe, J., *Nanotechnology* **2003,** 14, (7), 778-785.
15. Brinks, H. W.; Hauback, B. C.; Srinivasan, S. S.; Jensen, C. M., *J. Phys. Chem. B* **2005,** 109, 15780-15785.
16. Pan, X.; Fan, Z.; Chen, W.; Ding, Y.; Luo, H.; Bao, X., *Nature Mater.* **2007,** 6, 507-511.
17. Sietsma, J. R. A.; Meeldijk, J. D.; den Breejen, J. P.; Versluijs-Helder, M.; van Dillen, A.J.; de Jongh, P. E.; de Jong, K. P., *Angew. Chem. Int. Ed.* **2007,** 46, 4547-4549.
18. Feaver, A.; Sepehri, S.; Shamberger, P.; Stowe, A.; Autrey, T.; Cao, G., *J. Phys. Chem. B* **2007,** 111, (26), 7469 -7472.
19. Züttel, A.; Wenger, P.; Rentsch, S.; Sudan, P.; Mauron, P.; Emmenegger, C., *J. Power Sources* **2003,** 118, 1-7.
20. Vajo, J. J.; Olson, G. L., *Scr. Mater.* **2007,** 56, (10), 829-834
21. Van der Lee, M. K.; van Dillen, A. J.; Bitter, J. H.; de Jong, K. P., *J. Am. Chem. Soc.* **2005,** 127, (39), 13573-13582
22. Toebes, M. L.; van Heeswijk, E. M. P.; Bitter, J. H.; van Dillen, A.J.; de Jong, K. P., *Carbon* **2004,** 42 (2), 307-315.
23. Dreisbach, F.; Seif, R.; Lösch, H. W., *J. Therm. Anal. Calorim.* **2003,** 71, 73-82.
24. Lösch, H. W.; Kleinrahm, R.; Wagner, W., *Neue Magnetschwebewaagen für gravimertrische Messungen in der Verfahrentechnik.* VDI-Verlag Düsseldorf, 1994.
25. Haiduc, A. G.; Stil, H. A.; Schwarz, M. A.; Paulus, P.; Geerlings, J. J. C., *J. Alloys Compd.* **2005,** 393, (1-2), 252-263.
26. Kuipers, H. P. C. E., *Solid State Ion.* **1985,** 16, 15-21.
27. Kuipers, H. P. C. E.; Leuven, H. C. E. V.; Visser, W. M., *Surf. Interface Anal.* **1986,** 8, (6), 235-242.

28. *When $NaAlH_4$ is heated it decomposes via the following reactions: $NaAlH_4 \leftrightarrow \frac{1}{3} Na_3AlH_6 + \frac{2}{3} Al + H_2 \leftrightarrow NaH + Al + 1\frac{1}{2} H_2$. The material after desorption was used for XPS and TEM studies since $NaAlH_4$ is not stable under the conditions which TEM and XPS measurements are performed (low pressure and ionizing radiation).*

29. Neimark, A. V.; Kheifez, L. I.; Fenelonov, V. B., *Ind. Eng. Chem. Prod. Res. Dev.* **1981,** 20, 439-450.

30. Lekhal, A.; Glasser, B. J.; Khinast, J. G., *Chem. Eng. Sci.* **2001,** 56, (15), 4473-4487.

31. van Dillen, A. J.; Terörde, R. J. A. M.; Lensveld, D. J.; Geus, J. W.; de Jong, K. P., *J. Catal.* **2003,** 216, (1-2), 257-264.

32. Kissinger, H. E., *Anal. Chem.* **1957,** 29, 1702.

33. Luo, W.; Gross, K. J., *J. Alloys Compd.* **2004,** 385, 224–231.

34. Sandrock, G.; Gross, K.; Thomas, G., *J. Alloys Compd.* **2002,** 339, 299–308.

35. Marashdeh, A.; Olsen, R. A.; Løvvik, O. M.; Kroes, G. J., *Chem. Phys. Lett.* **2006,** 426, 180-186.

36. Marashdeh, A.; Olsen, R. A.; Løvvik, O. M.; Kroes, G. J., *J. Phys. Chem. C* **2007,** 111, 8206-8213.

37. Wagemans, R. W. P.; van Lenthe, J. H.; de Jongh, P. E.; van Dillen, A. J.; de Jong, K. P., *J. Am.Chem. Soc.* **2005,** 127, (47), 16675-16680.

38. Vegge, T., *Phys. Chem. Chem. Phys.* **2006,** 8, 4853 - 4861.

39. Jensen, J. O.; Li, Q.; He, R.; Pan, C.; Bjerrum, N. J., *J. Alloys Compd.* **2005,** 404-406, 653-656.

3

Linking Structure to Performance in Ti-catalyzed Nanosized-$NaAlH_4$

Abstract

The effects of a Ti-catalyst on sodium alanate ($NaAlH_4$) particles (<30 nm size) have been studied in relation to acceleration of hydrogen absorption and desorption kinetics. Ti-catalyzed $NaAlH_4$ nanoparticles were obtained by deposition onto carbon nanofibers (CNF). The order of Ti and $NaAlH_4$ deposition turned out to have a significant influence on the sorption characteristics of the final material. When $NaAlH_4$ is deposited first, Ti displays merely a catalytic role, decreasing the temperature of maximum H_2 desorption rate from above 160 °C (without Ti) to 132 °C in Ar. However, when Ti is deposited first, a "Ti-Al" catalyst is formed which has a twofold role: it functions as a catalyst and as an aid to further reduction of the $NaAlH_4$ particle size. Due to the ambivalent role of the Ti, the temperature for the maximum H_2 desorption rate is further decreased to 99 °C. Moreover, the Ti also lowers the initial uptake pressure of hydrogen from 20 (without Ti) to 10 bar H_2 pressure at 115 °C.

Introduction

Hydrogen is regarded as a future energy carrier and promising candidates for hydrogen storage are light-weight metal hydrides.[1] However, hydrogen release and absorption rates are often impeded in metal hydrides and need to be improved. Two generic solutions are put forward to address this issue, *i.e.* reducing the particle size in to the nm range (typically below 30 nm),[2-8] or addition of one or a combination of catalysts.[9-11] Nanoparticles have a larger surface to volume ratio than bulk materials and therefore exhibit modified properties. Besides that, mass transfer lengths of the solid are considerably reduced with nanoparticles, which is important for fast hydrogen release and uptake.

For catalyzed H_2 absorption and desorption in sodium alanate ($NaAlH_4$) a breakthrough has been realized by Bogdanovic and co-workers who discovered that mixing a few mol% Ti precursor with $NaAlH_4$ in solution led to enhanced sorption rates.[9] Later, it was found that ball milling the Ti precursor with the $NaAlH_4$ was more effective and facile.[12] Various studies indicate that the catalytic species in ball milled Ti-$NaAlH_4$ is a Ti-Al-alloy nanoparticle.[13-17] The $NaAlH_4$ particles, however, are typically 150-200 nm in these materials.[18, 19] The aim of the current research is to combine the Ti-based catalyst with $NaAlH_4$ particles smaller than 30 nm. Therefore, a preparation method had to be developed to create $NaAlH_4$ nanoparticles that mix with highly dispersed Ti catalyst particles. This has been achieved by deposition of $Ti(OBu)_4$ and $NaAlH_4$ on a carbon nanofiber (CNF) support material by performing two consecutive pore volume impregnations. Two Ti-catalyzed materials will be described in which the impregnation order was varied. Their characteristics will be compared to undoped nano-$NaAlH_4$ on CNF and ball milled $TiCl_3$-$NaAlH_4$. Structure activity relationships will be established by relating Ti K-edge Extended X-ray Absorption Fine Structure (EXAFS), in-situ X-ray Diffraction (XRD), and X-ray Photoelectron Spectroscopy (XPS) results with the hydrogen absorption and desorption characteristics of the samples.

Experimental

Sample preparation

Fishbone Carbon Nanofibers (CNF) of 20 to 30 nm in diameter were grown from 5 wt% Ni/SiO_2 (425-850 μm SiO_2 particles) using H_2/CO as described by Van der Lee *et al.*[20] After growth, SiO_2 was removed by refluxing twice in 1 M KOH for 1 hour. Subsequently, Ni was removed by

refluxing twice in fresh concentrated HCl for 1 hour. After each refluxing step, the CNF were thoroughly washed with demi-water until the supernatant had a pH of 5. Finally, the CNF were dried in an inert atmosphere at 500 °C and stored in the glovebox for further use. CNF prepared in this way comprised a low concentration (<0.02 $mmol.g^{-1}$) of oxygen-containing groups on the surface, had a specific surface area of 130 $m^2.g^{-1}$ and had a pore volume of 1.0 $ml.g^{-1}$.

All further sample handling was conducted under a dry and inert atmosphere using either Schlenk equipment or a glovebox equipped with a circulation purifier. The solvents, tetrahydrofuran (THF) and diethylether, were distilled over Na in N_2 atmosphere to remove H_2O and O_2 traces. $NaAlH_4$ (90%, Sigma Aldrich) was purified by dissolution in THF and filtrated to remove insoluble contaminants. The pure alanate was obtained as a white powder after evaporation of the THF under reduced pressure. It was stored in the glovebox afterwards and used within one day.

$Ti(OBu)_4$ (≥97%, Sigma-Aldrich) and purified $NaAlH_4$ were deposited on the CNF using pore volume impregnations followed by drying. Typically, 8 wt% $NaAlH_4$ with 10 mol % $Ti(OBu)_4$, relative to the $NaAlH_4$ loading, were deposited on the CNF. In the first sample, the pore volume of the CNF was first impregnated with $Ti(OBu)_4$ in diethylether until the pore volume was completely filled. The diethylether was removed by drying the impregnated sample at room temperature. Subsequently, 8wt% $NaAlH_4$ was impregnated using THF as a solvent. The sample was cooled to -40 °C in an acetone-dry-ice bath after the second impregnation step. Then, a drying procedure was performed from -40 to -15 °C over a period of 3 h by reducing the pressure to 6 mbar (denoted as low-temperature drying). This sample will be referred to as "$NaAlH_4$-Ti/CNF".

A second sample was prepared in which the impregnation order of $NaAlH_4$ and $Ti(OBu)_4$ was reversed. Thus, the CNF were first impregnated with $NaAlH_4$ and dried at low temperature. Next, the material was allowed to heat up in an Ar atmosphere to room temperature and the $Ti(OBu)_4$ dissolved in diethylether was impregnated to the $NaAlH_4$/CNF. The sample was immediately cooled down after impregnation to prevent thermal decomposition of the $NaAlH_4$ and dried at low-temperature. This sample will be referred to as "Ti-$NaAlH_4$/CNF". An uncatalyzed nano-$NaAlH_4$ with a similar $NaAlH_4$ loading was prepared via pore volume impregnation and low temperature drying. This sample will be referred to as "$NaAlH_4$/CNF".[3] For comparison, a bulk sample was prepared by ball milling $TiCl_3$ with purified $NaAlH_4$ (Ti:Al= 4.5 mol%) using a SPECS ball milling apparatus as described by Haiduc *et al.*.[21] This sample will be referred to as "ball milled $TiCl_3$-$NaAlH_4$". Due to the sensitive nature towards water, oxygen, and temperature, the as-prepared samples were stored at -20 °C under nitrogen atmosphere. Transport to the synchrotrons was conducted below 5 °C under nitrogen atmosphere to limit thermal decomposition of the $NaAlH_4$.

Hydrogen Sorption

Temperature Programmed Desorption (TPD) of H_2 was performed using a Micromeretics AutoChem II 2920. The quartz reactor was typically loaded with 0.2 g of sample and heated with a ramp of 2 °C.min^{-1} from -20 to 160 °C 25 ml/min Ar. H_2 concentrations were measured using a calibrated Thermal Conductivity Detector.

H_2 uptake characteristics were recorded with a high pressure magnetic suspension balance from Rubotherm.[22, 23] Typically, 0.25 gram $NaAlH_4$(-Ti)/CNF or 0.004 gram of ball milled $TiCl_3$-$NaAlH_4$ were loaded in the balance. The sample was desorbed at 0.1 bar H_2 (99.999%) pressure at 250 °C, after which the temperature was lowered to 115 °C and equilibrated for 1 hour. Next, the hydrogen pressure was increased to 100 bar with 1.38 barmin^{-1} during which the H_2 uptake was recorded (flow of H_2 was 300 ml.min^{-1}). When the pressure reached 100 bar, the sample was equilibrated for 1 hour in 30 ml.min^{-1} H_2 flow. The cycle was completed by desorbing the sample at 0.1 bar H_2 pressure for 1 hour. This cycle was repeated two more times. The amount of hydrogen uptake and desorption was determined after subtracting the weight changes of an empty sample holder and applying a buoyancy correction for the volume of the sample. The volume of the sample was determined from its weight and the true density of the sample.

Structural Investigation

X-ray absorption spectroscopy was performed on the Ti K-edge at station E4 of the DESY synchrotron (Hamburg, Germany). The storage ring was operated at 4.4 GeV with a mean current of 120 mA. The experimental station was equipped with a Si (111) double crystal monochromator which was detuned to 60% to suppress higher harmonics. The measuring cell was dried by heating under vacuum (10^{-4} mbar) for 1 hour. Afterwards, it was closed under reduced pressure and transferred to the glovebox. 120 mg sample was pressed in a pellet and mounted to the cell in the glovebox. Next, the cell (with sample and filled with Ar) was transferred to the beam-line to be flushed with He. XAS experiments were performed at 77 K in flowing He.

Extraction of the EXAFS data from the measured absorption data was performed with the XDAP program.[24] Three scans were averaged and the pre-edge background was approximated by a Victoreen function before subtraction.[25] The position of the edge energy was determined at the maximum of the first derivative of the spectrum and was calibrated using a Ti-foil as a reference in each scan. The spectrum was background corrected by employing a cubic spline routine.[26] Normalization was performed by dividing the absorption spectrum by the height of the background at 50 eV from the edge.

The Ti-Al backscattering amplitude and phase shift were calculated using the FEFF 8.0 code[27] and calibrated using an experimental measured spectrum of $TiAl_3$ (99%, Alfa Aesar) at 77 K. The same routines were applied to calibrate the Ti-C reference that was obtained from TiC (powder >4μm, Sigma-Aldrich) and the Ti-O reference from rutile-TiO_2 (99.99%, Sigma-Aldrich). Ti-Ti backscatter amplitude and phase shift were calibrated against a Ti foil recorded at room temperature. The FEFF input parameters are listed in Table 1. The experimental data were fitted in k^2 using the difference file technique in *R*-space from $3.1<k<11$ Å^{-1}.[28] The quality of the fit was checked by applying k^1 and k^3 weightings.

X-ray Photoelectron Spectroscopy (XPS) spectra were acquired from a Perkin Elmer (PHI) model 5580 spectrometer using Al K_α radiation. Samples were desorbed at 300 °C, crushed and pressed on double-sided adhesive conductive carbon tabs. The prepared samples were carefully passivated at room temperature in 0.5 ml.min^{-1} O_2 in 200 ml.min^{-1} N_2 in view of the presence of Ti. Shirley backgrounds were subtracted from the raw data to obtain the areas of the C_{1s}, Al_{2p} Ti_{2p} and Na_{1s} signals.

In-situ Powder X-ray Diffraction was recorded at the Synchrotron Radiation Source (Daresbury, UK) on station 6.2 using at a setup described by Jacques *et al.*.[29] The sample was crushed in a glovebox, loaded into a capillary which was sealed with wax. X-ray diffraction was performed at a wavelength of 1.4 Å during in-situ heating to 200 °C at 5 °C.min^{-1}.

Table 1. Input parameters to create FEFF references for EXAFS analysis.

Absorber - backscatterer	S_0^2	σ^2 / 10^{-3} Å^{-2}	V_r / eV	V_i / eV	Reference
Ti-Al	0.72	1.50	11.3	1.0	$TiAl_3$
Ti-C	0.52	3.71	-7.21	1.0	TiC
Ti-O	0.59	4.05	13.57	1.0	Rutile TiO_2
Ti-Ti	0.60	0	8.60	1.0	h.c.p. Ti Foil

Hedin-Lunqvist potentials were used for the calculations.

RESULTS

Performance for hydrogen storage

Figure 1 shows hydrogen evolution during the TPD for $NaAlH_4$/CNF, Ti-$NaAlH_4$/CNF, and $NaAlH_4$-Ti/CNF. H_2 started to desorb around 10 to 20 °C for all samples. The TPD profile of $NaAlH_4$-Ti/CNF displays a maximum at 99 °C (sample in which Ti was impregnated first to the CNF). For Ti-$NaAlH_4$/CNF ($NaAlH_4$ added first to the CNF followed by the Ti precursor), it is observed that the maximum shifts to 132 °C. The maximum increases to above 160 °C for $NaAlH_4$ on the CNF in the absence of Ti ($NaAlH_4$/CNF).

Figure 2 shows the H_2 uptake kinetics at 115 °C for increasing hydrogen pressures after the first desorption. The pure CNF (without $NaAlH_4$ or $Ti(OBu)_4$ deposition) was measured and showed that H_2 did not absorb from 0.1 to 100 bar H_2 pressure. Ball-milled $TiCl_3$-$NaAlH_4$ started to absorb H_2 from 45 bar H_2 pressure and absorbed 1.90 wt% H_2 at 100 bar. Uncatalyzed $NaAlH_4$ deposited on CNF ($NaAlH_4$/CNF) absorbed H_2 from a pressure of 20 bar. In the case of the $NaAlH_4$ catalyzed with Ti on the CNF ($NaAlH_4$-Ti/CNF), the absorption offset decreased to 10 bar H_2 pressure. The H_2 capacities for the first three absorption-desorption cycles are listed in Table 2. For $NaAlH_4$/CNF, the absorption capacity (based on the amount of $NaAlH_4$) in the first cycle was 0.85 wt% and decreased to 0.18 and 0.26 wt% in the second and third cycle. The absorption capacity for $NaAlH_4$-Ti/CNF was 1.38 wt% H_2 in the first cycle and decreased to 0.76 to 0.53 wt% H_2 for respectively the second and third cycle.

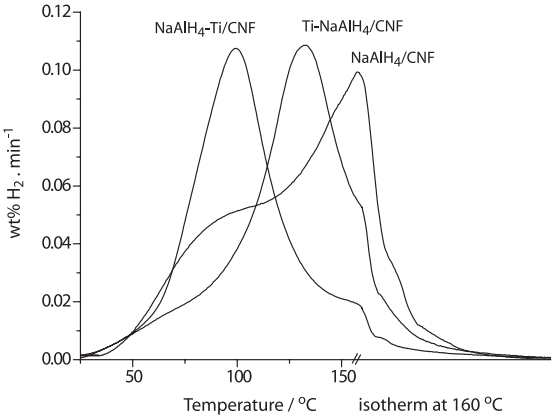

Figure 1. Hydrogen desorption profile for various samples from 0 to 160 °C under Ar atmosphere. Heating ramp 2 °C.min^{-1}, data normalized to the loading of $NaAlH_4$ on the CNF.

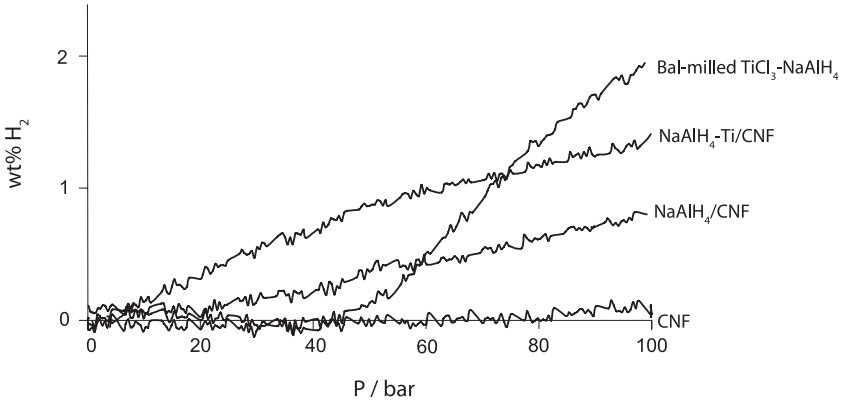

Figure 2. Initial H_2 absorption for 1st absorption step at 115 °C. $\Delta P/\Delta t$ = 1.38 barmin^{-1}; the uptake has been normalized to the weight of $NaAlH_4$ during measurement.

Table 2. Cycle tests of $NaAlH_4$/CNF and $NaAlH_4$-Ti/CNF. The maximum capacity for $NaAlH_4$-Ti/CNF is 2.50 wt% H_2. The mass of the CNF is not taken into account in this percentage.

	1st Abs (wt% H_2)	2nd Abs (wt% H_2)	3rd Abs (wt% H_2)
$NaAlH_4$-Ti/CNF	1.38	0.76	0.53
$NaAlH_4$/CNF	0.85	0.18	0.26

Structure of $NaAlH_4$

Figure 3 shows the X-ray diffraction patterns of as-prepared $NaAlH_4$/CNF, Ti-$NaAlH_4$/CNF and $NaAlH_4$-Ti/CNF at room temperature. Two broadened CNF diffractions were present at 2θ=23.55° and 38.86°. $NaAlH_4$ was detected at 2θ values of 26.85°, 28.56° and 32.33°. The inset in Figure 3 shows the full width at half maximum (FWHM) of the $NaAlH_4$ diffraction and shows that the FWHM was comparable for all measured samples; a crystallite size of ~20 nm was obtained using this FWHM in the Debye-Scherrer equation.

Diffraction peaks at 2θ = 34.79°, 40.34° and 43.70° were ascribed to Al and illustrate that the samples had lost H_2 during the transport to the XRD (see decomposition reactions in Eqs. (1) and (2) below). The FWHM of Al was comparable to that of $NaAlH_4$, also during hydrogen extraction, indicating a crystallite size of ~20 nm (Figure 3).

$$3\ NaAlH_4 \leftrightarrow Na_3AlH_6 + 2\ Al + 3\ H_2 \quad (1)$$

$$Na_3AlH_6 \leftrightarrow 3\ NaH + Al + 1½\ H_2 \quad (2)$$

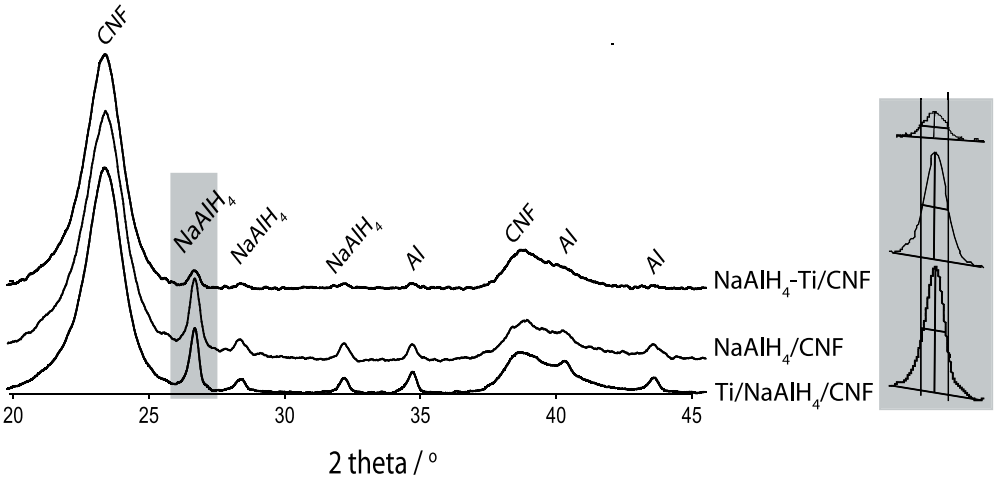

Figure 3. Powder XRD patterns from $NaAlH_4$/CNF, Ti-$NaAlH_4$/CNF and $NaAlH_4$-Ti/CNF at 25 °C (λ = 1.4 Å).

The evolution of the crystalline phases were recorded during in-situ desorption from room temperature to 200 °C for $NaAlH_4$/CNF and $NaAlH_4$-Ti/CNF. The integrated areas of the $NaAlH_4$, Na_3AlH_6, and Al diffraction peaks are shown in Figure 4 as a function of temperature. For $NaAlH_4$-Ti/CNF, the $NaAlH_4$ diffraction decreases starting from 20 °C and becomes zero at 115 °C. The Al diffraction grows steadily from 40 °C and stabilizes at 130 °C. Weak Na_3AlH_6 diffraction peaks were detected between 105 and 150 °C. For $NaAlH_4$/CNF, the $NaAlH_4$ diffraction starts to decrease from 20 °C and becomes zero at 150 °C. At the same temperatures the Al diffraction is constant. However above 150 °C, the Al diffraction shows a rapid increase and stabilizes at 190 °C. From 150 to 180 °C only weak diffraction of Na_3AlH_6 is detected.

The atomic compositions of the samples have been investigated with XPS after hydrogen extraction. Table 3 shows that the atomic Al:C ratio was 0.012 for Ti-$NaAlH_4$/CNF and increased to 0.031 in $NaAlH_4$-Ti/CNF. The Na:C ratio was an order of magnitude larger and was 0.16 and 0.26 for Ti-$NaAlH_4$/CNF and $NaAlH_4$-Ti/CNF, respectively.

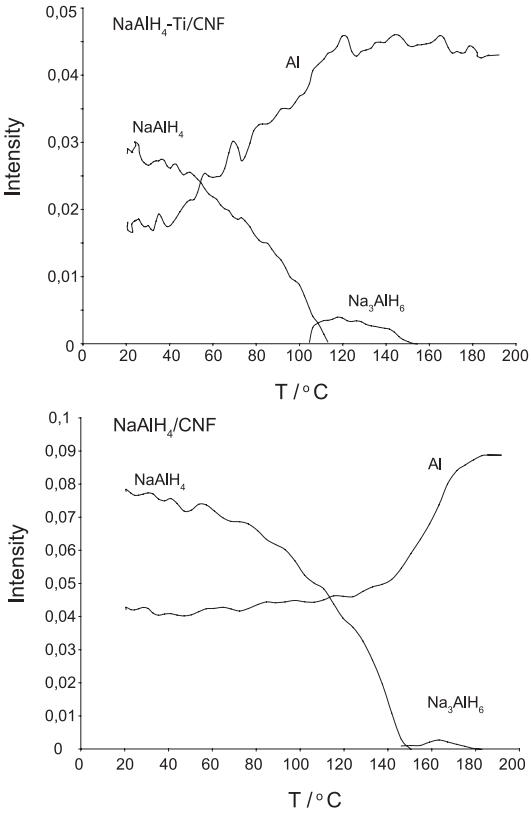

Figure 4. Integrated areas of $NaAlH_4$, Na_3AlH_6 and Al diffraction peaks during the in-situ desorption to 200 °C for $NaAlH_4$-Ti/CNF and $NaAlH_4$/CNF. Heating ramp 5 °C.min^{-1}, intensity has been normalized to the CNF diffraction.

Structure of Ti

A Ti-containing phase was not detected with XRD (Figures 3 and 4), which indicates that the Ti-phase was XRD-amorphous. XPS revealed that the Ti_{2p} signal appeared in the experiment and had an atomic Ti:C ratio of 0.005 and 0.007 for Ti-$NaAlH_4$/CNF and $NaAlH_4$-Ti/CNF (Table 3). Thus the Ti is presumably present at or near the surface of CNF and/or $NaAlH_4$. The local structure around the Ti was further investigated with Ti K-edge EXAFS. To show the quality of the data, the background subtracted EXAFS, $\chi(k)$, is shown in Figure 5. The *R*-space EXAFS fit of $NaAlH_4$-Ti/CNF is visualized in Figure 6 and shows that the fit describes the data well from 1.5 to 3.5 Å. The k^2 variances, shown in Table 4, were comparable for $NaAlH_4$-Ti/CNF and Ti-$NaAlH_4$/CNF, indicating that the quality of both fits were similar.

The EXAFS fit of $NaAlH_4$-Ti/CNF revealed that Ti is on average surrounded with 2.3 C atoms at 2.39 Å in its first shell (Table 4). In the next two shells, 2.9 Al atoms at 2.69 Å and 1.6 Al atoms at 3.09 Å were fitted. The first Ti atom was found at 3.63 Å with a coordination number of 0.7. The fit parameters of Ti-$NaAlH_4$/CNF are listed in Table 4 and reveal that Ti is surrounded with 3.9 O atoms at 2.02 Å and 6.2 C atoms at 2.49 Å. In the next shell, 3 Ti atoms are present at 2.85 Å.

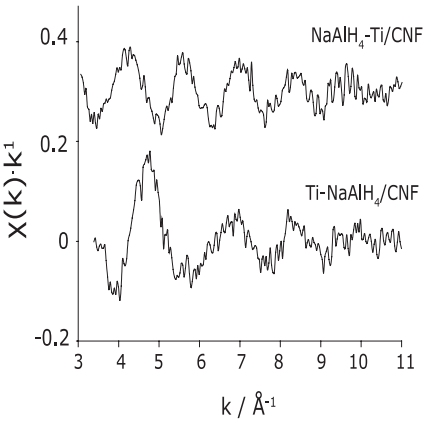

Figure 5. k^1 weighted background subtracted $\chi(k)$ for $TiAl_3$, Ti-$NaAlH_4$/CNF and $NaAlH_4$-Ti/CNF.

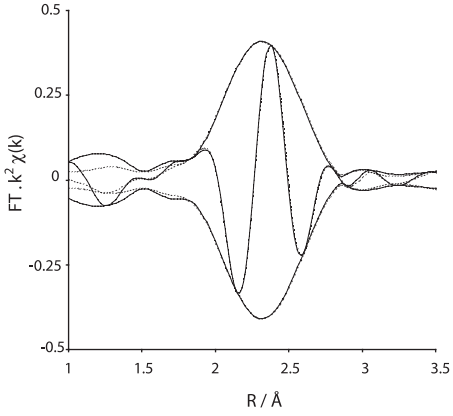

Figure 6. Raw data and EXAFS fit for $NaAlH_4$-Ti/CNF.

Table 3. Atomic ratios obtained from XPS after hydrogen extraction and careful oxidation.

	Al:C (at / at)	Na:C (at:at)	Ti:C (at:at)
Ti-$NaAlH_4$/CNF	0.012	0.16	0.007
$NaAlH_4$-Ti/CNF	0.031	0.26	0.005

Table 2. Ti K-edge EXAFS fit of as prepared $NaAlH_4$-Ti/CNF and Ti-$NaAlH_4$/CNF. Δk= 3.3-11 $Å^{-1}$.

Name	fitrange	Atom	N	$\Delta\sigma^2$ / 10^{-3} $Å^{-2}$	R / Å	E_o / eV	k^2 –variance	
							Im.	Abs.
$NaAlH_4$-Ti/CNF	1.5-3.8	Ti-C	2.3	4.48	2.39	8.75	0.40	0.17
		Ti-Al	2.9	3.36	2.69	3.42		
		Ti-Al	1.6	9.08	3.09	1.81		
		Ti-Ti	0.7	3.60	3.63	-3.10		
Ti-$NaAlH_4$CNF	1.3-2.9	Ti-O	3.9	7.03	2.02	2.18	0.09	0.07
		Ti-C	6.2	0.30	2.49	-12.20		
		Ti-Ti	3.0	7.01	2.85	-0.13		

Number of free parameters: 18 or 19.

Discussion

Hydrogen desorption characteristics of $NaAlH_4$/CNF, $NaAlH_4$-Ti/CNF and Ti-$NaAlH_4$/CNF have been investigated in TPD experiments (Figure 1). Clearly, H_2 evolves at a lower temperature when Ti is present in the sample. Literature provides two possible explanations for this, *i.e.*, the Ti species acts as a Ti catalyst,[9, 12, 30] or the particle size of the $NaAlH_4$ differs from one sample to another.[2, 3, 30, 31] In the following part we will discuss both explanations based on the structural characteristics of $NaAlH_4$/CNF, Ti-$NaAlH_4$/CNF and $NaAlH_4$-Ti/CNF. The structural characteristics of Ti-$NaAlH_4$/CNF will be discussed first.

The particle size of the $NaAlH_4$ is indicated by the FWHM of the $NaAlH_4$ diffraction peaks (Figure 3, illustrated in the inset). It is shown that the FWHM is similar in Ti-$NaAlH_4$/CNF and $NaAlH_4$/CNF, indicating that the average particle size (~20 nm) of the $NaAlH_4$ is comparable in both samples. The peak intensities of the $NaAlH_4$ diffraction patterns are also comparable such that the quantity of ~20 nm $NaAlH_4$ particles was the same. Therefore, it is concluded that the particle size distribution does not change significantly between Ti-$NaAlH_4$/CNF and $NaAlH_4$/CNF after synthesis. This implies that the decrease in T_{max} for Ti-$NaAlH_4$/CNF, compared to $NaAlH_4$/CNF (Figure 1), cannot be related to variations in the particle size of $NaAlH_4$ but, rather, suggests that the "Ti" acted as a catalyst.

Catalysts are often present at surfaces and for that reason the composition of the surface (first 2-5 nm) has been investigated with XPS. The amount of Ti in the sample was small, thus its appearance in XPS (Table 3) indicates that the majority of the Ti must be present at the surface as highly dispersed nanoparticles in Ti-$NaAlH_4$/CNF.

In order to verify the structure of the Ti-nanoparticles in Ti-$NaAlH_4$/CNF, its local structure has been investigated with EXAFS prior to hydrogen desorption. Table 4 shows the EXAFS fit parameters and reveal that Ti is surrounded by O, C and Ti atoms. The absence of Na or Al atoms in the local structure indicates that Ti had not reacted to the $NaAlH_4$ to a level detectable by EXAFS (10%). Since the local structure comprise the same atoms as the original Ti-precursor ($Ti(OBu)_4$), it is concluded that the majority of the Ti is present as nanoparticles of $Ti(OBu)_4$, or a decomposition product thereof, in the as-prepared Ti-$NaAlH_4$/CNF.

In the literature, the structure of the "Ti"-catalyst has been investigated by XAFS in ball milled $TiCl_3$-$NaAlH_4$ and this points to the local structure of the catalytic Ti-species comprising of Al atoms surrounding the Ti.[13-15] In contrast, the Ti in Ti-$NaAlH_4$/CNF has a local structure of O and C atoms (Table 4) prior to hydrogen desorption. This ostensible discrepancy might be explained

by the fact that the O and C atoms in the Ti species can be reduced to the catalytically active Ti-Al phase during the desorption step, as has been reported in an in-situ EXAFS dehydrogenation study of $Ti(OBu)_4$ ball milled $NaAlH_4$,[32] or that the Ti catalyst was present in a concentration non detectable by EXAFS (thus smaller than 10%).

The remaining part of the manuscript will focus on the properties of the sample that have the lowest T_{max} in the TPD profile ($NaAlH_4$-Ti/CNF in Figure 1). Similar to the previously described sample, the improved desorption kinetics will be discussed in relation to the $NaAlH_4$ particle size and/or the catalytic role of the "Ti". The crystallite size of the $NaAlH_4$ was indicated by its diffraction peak FWHM (inset in Figure 3). It reveals a FWHM for $NaAlH_4$-Ti/CNF that is comparable to those of $NaAlH_4$/CNF and Ti-$NaAlH_4$/CNF. However, the intensity of the diffraction has been reduced considerably. This is interpreted that a larger fraction of $NaAlH_4$ is amorphous in this sample, possibly because of a smaller particle size. Apparently, the averaged size and/or crystallinity of the $NaAlH_4$ has been decreased in $NaAlH_4$-Ti/CNF compared to $NaAlH_4$/CNF due to the presence of "Ti".

Evidence for the decrease in particle size was found in XPS performed on the samples after hydrogen extraction. The atomic Al:C and Na:C ratios are listed in Table 3 and show that the Al:C and Na:C ratios were respectively 3.8 and 1.6 times higher for $NaAlH_4$-Ti/CNF than for Ti-$NaAlH_4$/CNF. Since the elemental composition of both samples was identical and XPS probed the first 2 to 5 nm of the surface, the ratio provides a qualitative surface-to-volume ratio of the particles at the CNF. Hence, the higher Al:C and Na:C ratios in $NaAlH_4$-Ti/CNF indicate that NaH and Al particles had a higher surface-to-volume ratio, thus were more highly dispersed on the CNF.

Both XPS and XRD indicate that the average particle size of the $NaAlH_4$ is reduced in $NaAlH_4$-Ti/CNF compared to $NaAlH_4$/CNF and Ti-$NaAlH_4$/CNF. The literature shows that the reduction of particle size significantly increases H_2 desorption rates at lower temperatures.[2, 3, 30, 31] Thus, the particle size reduction of the $NaAlH_4$, induced by the presence of Ti, in $NaAlH_4$-Ti/CNF explains the lowest T_{max} in the TPD profile of Figure 1. However, this might not be the sole explanation of the observed kinetic improvements, as the Ti species can be active as a catalyst as well. Whether this is the case was verified in an in-situ XRD study that monitored the evolution of the crystalline phases during hydrogen desorption as a function of temperature.

As mentioned before, the FWHM of the $NaAlH_4$ diffraction was similar in $NaAlH_4$/CNF and $NaAlH_4$-Ti/CNF, *i.e.*, the crystalline part of the $NaAlH_4$ had a similar crystallite size (Figure 3); this allowed us to rule out the effect of particle/crystallite size on the decomposition rate for the crystalline nano-$NaAlH_4$. The role of the Ti on the $NaAlH_4$ decomposition could therefore be

independently investigated by monitoring the evolution of the diffraction patterns. It is observed in Figure 4 that the $NaAlH_4$ diffraction peaks reached zero intensity at a considerably lower temperature when Ti was present ($NaAlH_4$-Ti/CNF) than when Ti was absent ($NaAlH_4$/CNF). Apparently, "Ti" accelerates decomposition of the $NaAlH_4$ particles in $NaAlH_4$-Ti/CNF, thus acting as a catalyst.

The in-situ XRD experiment also monitored other crystalline phases during hydrogen desorption. It is observed that weak Na_3AlH_6 diffraction peaks were detected and disappeared for $NaAlH_4$/CNF and $NaAlH_4$-Ti/CNF (Figure 4). This indicates that Na_3AlH_6 was an intermediate in the decomposition regardless of the presence of "Ti". The diffraction peaks of Al, however, evolved differently in $NaAlH_4$/CNF and $NaAlH_4$-Ti/CNF. It is observed that the Al peaks grew after the $NaAlH_4$ diffraction peaks disappeared for $NaAlH_4$/CNF (Figure 4). In contrast, the Al peaks grew at the same temperature range that the $NaAlH_4$ peaks decreased when "Ti" was present ($NaAlH_4$-Ti/CNF). This indicates that the "Ti" species provides a nucleation site for Al growth during hydrogen extraction.

The previous discussions deals with the relation between the structures of Ti and $NaAlH_4$ and the hydrogen desorption characteristics. Next, the absorption of hydrogen characteristics of $NaAlH_4$-Ti/CNF will be addressed: Prior to the uptake experiment, the hydrogen is extracted at 250 °C for all measured samples. This implies that the $NaAlH_4$ decomposes to NaH and Al. The NaH has not been detected by XRD (Figures 3 and 4), indicating that it is XRD-amorphous for $NaAlH_4$-Ti/CNF and $NaAlH_4$/CNF. The hydrogen uptake properties for these Al and NaH particles in $NaAlH_4$-Ti/CNF are shown in Figure 2 and reveals that hydrogen absorbs from 10 to 100 bar hydrogen pressure. To rule out the possibility that the hydrogen uptake is caused by either chemisorption or absorption to the CNF, the experiment was repeated for pure CNF and revealed that the CNF did not absorb hydrogen (Figure 2). Thus, the uptake can be fully attributed to recombination of the NaH and Al to either Na_3AlH_6 and/or $NaAlH_4$ in $NaAlH_4$-Ti/CNF.

Figure 2 also shows that the hydrogen uptake properties for $NaAlH_4$-Ti/CNF improved compared to the sample without Ti ($NaAlH_4$/CNF), as the initial absorption pressure decreased and the uptake capacity increased. These improvements can be attributed to the previously mentioned roles of the Ti in this sample, namely the catalytic role of the Ti, as well as the effect of the Ti on the NaH/Al/$NaAlH_4$ dispersions.

In ball milled $TiCl_3$-$NaAlH_4$, the crystallite size of the $NaAlH_4$/NaH/Al was considerable larger (>100 nm)[14, 18] than the crystallite sizes of $NaAlH_4$(-Ti)/CNF (≤ ~20 nm). For bulk (>100 nm) Ti-catalyzed $NaAlH_4$ samples, it is reported in the literature that the rate limiting step for hydrogen absorption is the mass transfer in the solid-state.[33, 34] Since the Ti catalyst is present in

both $NaAlH_4$-Ti/CNF and ball milled $TiCl_3$ $NaAlH_4$, it is assumed that essentially only the particle sizes of the $NaAlH_4$/NaH and Al differed. Figure 2 shows that the initial absorption for $NaAlH_4$-Ti/CNF (Ti catalyzed nano-$NaAlH_4$) proceeded at 10 bar hydrogen pressure. In contrast, the ball milled $TiCl_3$-$NaAlH_4$ (>100 nm particles) absorbed H_2 from 45 bar hydrogen pressure. Thus, the decrease in initial absorption pressure is a result of decreasing the size of the $NaAlH_4$/NaH and Al phases. This is possibly caused by reduced mass-transfer in the solid-state and therewith facilitated H_2 uptake at low hydrogen pressures.

Several independent reports in the literature claim that ball milled mixtures of $TiCl_3$, carbon and $NaAlH_4$ show sustained H_2 absorption and desorption characteristics after multiple cycles.[35-37] In our research, Table 2 shows that the hydrogen uptake capacity for $NaAlH_4$-Ti/CNF of the first absorption was higher than the second and third absorption. Thus, we did not observe a stable catalytic function of the Ti due to the presence of carbon. Moreover, the reloading capacities at 100 bar are less than that the maximum capacity of 2.5 wt% H_2 (Table 2). The incomplete reversibility might be explained by the fact that although Al domains are small (~20 nm), the NaH was largely spread over the CNF surface and, therefore, the distance between the NaH and Al becomes too large at the CNF support. The NaH and Al cannot recombine to $NaAlH_4$ or Na_3AlH_6 completely for that reason. This can be circumvented by increasing the coverage of the nano-particles on the support. Another possible solution is to change the morphology of the support material from a convex surface (for the CNF) to a concave surface. This could, possibly, restrict the migration of the NaH and Al on the surface due to confinement.

The previous part in the discussion dealt with the effect of "Ti" addition on storage properties and structural characteristics of $NaAlH_4$ in $NaAlH_4$-Ti/CNF. However, the structural properties of the "Ti" species have not been discussed so far and will be discussed on the basis of EXAFS and XPS results. The EXAFS fit reveals that 2.3 C atoms at 2.39 Å surround the Ti atom in its first coordination shell (Table 4). The Ti-C bond distance in TiC is 2.16 Å.[38] The strong deviation to the Ti-C distance of 2.39 Å in $NaAlH_4$-Ti/CNF indicates that TiC did not form. Most logically, the carbon atom originated from the CNF support, implying that the Ti species was highly dispersed on the surface of the CNF. In the next shells 2.9 Al atoms were fitted at 2.69 Å and 1.6 Al atoms at 3.09 Å. The presence of Al atoms in the local structure indicates that the $Ti(OBu)_4$ reacts to $NaAlH_4$ during the synthesis.

In the literature, Ti-Al distances in ball milled $TiCl_3$-$NaAlH_4$ range from 2.71 to 2.92 Å.[13-15, 32] The shortest distance is comparable to the distance in our fit (Table 4), whereas the largest distance deviates significantly. This deviation might be explained since the Ti-Al alloy resides on the CNF surface in $NaAlH_4$-Ti/CNF and has, consequently, different bond distances.

The next shell contains 0.7 Ti atoms at 3.63 Å, indicating that the Ti:Al ratio of the $TiAl_x$ particle is on average ~1:6.4. The total coordination number of all the closest shells around Ti is 7.5, which is considerably smaller than the coordination number of 12 in bulk materials. This suggests that the $TiAl_{6.4}$ species has a high surface to volume ratio, *i.e.*, is very small, probably below 1 nm in size.[39] The highly dispersed nature of the $TiAl_{6.4}$ catalyst was confirmed by XPS, as the Ti was detectable by XPS despite its low concentration (Table 3).

The structure of the Ti catalyst and its ability to decrease the particle size of the $NaAlH_4$ in $NaAlH_4$-Ti/CNF has been discussed in the previous parts. Now, we will elaborate on an explanation of how the "Ti" addition disperses the $NaAlH_4$ during its preparation. The first step in the preparation was the impregnation of liquid $Ti(OBu)_4$ mixed with diethylether to the CNF. Subsequent drying deposited the liquid $Ti(OBu)_4$ on the fibers. In a second impregnation, the $NaAlH_4$ was added by dissolving in THF. The liquid $Ti(OBu)_4$ re-mixed with the impregnation solution, where it reacted to $NaAlH_4$ forming a homogenously-dispersed Ti-Al alloy. This Ti-Al catalyst was insoluble and precipitated on the CNF forming finely dispersed anchoring sites on the CNF. When the impregnated material was dried, the $NaAlH_4$ could deposit on the finely dispersed anchoring sites, which increased the dispersion of $NaAlH_4$ during the preparation.

Conclusions

$Ti(OBu)_4$ catalyzed $NaAlH_4$ nanoparticles have been synthesized on CNF by impregnation and drying techniques. It was elucidated that the order of impregnation was crucial for the nature of the Ti species and the particle size of the $NaAlH_4$. In the cases where the $NaAlH_4$ was impregnated first and $Ti(OBu)_4$ second, the particle size of the $NaAlH_4$ does not change compared to a uncatalyzed nano-$NaAlH_4$ and doping reaction does not substantially occur. The temperature at maximum desorption rate decreases from above 160 °C to 132 °C and has been ascribed to the catalytic role of the Ti in that sample. The best performing sample was prepared by impregnating the $Ti(OBu)_4$ first, and $NaAlH_4$ second. Samples prepared in this way show a H_2 desorption maximum at 99 °C in Ar and absorbed hydrogen from 10 bar H_2 pressure at 115 °C after hydrogen extraction. The outstanding hydrogen sorption properties can be ascribed to two roles of the "Ti". First, "Ti" further reduces the $NaAlH_4$ particle size in the nanometer range. Secondly, the Ti species itself is a highly dispersed "$TiAl_{6.4}$" nanoparticle on the CNF that possessed catalytic activity. This nanoparticle acts as an anchoring point for the growth of Al crystallites during the desorption of $NaAlH_4$. Further improvements are envisioned if the morphology of the support surface is changed from convex to concave when the loading of the nanoparticles will be increased.

Acknowledgements

HASYLAB (I-2006-0149-EC) and NWO/ACTS (Project number, 053.61.02) are acknowledged for funding. Elena Peláez-Jiménez and Johnny van Meurs are thanked for some sample preparation. Olivier Leynaud and Paul Barnes are acknowledged for making the in-situ XRD experiments possible. Paul Radstake (Utrecht University/Shell Global Solutions) is thanked to ball milling $TiCl_3$ with $NaAlH_4$. Ad van der Eerden (Utrecht University), Dr Dariusz Zajac and Dr Adam Webb from HASYLAB are thanked for their support during Ti-edge XAFS experiments.

References

1. Schlapbach, L.; Züttel, A., *Nature* **2001,** 414, 353-358.
2. Baldé, C. P.; Hereijgers, B. P. C.; Bitter, J. H.; de Jong, K. P., *Angew. Chem. Int. Ed.* **2006,** 45, 3501-3503.
3. Baldé, C. P.; Hereijgers, B. P. C.; Bitter, J. H.; de Jong, K. P., *submitted for publication* **2007**.
4. Gutowska, A.; Li, L.; Shin, Y.; Wang, C. M.; Li, X. S.; Linehan, J. C.; Smith, R. S.; Kay, B. D.; Schmid, B.; Shaw, W.; Gutowski, M.; Autrey, T., *Angew. Chem., Int. Ed.* **2005,** 44, 3578-3582.
5. Feaver, A.; Sepehri, S.; Shamberger, P.; Stowe, A.; Autrey, T.; Cao, G., *J. Phys. Chem. B* **2007,** 111, (26), 7469 -7472.
6. de Jongh, P. E.; Wagemans, R. W. P.; Eggenhuisen, T. M.; Dauviller, B. S.; Radstake, P. B.; Meeldijk, J. D.; Geus, J. W.; de Jong, K. P., *Chem. Mater.* **2007,** 19, (24), 6052-6057
7. Vajo, J. J.; Olson, G. L., *Scr. Mater.* **2007,** 56, (10), 829-834
8. Züttel, A.; Wenger, P.; Rentsch, S.; Sudan, P.; Mauron, P.; Emmenegger, C., *J. Power Sources* **2003,** 118, 1-7.
9. Bogdanovic, B.; Schwickardi, M., *J. Alloys Compd.* **1997,** 253-254, 1-9.
10. Yao, X.; Wu, C.; Du, A.; Zou, J.; Zhu, Z.; Wang, P.; Cheng, H.; Smith, S.; Lu, G., *J. Am. Chem. Soc.* **2007,** doi:/10.1021/ja0751431.
11. Bogdanovic, B.; Felderhoff, M.; Pommerin, A.; Schüth, F.; Spielkamp, N., *Adv. Mater.* **2006,** 18, 1198-1201.
12. Jensen, C. M.; Zidan, R.; Mariels, N.; Hee, A.; Hagen, C., *Int. J. Hydrogen Energy* **1999,** 24, (5), 461-465.

13. Baldé, C. P.; Stil, H. A.; van der Eerden, A. M. J.; de Jong, K. P.; Bitter, J. H., *J. Phys. Chem. C* **2007,** 111, 2797-2802.
14. Felderhoff, M.; Klementiev, K.; Grunert, W.; Spliethoff, B.; Tesche, B.; Colbe, J.M.B.V.; Bogdanovic, B.; Hartel, M.; Pommerin, A.; Schüth, F.; Weidenthaler, C., *Phys. Chem. Chem. Phys.* **2004,** 6, 4369-4374.
15. Léon, A.; Kircher, O.; Fichtner, M.; Rothe, J.; Schild, D., *J. Phys. Chem. B* **2006,** 110, 1192-1200.
16. Graetz, J.; Reilly, J. J.; Johnson, J.; Ignatov, A. Y.; Tyson, T. A., *Appl. Phys. Lett.* **2004,** 85 (3), 500-502
17. Chaudhuri, S.; Graetz, J.; Ignatov, A.; Reilly, J. J.; Muckerman, J. T., *J. Am. Chem. Soc.* **2006,** 128, (35), 11404 - 11415.
18. Brinks, H. W.; Hauback, B. C.; Srinivasan, S. S.; Jensen, C. M., *J. Phys. Chem. B* **2005,** 109, 15780-15785.
19. Gross, K. J.; Guthrie, S.; Takara, S.; Thomas, G., *J. Alloys Compd.* **2000,** 297, 270-281.
20. van der Lee, M. K.; van Dillen, A. J.; Bitter, J. H.; de Jong, K. P., *J. Am. Chem. Soc.* **2005,** 127, (39), 13573-13582
21. Haiduc, A. G.; Stil, H. A.; Schwarz, M. A.; Paulus, P.; Geerlings, J. J. C., *J. Alloys Compd.* **2005,** 393, (1-2), 252-263.
22. Dreisbach, F.; Seif, R.; Lösch, H. W., *J. Therm. Anal. Calorim.* **2003,** 71, 73-82.
23. Lösch, H. W.; Kleinrahm, R.; Wagner, W., *Neue Magnetschwebewaagen für gravimertrische Messungen in der Verfahrentechnik.* VDI-Verlag Düsseldorf, 1994.
24. Vaarkamp, M.; Linders, J. C.; Koningsberger, D. C., *Physica B* **1995,** 208/209, 159.
25. Teo, B. K., *EXAFS: Basic Principals and data analysis*. Springer: New York, 1986.
26. CookJr., J. W.; Sayers, D. E.; E., D., *52* **1981**, 5024.
27. Zabinsky, S. I.; Rehr, J. J.; Ankudinov, A. L.; Albers, R. C.; Eller, H. J.; J., H., *Phys. Rev. B: Condens. Matter Mater. Phys. B* **1995,** 52, 2995.
28. Koningsberger, D. C.; Mojet, B. L.; Dorssen, G. E. v.; Ramaker, D. E.; E., D., *Topics in Catalysis* **2000,** 10, ((3-4)), 143-155.
29. Jacques, S. D. M.; Leynaud, O.; Strusevich, D.; Beale, A. M.; Sankar, G.; Martin, C. M.; Barnes, P., *Angew. Chem. Int. Ed.* **2006,** 45, 445-448.
30. Bogdanovic, B.; Brand, R. A.; Marjanovic, A.; Schwickardi, M.; Tolle, J., *J. Alloys Compd.* **2000,** 302, 36-58.
31. Singh, S.; Eijt, S. W. H.; Huot, J.; Kockelmann, W.; Wagemaker, M.; Mulder, F. M., *Acta Mater.* **2007,** 55, 5549-5557.

32. Baldé, C. P.; van der Eerden, A. M. J.; Stil, H. A.; de Groot, F. M. F.; de Jong, K. P.; Bitter, J. H., *J. Alloys Compd.* **2007,** 446-447, 232-236.
33. Kiyobayashi, T.; Srinivasan, S. S.; Sun, D.; Jensen, C. M., *J. Phys. Chem. A* **2003,** 107, 7671-7674.
34. Von Colbe, J. M. B.; Schmidt, W.; Felderhoff, M.; Bogdanovic, B.; Schüth, F., *Angew. Chem. Int. Ed.* **2006,** 45, (22), 3663-3665.
35. Wang, J.; Ebner, A. D.; Prozorova, T.; Zidan, R.; Ritter, J. A., *J. Alloys Compd.* **2006,** 395, (1-2), 252-262.
36. Dehouche, Z.; Lafi, L.; Grimard, N.; Goyette, J.; Chahine, R., *Nanotechnology* **2005,** 16, (4), 402-409.
37. Pukazhselvan, D.; Gupta, B. K.; Srivastava, A.; Srivastava, O. N., **2005,** 403, (1-2), 312-317.
38. Ehrlich, P., *Zeitschrift fuer Anorganische und Allgemeine Chemie* **1949,** 259, 1-41.
39. Jentys, A., *Phys. Chem. Chem. Phys.* **1999,** 1, 4059 - 4063.

4

Active Ti Species in $TiCl_3$-Doped $NaAlH_4$

Mechanism for Catalyst Deactivation

Abstract

The nature of the active Ti species in $TiCl_3$-catalyzed $NaAlH_4$, a promising hydrogen storage material, was studied as a function of the desorption temperature with Ti K-edge extended X-ray absorption fine structure (EXAFS) spectroscopy, Ti K-edge X-ray absorption near-edge structure (XANES) spectroscopy, and X-ray diffraction (XRD). In the freshly prepared sample, Ti was amorphous and surrounded by 4.8 Al atoms divided between two shells at 2.71 and 2.89 Å. In the next shell, 1.9 Ti atoms were detected at 3.52 Å. It was concluded that 30% of Ti was incorporated into the surface of Al crystallites and 70% of Ti occupied interstitials in the $NaAlH_4$ lattice, possibly forming trimeric, triangular Ti entities. After hydrogen desorption at 125 °C, $NaAlH_4$ decomposed and the Ti-Al coordination number increased from 4.8 to 8.5. We propose that all Ti is incorporated into the surface layer of the formed Al. After the material was heated to 225 °C, the local structure of Ti, as inferred from EXAFS and XANES spectroscopy, was identical to the local structure of a $TiAl_3$ alloy. However, the formed alloy was amorphous and was only detected in XRD by an increase of the background intensity around the Al diffraction. These so-called "$TiAl_3$ clusters" agglomerated in the heat treatment to 475 °C, forming crystalline $TiAl_3$. Earlier work has shown that increasing the desorption temperature of $NaAlH_4$ lowers the absorption rate and capacity of hydrogen in the next step. Thus, by comparing our results with absorption properties published in the literature on similar samples, we could rank the activity of the Ti for hydrogen absorption as "Ti in the Al surface" > "$TiAl_3$ cluster" > "crystalline $TiAl_3$", therewith indicating that Ti incorporated into the surface of Al is the most active for the absorption of hydrogen.

Introduction

In the future new sustainable energy sources and carriers will be needed. Hydrogen is attractive as an energy carrier since it has a high energy to mass ratio and produces water as its only waste product.[1,2] Conventional storage technologies, such as gas compression or cryogenic liquid, have limitations related to safety aspects and low volumetric hydrogen densities.[2,3] Storing hydrogen by chemical bonding or physisorption may circumvent these problems. Several storage media are considered, *e.g.* nanosized magnesium hydride,[4] physisorption on carbon,[5,6] and sodium alanate (NaAlH4).[2,7] Sodium alanate is promising since its thermodynamic properties enable reversible storage of hydrogen at low temperatures for on-board applications. Hydrogen is desorbed in three steps (eqs 1-3) with respective equilibrium temperatures of 30, 110, and >400 °C at 1 bar of hydrogen pressure. The first two desorption temperatures are compatible with on-board storage and deliver a total of 5.6 wt % hydrogen storage capacity.

$$NaAlH_4 \leftrightarrow \tfrac{1}{3}\, Na_3AlH_6 + \tfrac{2}{3}\, Al + H_2 \qquad (1)$$

$$Na_3AlH_6 \leftrightarrow 3\, NaH + Al + 1\tfrac{1}{2}\, H_2 \qquad (2)$$

$$NaH \leftrightarrow Na + \tfrac{1}{2}\, H_2 \qquad (3)$$

The main hurdle to overcome for applying $NaAlH_4$ as a hydrogen storage material is the slow kinetics for hydrogen desorption and absorption. These unfavorable desorption and absorption rates can be improved by reducing the particle size of the $NaAlH_4$ to the nanometer range[8] or by adding a catalyst, for example, $TiCl_3$ or titanium butoxide, to the alanate.[7,9,10] Generally, the most active catalyst is prepared by ball milling $NaAlH_4$ with the $TiCl_3$,[10] resulting in a reaction to form NaCl, Al, and a reduced Ti entity as shown in reaction 4.[11]

$$TiCl_3 + 3\, NaAlH_4 \rightarrow \text{“Ti”} + 3\, Al + 3\, NaCl + 6\, H_2 \qquad (4)$$

The correlation among the catalytic role, structure, and location of the Ti for (de)hydriding catalysis is not fully understood, although it has been the subject of many investigations in the past years.[12-28] A H_2/D_2 scrambling study performed by Schüth *et al.* points out that the Ti after preparation dissociates hydrogen at room temperature, suggesting that one of the roles of the Ti catalyst might be to split hydrogen.[12] Alternatively, it is suggested that Ti facilitates migration of H via interstitials[13] or facilitates migration of metal atoms in the form of AlH_3 units.[14,15] It has also been reported that the Ti does not solely change the kinetics, but also alters the thermodynamics

of the Ti-catalyzed $NaAlH_4$ system.[16] The structure and catalytic cycle of the active Ti species for these functions have not been identified in these studies.

A variety of Ti species have been proposed or calculated to be catalytically active. Some authors claim that Ti alloys with Al as an amorphous species when $TiCl_3$ reacts to $NaAlH_4$,[9,17-19] while others observed the formation of metallic Ti clusters.[20] Jensen *et al.* claim on the basis of an IR spectroscopy study that Ti is located in the vicinity of the AlH_4^- unit and influences the Al-H asymmetric stretching frequency.[21] Some DFT calculations show that Ti preferably substitutes Na sites[14,22,23] or occupies interstitial positions in the $NaAlH_4$ lattice.[24] Contrarily, Løvvik and Opalka claim that Ti primarily moves to interfaces between Al and $NaAlH_4$, grain boundaries, or to defects in the $NaAlH_4$ particles.[25] Alternatively, it is also reported that Ti on an Al surface might be the active Ti entity.[26-28]

Geerlings *et al.* showed that the rate of hydrogen reloading decreases with increasing temperature of the preceding hydrogen desorption step.[9] Thus, by comparing the Ti species in the samples after different desorption temperatures, more information might be obtained on the nature of the (in)active Ti species. Ti was mostly present as an amorphous phase, making analysis challenging with a single technique. Therefore, the structure of Ti-containing $NaAlH_4$ was characterized using extended X-ray absorption fine structure (EXAFS) spectroscopy, X-ray absorption near-edge structure (XANES) spectroscopy, and X-ray diffraction (XRD) in this paper. A structure-activity relationship is proposed on the basis of the derived structure of Ti.

Experimental

Sample Preparations

All sample preparations were performed under a nitrogen or argon atmosphere in a glovebox equipped with a circulation purifier. Chemical operations were conducted using Schlenk techniques. To prevent hydrogen desorption and possible changes in the samples, transportation and storage were performed at 5 °C or below under an inert atmosphere. Commercially available $NaAlH_4$ (tech. 90%, Sigma-Aldrich) was purified and ball-milled with 10 mol % $TiCl_3$ by the authors of ref 9 as described before. This sample is referred to as "SAH-start". This sample was split into three parts; the respective parts were heated in Ar to 125, 225, and 475 °C with a ramp of 5 °C.min^{-1}. The samples were kept at the final temperature until no detectable hydrogen desorption was recorded by volumetric analysis. The samples are called "SAH-125", "SAH-225", and "SAH-475", respectively. The XRD diffraction patterns, curves of the first desorption step, and hydrogen storage capacities are identical to those reported in a previous paper.[9]

EXAFS Spectroscopy

X-ray absorption spectroscopy was performed on the Ti K-edge at station E4 of the DESY synchrotron (Hamburg, Germany). The storage ring was operated at 4.4 GeV with a mean current of 120 mA, using a Si(111) double-crystal monochromator that was detuned to 80% to suppress higher harmonics. Measurements were performed at 77 K in flowing He to exclude thermal decomposition of the sample. The samples (11 mg of Ti-catalyzed $NaAlH_4$ or 6 mg of $TiAl_3$) had a total absorption of 2.55 and were homogeneously diluted with 50 mg of BN, pressed into a pellet, mounted to the cell, and transferred to the beamline in a closed cell.

Extraction of the EXAFS data from the measured absorption data was performed with the XDAP program.[29] Three scans were averaged and the pre-edge background was approximated by a Victoreen function before subtraction.[30] The position of the edge energy was determined at the maximum of the first derivative of the spectrum and was calibrated using a Ti foil as a reference in each scan. The spectrum was background corrected by employing a cubic spline routine.[31] Normalization was performed by dividing the absorption spectrum by the height of the background 50 eV from the edge. The Ti-Al backscattering amplitude and phase shift were calculated using the FEFF 8.2 code[32] and calibrated using an experimentally measured spectrum of $TiAl_3$ at 77 K. EXAFS spectroscopy of a Ti foil at room temperature was used to calibrate the Ti-Ti calculated reference. The FEFF input parameters for the references are listed in Table 1.

Experimental data were fitted in k^2 using the difference file technique in R space[33] at $3 < k$ (Å^{-1}) < 10 or $3 < k$ (Å^{-1}) < 12 depending on the quality of the data. The quality of the fit was checked by applying k^1, k^2, and k^3 weightings, ensuring that the correct coordination number and Debye-Waller factor (σ^2) were fitted.[33] Errors in the numerical values obtained by EXAFS data analysis are estimated to be 10% in the coordination number (N), 1% in the distance (R), 5% in the Debye-Waller factor (σ^2), and 10% for inner potential correction (E_0).[34]

Table 1. Input parameters to create FEFF calculated Ti-Al and Ti-Ti references.

Absorber - Backscatterer	Reference compound	S_0^2	σ^2 / 10^{-3} Å^{-2}	V_r / eV	V_i / eV	Potential
Ti-Al	$TiAl_3$	0.72	1.5	11.3	1.0	Hedin-Lunqvist
Ti-Ti	*h.c.p.* Ti foil	0.60	0	8.6	1.0	Hedin-Lunqvist

XANES Spectroscopy

XANES spectra were recorded from 4950 to 5050 eV with a step size of 0.3 eV. The position of the edge was set at the maximum of the first derivative (inflection point) of the first rising edge. The spectra were normalized to 5020 eV.

XRD

X-ray diffraction patterns were recorded on a Panalytical X'pert Pro system using Cu K_α radiation. Samples were transferred to the instrument in airtight sample holders. The data were collected in the range 2θ 15-85° with a step size of 0.033°. Qualitative analysis was done by comparison with entries from the ICDD PDF22000 database.

Results

To confirm that our samples were identical to those described in ref 9, an XRD study was carried out. Figure 1 shows the XRD pattern of the materials after they were heated to different temperatures. Different phases were identified ($NaAlH_4$, Na_3AlH_6, Al, Na, NaCl, NaH, $TiAl_3$) and are indicated in the figure. In SAH-start, $NaAlH_4$, NaCl, and Al were detected. The latter two phases were expected on the basis of reaction (eq 4). After the material was heated to 125 °C, the diffraction lines representing $NaAlH_4$ disappeared (Figure 1, SAH-125), while those of NaCl, NaH, Al, and Na_3AlH_6 were present. This is in line with the desorption reactions shown in eqs 1 and 2. In SAH-225 only diffractions from NaH, Al, and NaCl were present, indicating that all hydrogen relating to reactions 1 and 2 was desorbed. After the hydrogen was desorbed at 475 °C, Al, Na, NaCl, NaH, and $TiAl_3$ were observed. The presence of Na indicates that at this high temperature NaH was partly dehydrogenated.

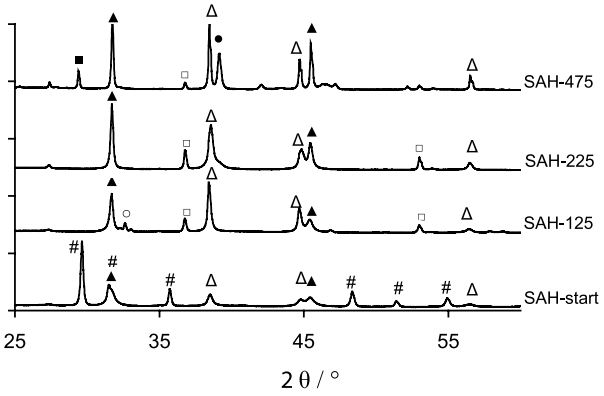

Figure 1. XRD patterns of SAH-start, SAH-125, SAH-225 and SAH-475. # = $NaAlH_4$, Δ = Al, ▲ = NaCl, □ = NaH, ○ = Na_3AlH_6, ■ = Na, ● = $TiAl_3$.

Titanium was only detectable as a crystalline $TiAl_3$ phase in SAH-475. Amorphous Ti species have been claimed to be indirectly visible in XRD via the Al diffraction peaks.[9,18,19] Therefore, the diffraction peak of Al metal is shown in detail in Figure 2. An increase of the background was observed for 2θ = 38.7-39.5° after the sample was heated to 225 °C (SAH-225), indicating the presence of an amorphous phase. In contrast, the materials after ball milling (SAH-start) and after desorption at 125 °C (SAH-125) and 475 °C (SAH-475) did not show this increase in background intensity.

To get more insight regarding the structure of the amorphous Ti, the local structure of Ti was investigated with EXAFS spectroscopy. The background-subtracted EXAFS data, $\chi(k)$, of SAH-Start, SAH-125, SAH-225, and SAH-475 are shown in Figure 3. It can be seen that the quality of the data was good. The k^1-weighted Fourier-transformed data are shown in Figure 4 (top panel, magnitude; lower panel, imaginary part). From the changes in the magnitude and the positions of the nodes in the imaginary part it can be concluded that the local environment around Ti changed significantly with the desorption temperature. The fitted and raw data for SAH-start are shown in Figure 5.

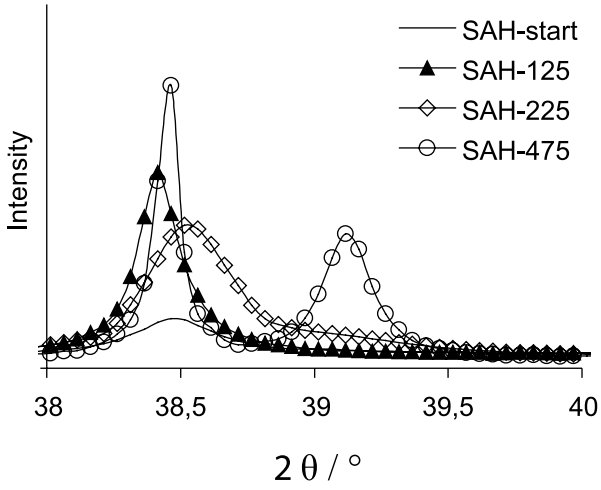

Figure 2. XRD Al-diffraction lines for SAH-start, SAH-125, SAH-225 and SAH-475.

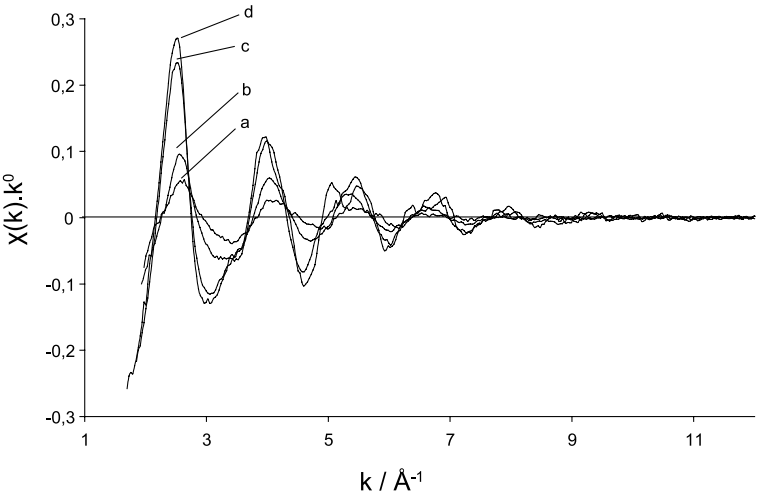

Figure 3. k^0 weighted background subtracted $\chi(k)$ of: a) SAH-start, b) SAH-125, c) SAH-225 and d) SAH-475.

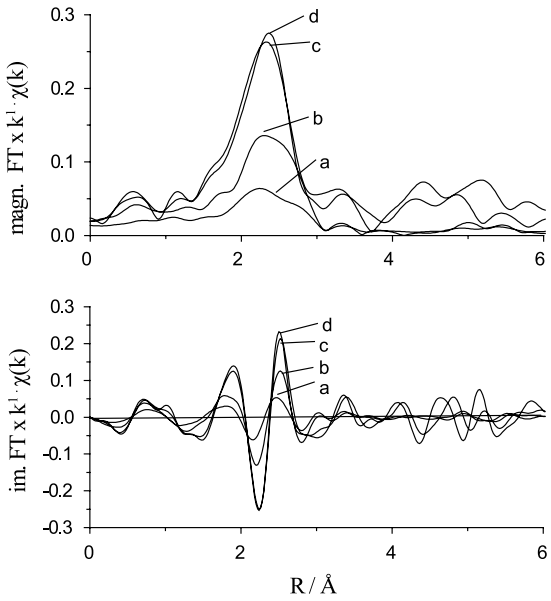

Figure 4. Magnitude and imaginary part of Fourier Transformed $\chi(k)$:

a) SAH-start, b) SAH-125, c) SAH-225 and d) SAH-475. (k^1 ; Δk; 3-12 Å^{-1}).

Table 2 shows the fit parameters and k^2 variances of SAH-start, SAH-125, SAH-225, SAH-475, and the reference $TiAl_3$. The k^2 variances were low and in the same range, indicating that the fits were of comparable quality. For all measured samples, Al always surrounded Ti in the first two coordination shells. In the third shell, Ti was found at a longer distance. The fit for $TiAl_3$ exactly matches the known crystallographic data[35] of this sample; *i.e.*, Al is distributed in two shells located at 2.73 and 2.88 Å with, respectively, four and eight Al atoms (please note that the first Ti-Al shell was used to calibrate the Ti-Al reference), and four Ti atoms were detected at 3.89 Å. Taking into account the 10% error of the coordination number and the 1% error in distance,[34] the local environment of Ti in SAH-475 and SAH-225 was identical to that of Ti in the reference sample $TiAl_3$.

In contrast, the local structure of SAH-125 comprised in total 8.5 Al atoms in its first and second Al shells, 3.9 Al at 2.76 Å and 4.6 Al atoms at 2.92 Å. Thus, the total coordination number of the Al sphere (8.5) was significantly lower than in $TiAl_3$, in which 12 Al atoms surround Ti. In addition, the Ti-Ti distance in SAH-125 was 3.49 Å, which is significantly shorter than the Ti-Ti distance of 3.89 Å in $TiAl_3$. For the sample prior to hydrogen desorption (SAH-start), 2.3 Al atoms at 2.71 Å and 2.5 Al atoms at 2.89 Å surrounded Ti in the first coordination sphere. The next sphere contained 1.9 Ti atoms at 3.49 Å, which was approximately the same as in SAH-125.

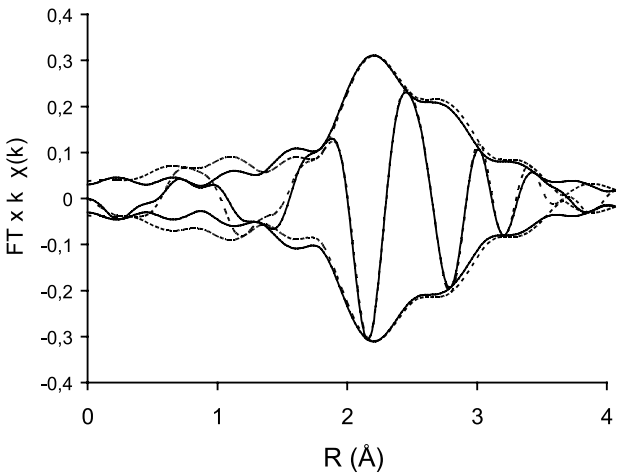

Figure 5. k^2 weighted phase uncorrected Fourier Transform of SAH-start (solid line) and fit (Δk; 3-12 $Å^{-1}$; ΔR; 1.2-3.5 Å) (dashed line).

Table 2. EXAFS fits of SAH-start, SAH-125, SAH-225 and SAH-475.

Name	Shell	Atom	*N*	$\Delta\sigma^2$ / 10^{-3} Å^{-2}	*R* / Å	*Eo* / eV	k^2 –variance	
							Im.	Abs.
SAH-start	1	Ti-Al	2.3	0.04	2.71	-0.96	0.63	0.40
	2	Ti-Al	2.5	0.18	2.89	0.96		
	3	Ti-Ti	1.9	0.81	3.52	1.93		
SAH-125	1	Ti-Al	3.9	0.20	2.76	-1.19	0.90	0.44
	2	Ti-Al	4.6	0.20	2.92	0.23		
	3	Ti-Ti	1.3	2.70	3.49	4.30		
SAH-225	1	Ti-Al	4.6	0.10	2.73	1.53	0.36	0.23
	2	Ti-Al	7.8	0.82	2.84	4.97		
	3	Ti-Ti	3.8	6.36	3.90	4.31		
SAH-475	1	Ti-Al	4.2	0.36	2.75	3.11	0.43	0.27
	2	Ti-Al	8.3	1.95	2.89	3.70		
	3	Ti-Ti	3.8	3.25	3.84	5.44		
$TiAl_3$	1	Ti-Al	4.0	0.00	2.73	-0.47	2.13	1.00
	2	Ti-Al	8.0	1.53	2.88	4.12		
	3	Ti-Ti	4.0	4.83	3.89	1.85		

Number of independent parameters (Nyquist theorem) was 17 and the data was fitted with 12 parameters.[39]

XANES spectra of SAH-start, SAH-125, SAH-225, SAH-475, and $TiAl_3$ are shown in Figure 6. It is observed that the XANES spectra of TiAl3, SAH-475, and SAH-225 are identical. In contrast, the XANES spectra of SAH-start and SAH-125 show similar characteristics and differed from that of $TiAl_3$. The positions of the absorption edge for the measured samples are listed in Table 3 and were between those of Ti-foil and $TiAl_3$.

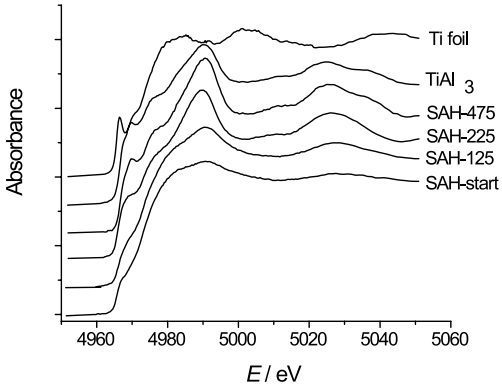

Figure 6. XANES of SAH-start, SAH-125, SAH-225, SAH-475 and $TiAl_3$.

Table 3. Positions of Ti-edges in SAH-start, SAH-125, SAH-225, SAH-475, $TiAl_3$ and Ti-foil.

	Edge position (eV)
SAH-start	4965.7
SAH-125	4965.7
SAH-225	4966.1
SAH-475	4966.7
$TiAl_3$	4966.7
Ti foil	4965.5

Discussion

Structure of Ti as a Function of the Desorption Temperature

The position of the Ti absorption edge is affected by the oxidation state of Ti. When the formal oxidation state of Ti was zero, for instance, in Ti metal and $TiAl_3$, the edge positions were, respectively, at 4965.5 and 4966.7 eV (Table 3). After preparation (SAH-start), the position of the Ti edge was at 4965.7 eV, which was between that of $TiAl_3$ and Ti (Figure 6 and Table 3). Thus, Ti had a (close to) zero oxidation state after preparation, which is in agreement with the reaction 4. Linear analysis methods did not indicate substantial (>10%) oxidation of the Ti. The XANES features of SAH-start and $TiAl_3$ were different, indicating a different geometry and/or electronic state for Ti in SAH-start compared to $TiAl_3$. The structural differences were further revealed by EXAFS spectroscopy. In SAH-start (Table 2) Ti was surrounded by on average 2.3 and 2.5 Al atoms at 2.71 and 2.89 Å in the two closest coordination shells. This is significantly lower than the Ti-Al coordination number in $TiAl_3$, which was 4 in the first shell and 8 in the second (Table 2 and ref 35). The structure of the subcoordinated Ti species in SAH-start will be discussed now.

XRD (Figure 1) shows that in SAH-start $NaAlH_4$, Al, and NaCl are present as crystalline materials. Since Ti is inert toward NaCl, Ti must have interacted with either Al or $NaAlH_4$ or formed a separate Ti phase. Since fitting of one or both of the first shells with Ti-Ti scattering (not shown) did not result in satisfactory fits, it was concluded that no measurable concentration of Ti clusters was formed during the preparation. Thus, Ti must have interacted with Al or $NaAlH_4$. When Ti interacts with $NaAlH_4$, it has been reported that Ti can substitute for Na[14,22,23] or occupies an interstitial position among three AlH_4^- units.[24] In the case that Ti substitutes for Na, the resulting Al-Ti distance would be approximately 3.5 Å, which is a distance that was not observed for Ti-Al scattering in our EXAFS analysis (Table 2). Therefore, we conclude that the Ti did not substitute for Na to a measurable extent. When Ti is interstitial in the $NaAlH_4$ lattice, the DFT-calculated Ti-Al distance is approximately 2.6 Å.[24] This distance is, within the error limits of the calculation, similar to that was found in our EXAFS analysis, hence interstitial Ti in $NaAlH_4$ is a reasonable suggestion for a phase present in SAH-start. Three aluminum atoms surrounded the Ti in this species; thus, assuming that all Ti is interstitial, the Ti-Al coordination number should be 3. Since the observed Ti-Al coordination number is 4.8 (Table 2), Ti must also be present in another phase as well with a higher coordination number. Two other locations for the Ti can be envisioned, *i.e.*, on/in the Al phase or as a Ti-Al alloy. XRD (Figures 1 and 2) did not indicate that Ti formed a crystalline phase with Al; thus, bulk alloying did not occur to a large extent. Chaudhuri *et al.* have calculated that a Ti capped by H atoms and incorporated into the Al surface is stable.[26]

When Ti is incorporated into the surface of Al metal, the Ti-Al distance is expected to be in the range of 2.7-2.9 Å.[26] These values agree with those found in our EXAFS analysis (Table 2); therefore, we propose that part of the Ti is located at the Al surface. When the Ti is incorporated into a surface, the close-packed fcc structure of Al metal is 9 Al atoms around the Ti. On the basis of the use of fractional coordination numbers, it can be calculated that 30% of the Ti resided in the Al surface with a coordination number of 9 and 70% was located in an interstitial place in $NaAlH_4$ with a coordination number of 3 ((0.7 x 3) + (0.3 x 9) = 4.8).

The structure of the interstitial Ti during the preparation is schematically represented in Scheme 1. Scheme 1a shows the $NaAlH_4$ lattice; after ball milling $TiCl_3$ reacts with $NaAlH_4$, forming NaCl and Al metal (eq 4). The formed NaCl and Al are excluded from the picture to clarify the Ti occupying an interstitial site in the $NaAlH_4$ lattice (Scheme 1b). EXAFS analysis of SAH-start (Table 2) also shows that a Ti-Ti distance at 3.52 Å was present. This Ti-Ti distance does not appear in Ti metal, any titanium hydride phase, or Ti-Al alloy. In $TiCl_3$, the Ti-Ti distance is 3.53 Å.[36] However, if the $TiCl_3$ is present, Ti-Cl bonds at 2.46 Å must be detected too. Attempts to fit this distance with an FEFF 8.2 calculated Ti-Cl reference were not successful. Moreover, an XPS depth profiling study indicates that the $TiCl_3$ is completely reduced after 30 min of ball milling,[37] whereas the samples investigated in the current study were milled for 1 h. Thus, $TiCl_3$ was most likely not present in SAH-start. The distance between two interstitial spaces in an unperturbed $NaAlH_4$ lattice is 3.7 Å. Thus, we hypothesize that the Ti-Ti distance found in

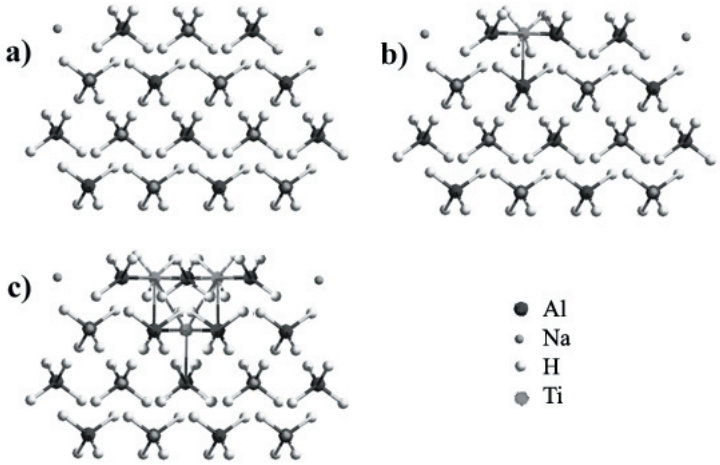

Scheme 1. a) Structure of $NaAlH_4$ *(1 1 0)*, b) interstitial Ti in $NaAlH_4$, c) two Ti atoms added to adjacent interstitial positions forming a trimeric triangular entity.

EXAFS analysis originated from Ti atoms occupying adjacent interstitial spaces in the $NaAlH_4$ lattice. The observed coordination number of Ti-Ti is 1.9; thus, a trimeric triangular Ti species occupying three neighboring interstitials is proposed to explain these observations (Scheme 1c). The deviation between interstitial distances in $NaAlH_4$ (3.7 Å) and the interstitial Ti-Ti distance (3.5 Å) found in EXAFS analysis is possibly due to the fact that the presence of Ti atoms in adjacent interstitial spaces distorts the local structure.

The evolution of the Ti species was further investigated after hydrogen desorption at different temperatures. After desorption at 125 °C, the XRD pattern of SAH-125 revealed that NaH, Al, Na_3AlH_6, and NaCl were present (Figure 1), indicating that $NaAlH_4$ was completely converted. In the starting material (SAH-start), 70% of Ti was present in $NaAlH_4$ interstitials; thus, the local structure of Ti must have been changed during desorption since $NaAlH_4$ was absent in SAH-125. In the EXAFS fits (Table 2) the total coordination number of the first two Ti-Al shells increased from 4.8 to 8.5 (SAH-start to SAH-125). The Ti-Al coordination of 8.5 in SAH-125 is very close to the coordination number when Ti is substituted in the Al(111) surface, in which Ti has 9 Al atoms in its coordination sphere (see Scheme 2a). The aluminum was present in two shells around Ti, at distances of 2.76 and 2.92 Å. In an ideal fcc lattice, the Ti is only surrounded by a single Ti-Al shell. This indicates that the local structure was probably distorted with respect to the ideal fcc geometry. Thus, we conclude that the majority of the Ti was present at the Al surface having a distorted local structure after desorption at 125 °C, which is schematically shown in Scheme 2a.

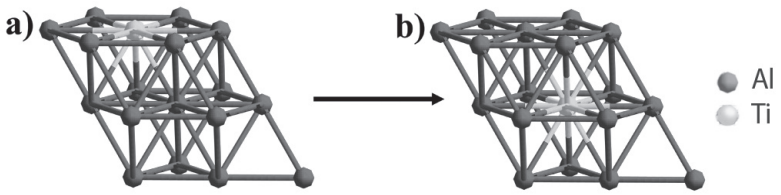

Scheme 2. a) View parallel to the *(111)* Al surface (dark) with Ti (bright) incorporated in the surface having a distorted local structure; the Ti in SAH-125 displayed predominantly this structure. b) View parallel to (111) Al surface of Ti that migrated from the surface into the bulk, forming a $TiAl_3$-cluster; this resembles the composition of SAH-225.

The local structure of Ti in SAH-125 revealed a Ti at 3.49 Å (Table 2), whereas a Ti atom at 3.8 Å would be expected on the basis of the structure of $TiAl_3$.[35] This led us to the speculation that a distorted surface Ti-Al species was formed, leading to a Ti atom in a contracted third shell.

When the hydrogen was desorbed at 225 °C, it was found that the local structures of SAH-225 and $TiAl_3$ were the same within the sensitivity of EXAFS spectroscopy (Table 2). This was also confirmed by XANES spectroscopy (Figure 6), which showed a high similarity of the spectra SAH-225 and $TiAl_3$. The diffraction line of crystalline $TiAl_3$ was not detected in XRD (Figure 1), but the magnification of the Al diffraction (Figure 2) shows that the background was increased from $2\theta = 38.7°$ to $2\theta = 39.5°$. This indicates that an amorphous Ti-Al alloy is formed and has been explained by the presence of an intermetallic $TiAl_x$ species by Geerlings *et al.*[9] Thus, the local structure of Ti was identical to the local structure of $TiAl_3$, and we suggest that $TiAl_3$ clusters were formed at 225 °C. Thus, between 125 and 225 °C, Ti had migrated from the Al surface to the bulk of aluminium, which is visualized in Scheme 2.

When the desorption temperature was 475 °C, the local structure around Ti did not change significantly compared to that after desorption at 225 °C, as seen in Table 2. However, XRD showed that a crystalline $TiAl_3$ alloy was formed at this temperature (Figure 2). Thus, the $TiAl_3$ clusters in SAH-225 had agglomerated to a crystalline $TiAl_3$ phase on going from 225 to 475 °C.

Catalyst Deactivation.

The XRD study reproduced the results of Geerlings *et al.* (ref 9), indicating that the current samples are identical to the ones used before. Their research indicated that the hydriding activity decreased with an increasing desorption temperature in the preceding step. The activity of the Ti catalyst increased thus in the order SAH-125 > SAH-225 > SAH-475. In the most active sample (SAH-125), it was concluded in the preceding chapter that the majority of Ti was incorporated into the Al surface having a distorted local structure. Thus, we propose that this is the most active form of Ti in the Ti-catalyzed $NaAlH_4$. The Ti catalyst deactivated as the Ti migrated into the Al metal, which occurred between 125 and 225 °C (Scheme 2). The deactivation continued when the $TiAl_3$ clusters agglomerated, forming crystalline $TiAl_3$, which occurred between 225 and 475 °C. This decreases the dispersion of the Ti catalyst, probably resulting in an impaired accessibility of the Ti catalyst. Thus, the activity of the Ti catalyst can be summarized in the following sequence:

$$Ti \text{ in the Al surface} > TiAl_3 \text{ cluster} > \text{crystalline } TiAl_3$$

Conclusion

In $NaAlH_4$ ball milled with $TiCl_3$, the majority (70%) of Ti occupied interstitial spaces in the $NaAlH_4$ lattice. The remaining Ti was present at the surface of Al. After desorption at 125 °C the majority of Ti was present at the Al surface having a distorted local structure, which appeared to be the most active Ti species for hydriding catalysis of a desorbed $NaAlH_4$. At 225 °C, Ti migrated from the Al surface to the bulk, forming amorphous $TiAl_3$ clusters. This surface to bulk migration of the Ti atoms was accompanied by a deactivation of the catalyst. Subsequently, the $TiAl_3$ clusters agglomerated during the heat treatment to 475 °C to crystalline $TiAl_3$, leading to a lower dispersion of the Ti catalyst and consequently a lower hydriding activity.

Acknowledgments

This work was financially supported by ACTS, Project Number 053.61.02, and HASYLAB, Project Number I-05-062 EC. We thank Dr. Peter Paulus and Hans Stil (Shell Research and Technology Centre) for the XRD measurements and sample preparation. Ad van der Eerden is thanked for assistance during the EXAFS measurements. We also thank Dr. Konstantin Klementiev from HASYLAB for providing $TiAl_3$. Dr. Andy Beale and Prof. Dr. Diek Koningsberger from Utrecht University are thanked for useful discussions regarding EXAFS analysis.

References

1. Grant, P. *Nature* **2003**, *424*, 129-130.
2. Schlapbach, L.; Züttel, A. *Nature* **2001**, *414*, 353-358.
3. Schüth, F. *Nature* **2005**, *434*, 712-713.
4. Wagemans, R. W .P.; Van Lenthe, J. H.; De Jongh, P. E.; Van Dillen, A. J.; De Jong, K. P. *J. Am. Chem. Soc.* **2005**, *127* (47), 16675-16680.
5. Nijkamp, M. G.; Raaymakers, J. E. M. J.; Van Dillen, A. J.; De Jong, K. P. *Appl. Phys. A: Mater. Sci. Process.* **2001**, *72* (5), 619-623.
6. Weitkamp, J.; Fritz, M.; Ernst, S. *Int. J. Hydrogen Energy* **1995**, *20*, 967-970.
7. Bogdanovic, B.; Schwickardi, M. *J. Alloys Compd.* **1997**, *253-254*, 1-9.
8. Baldé, C. P.; Hereijgers, B. P. C.; Bitter, J. H.; De Jong, K. P. *Angew. Chem., Int. Ed.* **2006**, *45* (21), 3501-3503.

9. Haiduc, A. G.; Stil, H. A.; Schwarz, M. A.; Paulus, P.; Geerlings, J. J. C. *J. Alloys Compd.* **2005**, *393* (1-2), 252-263.
10. Jensen, C. M.; Zidan, R. A.; Mariels, N.; Hee, A. G.; Hagen, C. *Int. J. Hydrogen Energy* **1999**, *24*, 461.
11. Bellosta von Colbe, J. M.; Bogdanovic, B.; Felderhof M.; Pommerin, A.; Schuth, F. *J. Alloys Compd.* **2004**, *370*, 104-109.
12. Bellosta Von Colbe, J. M.; Schmidt, W.; Felderhoff, M.; Bogdanovic, B.; Schu¨th, F. *Angew. Chem., Int. Ed.* **2006**, *45* (22), 3663-3665.
13. Palumbo, O.; Paolone, A.; Cantelli, R.; Jensen, C. M.; Sulic, M. *J. Phys. Chem. B* **2006**, *110*, 9105-9111.
14. Moyse´s Arau´jo, C.; Li, S.; Ahuja, R.; Jena, P. *Phys. Rev. B: Condens. Matter Mater. Phys.* **2005**, *72*, 165101.
15. Fu, Q. J.; Ramirez-Cuesta, A. J.; Tsang, S. H. *J. Phys. Chem. B***2006**, *110*, 711-715.
16. Streukens, G.; Bogdanovic, B.; Felderhof, M.; Schüth, F. *Phys. Chem. Chem. Phys.* **2006**, *8*, 2889-2892.
17. Felderhoff, M.; Klementiev, K.; Grunert, W.; Spliethoff, B.; Tesche, B.; Bellosta Von Colbe, J. M.; Bogdanovic, B.; Hartel, M.; Pommerin, A.; Schüth, F.; Weidenthaler, C. *Phys. Chem. Chem. Phys.* **2004**, *6*, 4369-4374.
18. Bogdanovic, B.; Felderhof, M.; Germann, M.; Pommerin, A.; Schüth, F.; Weidentaler, C.; Zibrowius, B. *J. Alloys Compd.* **2003**, *350*, 246-255.
19. Brinks, H. W.; Jensen, C. M.; Srinivasan, S. S.; Hauback, D. C.; Blanchard, D.; Murphy, K. *J. Alloys Compd.* **2004**, *376*, 215.
20. Léon, A.; Kircher, O.; Fichtner, M.; Rothe, J.; Schild, D. *J. Phys. Chem. B* **2006**, *110*, 1192-1200.
21. Gomes, S.; Renaudin, G.; Hagemann, H.; Yvon, K.; Sulic, M.; Jensen, C. M. *J. Alloys Compd.* **2005**, *390*, 305.
22. Arau´jo, C. M.; Ahuja, R.; Guille´n, J. M. O.; Jena, P. *Appl. Phys.Lett.* **2005**, *86*, 251913
23. Iniguez, J.; Yildirim, T.; Udovic, T. J.; Sulic, M.; Jensen, C. M. *Phys. Rev. B: Condens. Matter Mater. Phys.* **2004**, *70*, 060101(R).
24. Liu, J.; Ge, Q. *Chem. Commun.* **2006**, 1822-1824.
25. Løvvik, O. M.; Opalka, S. M. *Appl. Phys. Lett.* **2006**, *88*, 161917.
26. Chaudhuri, S.; Muckerman, J. T. *J. Phys. Chem. B* **2005**, *109* (15), 6952-6957.

27. Løvvik, O. M.; Opalka, S. A. *Phys. Rev. B: Condens. Matter Mater. Phys.* **2005**, *71* (5), 054103.
28. Graetz, J.; Reilly, J. J.; Johnson, J.; Ignatov, A. Y.; Tyson, T. A. *Appl. Phys. Lett.* **2004**, *85* (3), 500-502.
29. Vaarkamp, M.; Linders, J. C.; Koningsberger, D. C. *Physica B* **1995**, *208/209*, 159.
30. Teo, B. K. *EXAFS: Basic Principals and data analysis*; Springer: New York, 1986.
31. Cook J. W., Jr.; Sayers, D. E. *J. Appl. Phys.* **1981**, *52*, 5024.
32. Zabinsky, S. I.; Rehr, J. J.; Ankudinov, A. L.; Albers, R. C.; Eller, H. J. *Phys. Rev. B: Condens. Matter Mater. Phys.* **1995**, *52*, 2995.
33. Koningsberger, D. C.; Mojet, B. L.; Van Dorssen, G. E.; Ramaker, D. E. *Top. Catal.* **2000**, *10* (3-4), 143-155.
34. Li, G. G.; Bridges, F.; Booth, C. H. *Phys. Rev. B* **1995**, *52*, 6332.
35. Norby, P.; Christensen, A. N. *Acta Chem. Scand., Ser. A* **1986**, *40*, 157-159.
36. Klemm, W.; Krose, E. *Z. Anorg. Allg. Chem.* **1947**, *253*, 218- 225.
37. Léon, A.; Schild, D.; Fichtner, M. *J. Alloys Compd.* **2005**, *404*, 766-770.
38. Stern, E. A. *Phys. Rev. B* **1993**, *48*, 9825.

5

On the local structure of Ti during in-situ desorption of $Ti(OBu)_4$ and $TiCl_3$ catalyzed $NaAlH_4$

Abstract

The local structures of $Ti(OBu)_4$ and $TiCl_3$ catalyzed $NaAlH_4$ were investigated with extended X-ray absorption fine structure (EXAFS) and X-ray absorption near edge structure (XANES). The local structures were linked to literature data on hydrogen desorption and absorption kinetics. In the $Ti(OBu)_4$ catalyzed $NaAlH_4$, butoxide or decomposition products thereof (C, O atoms) were bonded to Ti after ball-milling, where they inhibited the performance of the Ti catalyst. C and O atoms were removed upon heating and Ti–Al species were formed. The thermodynamical most stable specie, $TiAl_3$, was not formed at $T \leq 300$ °C, contrarily to $TiCl_3$ catalyzed $NaAlH_4$. Probably, the initially present butoxide groups inhibited its formation. Besides that, the butoxide or decompostion products thereof (C, O atoms) are also suspected to interfere with the hydrogen uptake of a desorbed $NaAlH_4$.

Introduction

Since the innovative work of Bogdanovic and Schwickardi from 1997,[1] hydrogen storage using Ti catalyzed sodium alanate ($NaAlH_4$) has been subject of much research. This is mainly because sodium alanate displays suitable thermodynamic properties that enable reversible storage of hydrogen at temperatures suitable for mobile applications. The hydrogen is desorbed in two steps (Eqs. (1) and (2)) with respective equilibrium temperatures of 30 and 110 °C at 1 bar hydrogen pressure and delivers 5.6 wt% reversible hydrogen storage capacity.

$$NaAlH_4 \leftrightarrow \tfrac{1}{3}\, Na_3AlH_6 + \tfrac{2}{3}\, Al + H_2 \quad (1)$$

$$Na_3AlH_6 \leftrightarrow 3\, NaH + Al + 1\tfrac{1}{2}\, H_2 \quad (2)$$

The main difficulties to overcome for applying $NaAlH_4$ as a hydrogen storage material are the slow kinetics for hydrogen desorption and absorption. These unfavorable desorption and absorption rates can be improved by reducing the particle size of the $NaAlH_4$ to the nanometer range,[2] or by adding a catalyst, for example $TiCl_3$ or $Ti(OBu)_4$, to the alanate.[1,3-5] The $TiCl_3$ precursor reacts to $NaAlH_4$ forming NaCl, Al, and a reduced Ti entity as shown in Eq. (3).[5] When $Ti(OBu)_4$ is used, the Ti is supposed to be reduced via Eq. (4).[5]

$$TiCl_3 + 3\, NaAlH_4 \rightarrow \text{“Ti”} + 3Al + 3\, NaCl + 6\, H_2 \quad (3)$$

$$Ti(OBu)_4 + NaAlH_4 \rightarrow \text{“Ti”} + NaAl(OBu)_4 + 2\, H_2 \quad (4)$$

Several experimental studies reported that the Ti is finely dispersed and is present as amorphous nano-particles in the $NaAlH_4$ or Al.[6-9] Therefore, characterization of the Ti on atomic scale is necessary and suitable techniques are extended X-ray absorption fine structure (EXAFS) and X-ray absorption near edge structure (XANES). It has been reported that the precursor has an influence on the initial hydrogen desorption and absorption properties, *i.e.*, $TiCl_3$ catalyzed $NaAlH_4$ display faster hydrogen desorption kinetics and also show enhanced hydrogen absorption rates compared to $Ti(OBu)_4$ catalyzed $NaAlH_4$.[4,10,11] Therefore, the proposed Ti entity after ball-milling $TiCl_3$ or $Ti(OBu)_4$ might not possess the same structure, which could be the origin of the difference in the initial kinetics. The atomic structure of Ti in $NaAlH_4$ has been investigated for $TiCl_3$.[6–9] However, the atomic structure has not been investigated for $Ti(OBu)_4$ and is presented here. The structures are investigated for $Ti(OBu)_4$ and $TiCl_3$ catalyzed $NaAlH_4$ after ball-milling and during the in-situ desorption of hydrogen.

Experimental

All sample preparations were performed under a nitrogen or argon atmosphere in a glovebox equipped with a circulation purifier. Commercially available $NaAlH_4$ (tech. 90% Sigma Aldrich) was purified and ball-milled with 10 mol% $TiCl_3$ and 12 mol% $Ti(OBu)_4$ as described before.[4] These samples are referred to as $TiCl_3/NaAlH_4$ and $Ti(OBu)_4/NaAlH_4$. One part of the $TiCl_3/NaAlH_4$ was heated in Ar to 225 °C with a ramp of 5 °C.min^{-1} until no detectable hydrogen desorption was recorded by volumetric analysis ($TiCl_3/NaAlH_4$-225). The $Ti(OBu)_4/NaAlH_4$ was desorbed in situ to 90 °C, kept isothermal for 30 min, and cooled down ($Ti(OBu)_4/NaAlH_4$-90). Next, the sample was desorbed at 150 °C isothermal for 12 h ($Ti(OBu)_4/NaAlH_4$-150). After that, the temperature was increased to 300 °C and kept isothermal for 30 min ($Ti(OBu)_4/NaAlH_4$-300).

X-ray absorption spectroscopy was performed on the Ti K-edge at station E4 of the DESY synchrotron (Hamburg, Germany), using a Si (1 1 1) double crystal monochromator that was detuned to 80% to suppress higher harmonics. All measurements were performed at 77 K in flowing He to exclude thermal decomposition of the sample. The samples (11 mg of Ti-catalyzed $NaAlH_4$) were homogeneously diluted with 50 mg BN, pressed in a pellet, mounted to the cell and transferred to the beam-line in a closed cell under inert atmosphere. Extraction of the EXAFS data was performed as described in chapter 4 of this thesis and described earlier in literature.[9,12] The Ti–Al backscattering amplitude and phase shift were calculated using the FEFF 8.2 code[13] and calibrated using an experimental measured spectrum at 77 K so that E_0 and σ^2 of the references were zero. The FEFF input parameters and used references are listed in Table 1.

Table 1. Input parameters for FEFF to create the reference files.

Absorber - backscatterer	S_0^2	σ^2 / 10^{-3}Å^{-2}	V_r / eV	V_i / eV	Reference compound
Ti-Al	0.72	1.50	11.3	1.0	$TiAl_3$
Ti-Ti	0.60	0	8.6	1.0	h.c.p. Ti-foil
Ti-O	0.59	4.05	13.57	1.0	TiO_2 rutile
Ti-C	1	0	0	1.0	----

Hedin-Lunqvist potentials were used for the calculations.

Experimental data were fitted in k^2 using the difference file technique in R-space from $3 < k < 10$ or $3 < k < 12$ (Å^{-1}) depending on the quality of the data. The quality of the fit was checked by applying k^1, k^2 and k^3 weightings. XANES was recorded from 4950 to 5050 eV with a stepsize of 0.3 eV. The position of the edge was set at the maximum of the first derivative (inflection point) of the absorption edge. Spectra were normalized to 5020 eV.

Results

The magnitude of the uncorrected Fourier Transform (FT) of $Ti(OBu)_4/NaAlH_4$ and $TiCl_3/NaAlH_4$ treated at various temperatures are shown in Figure 1. It is observed that the FT changed significantly upon changing temperature and/or precursor. The changes were quantified in the fits of the different samples. The k^2 variances of the fits (Table 2) are low, indicating that the fits were of a comparable and good quality. The fit parameters of $Ti(OBu)_4/NaAlH_4$ are listed in Table 2. It was observed that 4.5 oxygen atoms surrounded Ti in its closest shell at 1.99 Å, which is a typical distance for Ti–O in Ti-oxides.[14] The next shell contained 3.4 Ti–C bonds at 2.49 Å. This distance is relatively long for a Ti–C distance, which is typically at 2.1–2.2 Å.[15] However, Ti–C distances of ~2.4 Å have been reported as well.[15] No atoms were observed in higher shells.

After heating $Ti(OBu)_4/NaAlH_4$ to 90 °C, the distances of the first two shells altered only slightly. In contrast, the coordination numbers decreased from 4.5 to 1.9 (Ti–O), and from 3.4 to 1.9 (Ti–C). Besides that, the third shell displayed an Al atom at 2.82 Å. After heating the sample to 150 °C, the nearest shells did not contain O or C atoms (Table 2, $Ti(OBu)_4/NaAlH_4$-150). The fit parameters show that Al atoms surrounded the Ti at 2.76 and 2.92 Å, which are at typical distances for $TiAl_x$ alloys.[6–9,16] Further heating to 300 °C increased the Ti–Al bond distances slightly, however the Ti–Al coordination number increased significantly from 3.3 to 6.7, and from 2.0 to 3.0 in the two nearest shells ($Ti(OBu)_4/NaAlH_4$-300).

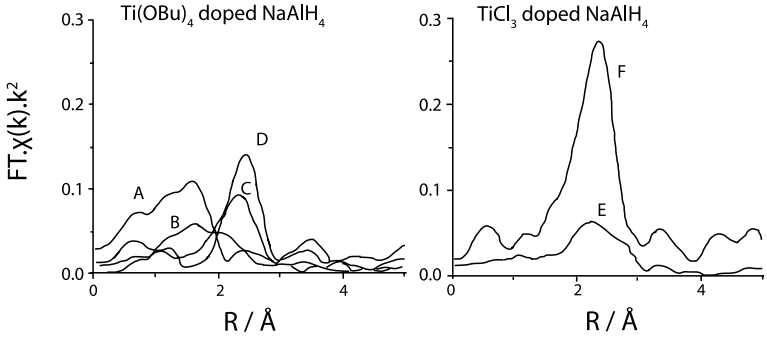

Figure 1 Magnitude of Fourier Transformed *χ(k)*: A) $Ti(OBu)_4/NaAlH_4$, B) $Ti(OBu)_4/NaAlH_4$-90, C) $Ti(OBu)_4$ / $NaAlH_4$-150 D) $Ti(OBu)_4/NaAlH_4$-300, E) $TiCl_3/NaAlH_4$, F) $TiCl_3/NaAlH_4$-225. (k^1 ; Δk; 3-12 Å^{-1}).

Table 2. EXAFS fits of $Ti(OBu)_4$ / $NaAlH_4$ after ball milling, and after desorption at 90 °C, 150 °C, 300 °C, and EXAFS fits of $TiCl_3$ / $NaAlH_4$ after ball milling and desorption at 225 °C.

Name	Fitrange / Å	Shell	Atom	*N*	$\Delta\sigma^2$ / 10^{-3} Å^{-2}	*R* / Å	*Eo* / eV	k^2 –variance	
								Im.	Abs.
$Ti(OBu)_4/NaAlH_4$	1.1 to 2.1	1	Ti-O	4.5	8.6	1.99	3.09	0.24	0.17
		2	Ti-C	3.4	0.9	2.48	-0.60		
$Ti(OBu)_4/NaAlH_4$-90	1.0 to 2.8	1	Ti-O	1.9	1.8	1.91	2.40	0.40	1.02
		2	Ti-C	1.9	0.6	2.52	-7.00		
		3	Ti-Al	1.5	3.2	2.83	-1.05		
$Ti(OBu)_4/NaAlH_4$-150	1.8 to 3.6	1	Ti-Al	3.3	0.5	2.76	-1.32	0.07	0.10
		2	Ti-Al	2.0	0.5	2.92	0.57		
		3	Ti-Ti	1.3	8.8	3.39	4.06		
$Ti(OBu)_4/NaAlH_4$-300	1.9 to 3.3	1	Ti-Al	6.7	0.6	2.82	-1.65	0.46	0.25
		2	Ti-Al	3.0	0.5	3.00	4.91		
		3	Ti-Ti	2.0	3.6	3.39	8.83		
$TiCl_3/NaAlH_4$	1.2 to 3.5	1	Ti-Al	2.3	0.04	2.71	-0.96	0.63	0.40
		2	Ti-Al	2.5	0.18	2.89	0.96		
		3	Ti-Ti	1.9	0.81	3.52	1.93		
$TiCl_3/NaAlH_4$-225	1.2 to 3.5	1	Ti-Al	4.6	0.10	2.73	1.53	0.36	0.23
		2	Ti-Al	7.8	0.82	2.84	4.97		
		3	Ti-Ti	3.8	6.36	3.90	4.31		

The local structure for $TiCl_3/NaAlH_4$ is listed in Table 2 and it is observed that Al surrounded the Ti. A detailed description of this structure can be found in chapter 4.[9] After heating to 225 °C ($TiCl_3/NaAlH_4$-225), the local structure around Ti was similar to that of $TiAl_3$,[16] *i.e.* 4 Al atoms at 2.73 Å, 8 Al atoms at 2.84 Å, and 4 Ti atoms at 3.90 Å.

The XANES of several samples are shown in Figure 2. The edge positions of all measured samples are listed in Table 3. The two features at 4696.3 and 4972.4 eV in the Ti edge for Ti-oxides are pre-edge features,[17] thus the edge position was determined at the inflection point (maximum of first derivative) of the second rising edge for the samples that contained oxygen (E_{edge}=4972.3 eV for $Ti(OBu)_4/NaAlH_4$ and E_{edge}=4976.5 eV for TiO_2). The inflection point of first rising edge was taken as the absorption edge for the samples that did not contain oxygen in the EXAFS fit. The edge energy was the same for $Ti(OBu)_4/NaAlH_4$-150 and $Ti(OBu)_4/NaAlH_4$-300, *i.e.* E_{edge}=4967.0 eV. This is close to the values for $TiAl_3$ and Ti metal references (4966.7 and 4965.5 eV) and the $TiCl_3$ ball milled $NaAlH_4$ samples (E_{edge}=4965.7 eV for $TiCl_3/NaAlH_4$ and E_{edge}=4966.1 eV for $TiCl_3/NaAlH_4$-225). The edge energy of the first rising edge has been determined for $Ti(OBu)_4/NaAlH_4$-90, although the EXAFS fit indicated that the local structure involved both oxygen and aluminum atoms (Table 2), implying that the absorption edge consists of a combination of two oxidation states. It was also observed that the resonances of $Ti(OBu)_4/NaAlH_4$ and $Ti(OBu)_4/NaAlH_4$-150 were less pronounced than those of the crystalline references $TiAl_3$ and TiO_2 (Figure 2).

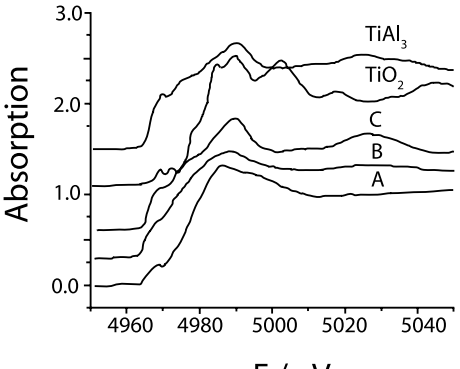

Figure 2. XANES of A) $Ti(OBu)_4/NaAlH_4$, B) $Ti(OBu)_4/NaAlH_4$-150, C) $TiCl_3/NaAlH_4$-225, and references TiO_2 and $TiAl_3$.

Table 3. Positions of Ti-edges in various samples.

	Edge position (eV)
$TiCl_3/NaAlH_4$	4965.7
$TiCl_3/NaAlH_4$-225	4966.1
$Ti(OBu)_4/NaAlH_4$	4972.3
$Ti(OBu)_4/NaAlH_4$-90	4967.0
$Ti(OBu)_4/NaAlH_4$-150	4967.0
$Ti(OBu)_4/NaAlH_4$-300	4967.0
TiO_2	4976.5
$TiAl_3$	4966.7
Ti foil	4965.5

Discussion

The position of the Ti absorption edge energy represents the oxidation state of Ti in Ti-butoxide catalyzed $NaAlH_4$. Table 3 shows that the position of the edge energy was significantly higher for $Ti(OBu)_4/NaAlH_4$ than the position of the edge in Ti-metal. The shift in edge energy is linearly dependant of the oxidation state of Ti (○ symbols in Figure 3).[6] Note that the edge shift of TiO_2 differs 3 eV with TiO_2 obtained from literature, probably due to differences in the determination of the edge energy. When assuming a linear relationship between oxidation state and edge shift of our recorded Ti-metal and TiO_2 (Figure 3), it is calculated that the formal valency of Ti was +2.5 in $Ti(OBu)_4/NaAlH_4$ after ball-milling. These findings are in contradiction with the reaction between $Ti(OBu)_4$ and $NaAlH_4$ Eq. (4), in which the Ti is claimed to be reduced to Ti^0. Contrarily, the oxidation state was +0.3 when $TiCl_3$ is used ($TiCl_3/NaAlH_4$), and indicated that the Ti was reduced to a low oxidation state during the preparation (Figure 3).

It was also observed that the XANES resonances of $Ti(OBu)_4$ catalyzed $NaAlH_4$ were damped compared to crystalline materials such as $TiAl_3$ and TiO_2 (Figure 2). Similar damped resonances were reported and explained by Graetz *et al.* by presence of surface nano-entities.[6] Probably, in the case of $Ti(OBu)_4/NaAlH_4$ the Ti is highly dispersed on the $NaAlH_4$. The structural properties of these highly dispersed Ti-entities were further investigated with EXAFS. The EXAFS fit parameters in Table 2 revealed that Ti was surrounded by oxygen and carbon atoms after ball-milling $Ti(OBu)_4$ with $NaAlH_4$. The carbon and oxygen atoms originated from the butoxide group of the Ti-precursor, thus most probably the Ti was not in the close vicinity of the $NaAlH_4$ in this stage of the experiment.

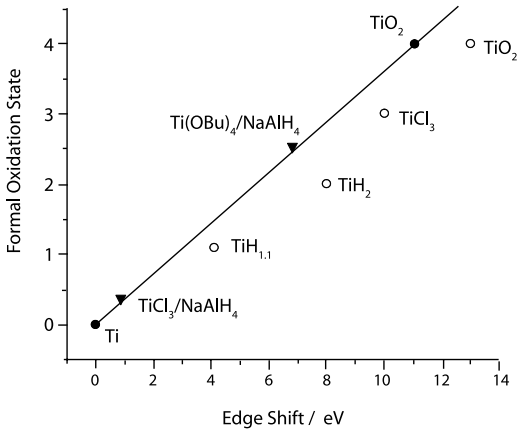

Figure 3. Shift in Ti K-edge, ● measured references, used to calibrate samples with unknown valency (▼), ○ Ti standards taken from ref 6.

Upon heating to 90 °C, the coordination number of the Ti–O and Ti–C shells decreased from 4.5 to 1.9 (Ti–O), and 3.4 to 1.9 (Ti–C), as observed in the EXAFS fit of $Ti(OBu)_4/NaAlH_4$-90 (Table 2). This indicates that the C and O atoms of the Ti were removed for approximately 50% during this temperature treatment. At the same time Ti–Al scattering at 2.82 Å appeared in the fit (Table 2). This indicates that the heat treatment partly broke the Ti–O, and Ti–C bonds and Ti reacted with the formed Al metal (see Eq. (1)). This process prolonged when the sample was heated to 150 °C. Namely, in $Ti(OBu)_4/NaAlH_4$-150, no Ti–O or Ti–C bonds were detected in the closest coordination spheres (Table 2) and the Ti was surrounded by Al atoms at 2.76 and 2.92 Å. The coordination number of Al surrounding the Ti was low (3.3 + 2.0 = 5.3, see Table 2) compared to a Ti in crystalline $TiAl_3$ alloy (4+8=12 Al neighbours). Most likely, the Ti is present as Ti–Al nano entities as was also inferred from XANES. The coordination number of Al increased further when the sample was heated to 300 °C ($Ti(OBu)_4/NaAlH_4$-300), but the local structure differed to the local structure of $TiAl_3$.

In the EXAFS fits of $TiCl_3$ milled $NaAlH_4$, the chloride precursor ion did not appear in the fits (Table 2), but only Ti–Al distances were observed in the first two shells. This illustrates that Ti in $TiCl_3$ was more easily reduced than Ti in $Ti(OBu)_4$. When $TiCl_3/NaAlH_4$ was heated to 225 °C ($TiCl_3/NaAlH_4$-225) the local structure was identical to that of $TiAl_3$, thus comprised 4+8=12 Al atoms. This indicates that thermodynamical lowest state ($TiAl_3$) had been reached. After heating the Ti in $Ti(OBu)_4$ catalyzed $NaAlH_4$, the Ti also enriched with Al atoms. However, its first coordination sphere contained 3 + 6.7 = 9.7 Al atoms after the final temperature treatment to 300 °C ($Ti(OBu)_4/NaAlH_4$-300). Thus, did not reach the thermodynamical lowest state ($TiAl_3$).

Several reports indicate that the hydrogen desorption rates are faster for the $TiCl_3$ catalyst than for $Ti(OBu)_4$,[4,10,11] which has also been confirmed for our investigated samples (not shown). It was observed that the oxidation state of the Ti was +2.5 in $Ti(OBu)_4/NaAlH_4$ and +0.3 in $TiCl_3/NaAlH_4$ (Figure 3). It might be that the oxidation state of Ti is of crucial importance for its catalytic performance. Another, related, explanation is that the butoxide groups occupy space around Ti and shield the Ti from $NaAlH_4$ leading to a less effective Ti-catalyst.

Besides improved desorption rates, hydrogen absorption rates and capacities are also better using $TiCl_3$ than Ti-butoxide.[4,10,11] The coordination number of Al around Ti was low in $Ti(OBu)_4/NaAlH_4$-150, which is interpreted that Ti particles were small and/or at the surface. In contrast, the coordination number for $TiCl_3$ catalyzed $NaAlH_4$ was higher, but still displays better absorption rates and capacities.[4,10,11] As Ti–Al surface or nano entities are considered as the active species,[6–9] this kinetic difference cannot be explained on basis of EXAFS/XANES results. As mentioned before, the butoxide groups were removed from the Ti during heating. These

butoxide groups could have desorbed as a gas, or formed bulk oxides/carbides. The presence of gaseous hydrocarbons or alcohols was tested in an in-situ gas phase IR experiment to 450 °C and revealed that no detectable amounts of gasses were desorbed. Thus, the butoxide must have reacted with $NaAlH_4$, NaH or Al in the bulk. The ratio of carbon to aluminum is high in the sample (C/Al ratio = 1.9). It might be that a phase comprising the C and O atoms block the Ti-catalyst and interfere with the H_2 absorption process.

Conclusions

$NaAlH_4$ catalyzed with $Ti(OBu)_4$ and $TiCl_3$ yields different Ti species under identical preparation conditions. For $TiCl_3$, Ti was reduced to $Ti^{0.3}$ and was surrounded by Al atoms. Whereas for $Ti(OBu)_4$, the Ti oxidation state was +2.5 and C and O atoms were detected around Ti. The presence of carbon and oxygen inhibited the Ti catalyst for hydrogen desorption. The C and O groups were removed in between 90 and 150 °C and delayed the formation of the thermodynamical most stable state ($TiAl_3$ alloy). The presence of carbon and oxygen atoms in the bulk interferes possibly with hydrogen uptake, explaining the lower the activity of the Ti-catalyst.

Acknowledgements

This work was financially supported by ACTS, project number 053.61.02, and HASYLAB project number I-05-062 EC. We thank Dr. Konstantin Klementiev from HASYLAB for providing $TiAl_3$. Hans Stil from Shell Research and Technology Centre is thanked for sample preparation. We also thank Fouad Soulimani and Ad van der Eerden from Utrecht University for assistance during the IR and XAFS experiments.

References

1. Bogdanovic, B.; Schwickardi, M.*J. Alloys Compd.* **253–254** (1997) 1–9.
2. Baldé, C.P.; Hereijgers, B.P.C.; Bitter, J.H.; de Jong, K.P. *Angew. Chem. Int. Ed*. **45** (2006) 3501–3503.
3. Jensen, C.M.; Zidan, R.A.; Mariels, N.; Hee, A.G.; Hagen, C. *Int. J. Hydrogen Energy* **24** (1999) 461.
4. Haiduc, A.G.; Stil, H.A.; Schwarz, M.A.; Paulus, P.; Geerlings, J.J.C. *J. Alloys Compd.* **393** (2005) 252–263.
5. Bellosta von Colbe, J.M.; Bogdanovic, B.; Felderhof, M.; Pommerin, A.; Schüth, F. *J. Alloys Compd.* **370** (2004) 104–109.
6. Graetz, J.; Reilly, J.J.; Johnson, J.; Ignatov, A.Y.; Tyson, T.A. *Appl. Phys. Lett.* **85** (2004) 500–502.
7. Felderhoff, M.; Klementiev, K.; Grunert, W.; Spliethoff, B.; Tesche, b.; Bellosta Von Colbe, J.M.; Bogdanovic, B.; Hartel, M.; Pommerin, A.; Schüth, F.; Weidenthaler, C. *Phys. Chem. Chem. Phys.* **6** (2004) 4369–4374.
8. Léon, A.; Kircher, O.; Rothe, J.; Fichtner, M. *J. Phys. Chem. B* **108** (2004) 16372–16376.
9. Baldé, C.P.; Stil, H.A.; van der Eerden, A.M.J.; de Jong, K.P.; Bitter, J.H. *J. Phys. Chem. C*, **2007**, *111*, 2797-2802.
10. Bogdanovic, B.; Brand, R.A.; Marjanovic, A.; Schwickardi, M.; Tölle, J. *J. Alloys Compd.* **302** (2000) 36–58.
11. Schüth, F.; Bogdanovic, B.; Felderhof, M.; *Chem. Commun.* **37** (2004) 2249–2258.
12. Koningsberger, D.C.; Mojet, B.L.; van Dorssen, G.E.; Ramaker, D.E. *Top. Catal.* **10** (2000) 143–155.
13. Zabinsky, S.I.; Rehr, J.J.; Ankudinov, A.L.; Albers, R.C.; Eller, H.J. *Phys. Rev. B: Condens. Matter* **52** (1995) 2995.
14. Vegard, L. *Philos. Mag.* **32** (1916) 505–518.
15. Wasserman, E.P.; Westwood, A.D.; Yu, Z.; Oskam, J.H.; Duenas, S.L. *J. Mol. Catal. A: Chem.* **172** (2001) 67–80.
16. Norby, P.; Christensen, A.N.; *Acta Chem. Scand., Series A* **40** (1986) 157–159.
17. Farges, F.; Brown Jr., G.E.; Rehr, J.J. *Phys. Rev. B: Condens. Matter* **56** (1997) 1809–1819.

6

XAFS study of the Al K-edge in $NaAlH_4$

Abstract

Al K-edge (1561.1 eV) XANES and EXAFS spectra of unoxidized $NaAlH_4$, a hydrogen storage material, have been recorded in He atmosphere in a special in-situ low energy cell. The XANES spectrum of $NaAlH_4$ was reported and compared to an oxidized $NaAlH_4$ and illustrated the power of XANES as a quick qualitative check of the $NaAlH_4$. Self-consistent real-space multiple-scattering calculations could reproduce the features of the XANES of $NaAlH_4$ for a cluster of 74 atoms. For EXAFS, reliable fits of the Al K-edge spectra could be obtained when all scattering contributions, *i.e.* Al-H, Al-Na and Al-Al, were incorporated in the fit. The hydrogen atoms had a significant contribution to the Al K-edge EXAFS signal of $NaAlH_4$, which stresses the importance of hydrogen scattering when analyzing EXAFS data of this metal hydride.

Introduction

In realizing a society applying sustainable energy schemes, storage of energy is essential. Hydrogen is regarded as a candidate to store energy for stationary and mobile applications. However for implementation the hydrogen technology in society, the challenge of hydrogen storage has to be addressed. Sodium alanate ($NaAlH_4$) is regarded as a promising hydrogen storage material as it has a high hydrogen capacity (5.6 wt%) and suitable thermodynamic stability for reversible hydrogen storage.[1,2] The hydrogen is released in two steps when $NaAlH_4$ is heated (equation 1), and hydrogen is reabsorbed by applying H_2 pressure.

$$NaAlH_4 \leftrightarrow \tfrac{1}{3}\, Na_3AlH_6 + \tfrac{2}{3}\, Al + H_2 \leftrightarrow NaH + Al + 1\tfrac{1}{2}\, H_2 \qquad (1)$$

Unfortunately the kinetics of hydrogen desorption and reloading of a desorbed alanate are unfavorable, the latter is most likely a result of segregation of NaH and Al phases.[3,4] We expect that the dynamics of the local structure around Al (and Na) can give insight in the mechanism of phase segregation which will allow us to develop improved storage materials. Up to now most structural properties of sodium alanate have been investigated with (synchrotron) X-ray diffraction [5-7], neutron diffraction [7,8], ^{1}H-NMR, and ^{27}Al-NMR. [9-11] The diffraction techniques require long-range ordering, thus do not necessarily give information on the local environment around Al, and NMR of solid materials is challenging to interpret. X-ray absorption spectroscopy, *i.e.* Extended X-Ray Absorption Fine Structure (EXAFS) and X-ray Absorption Near Edge Structure (XANES) are suitable for determining local structures (EXAFS) and electronic/geometrical (XANES) parameters of a specimen and have been applied to determine the local structure of Ti in Ti doped $NaAlH_4$ systems.[12-16] Recently, an Al K-edge XANES study was reported on $NaAlH_4$.[17]

X-ray absorption measurements of low Z elements, like Na and Al, are challenging due to the low X-ray intensity of the synchrotron radiation at the required energy range (1000-2000 eV). Nevertheless some successful studies on the Al K-edge have been reported for solid oxides and Al-oxide gels [18-20] either in vacuum or in-situ using a specially designed cell (ILEXAFS[21]). Contrarily to Al-oxides, measuring XAFS of a metal hydride is experimentally challenging due to its sensitive nature towards oxygen, water, vacuum, and temperature. Therefore, sample handling prior and during XAFS recording require extra attention to obtain reliable data.

In this work, Al K-edge X-ray absorption spectra of $NaAlH_4$ were recorded in the ILEXAFS cell.[21] Due to the sensitivity of $NaAlH_4$ towards air and water, its XANES and EXAFS will be compared to those of an oxidized $NaAlH_4$ and a discrepancy with recent XANES spectra reported by Fichtner et al.[17] will be discussed. For EXAFS fitting, the significance of including aluminum-hydrogen scattering is discussed for $NaAlH_4$. No Al K-edge EXAFS study has been published before for $NaAlH_4$.

Experimental Section

Sample preparations

All sample preparations were carried out in a nitrogen-filled glovebox equipped with a circulation purifier. Chemical operations were conducted using Schlenk techniques. The solvents (THF and diethylether) were dried by distillation over Na. Commercially available $NaAlH_4$ (Sigma-Aldrich) was purified by dissolving it in an excess of THF; remaining solids were removed by filtration. Next, the THF was evaporated by at reduced pressure until precipitation started. In the following step the $NaAlH_4$ was further precipitated by drop wise addition of diethylether. The crystallinity of the obtained $NaAlH_4$ was checked with X-ray diffraction and only displayed sharp diffractions of the $NaAlH_4$ were present (not shown). A part of this $NaAlH_4$ was exposed to ambient air for two days and will be referred to as 'oxidized $NaAlH_4$'.

XAFS recording

X-ray absorption spectroscopy was performed on the Al K-edge (1561.1 eV) using the ILEXAFS cell [21] in fluorescence mode with a gas proportional detector. Measurements were conducted on station 3.4 at the SRS (Synchrotron Radiation Source, Daresbury, UK) that was equipped with a YB_{66} double crystal monochromator. Higher harmonics were removed by increasing the incident angle for the plane pre-mirror to 0.8 degrees and using a dual carbon on silicon coating. The storage ring operated at 2.0 GeV and a mean current of 130 mA. $NaAlH_4$ was diluted 1:2 on volume basis with BN to prevent self-absorption and loaded to the cell in a glovebox. Afterwards, the cell was closed and transferred to the beamline. All EXAFS spectra were recorded at room temperature in flowing He that was purified using O_2 and H_2O gas clean filters from Varian Inc.

EXAFS data handling

EXAFS data analysis was done using XDAP.[22] The pre-edge background was approximated by a Victoreen function before subtraction.[23] The edge energy was determined at the maximum of the first derivative of the spectrum and was calibrated to the edge energy of Al-foil (1559.0 eV). The spectrum was corrected for the background with a cubic spline.[24] During the background extraction procedure, the AXAFS was removed from the data, by minimizing the intensity from 0-1 Å in R-space without significantly reducing the intensity of the most intense peak.[25,26] Normalization was performed by dividing the absorption spectrum by the height of the background at 50 eV above the edge. Four spectra were averaged to improve the signal to noise ratio.

Phase shifts and backscattering amplitudes of the different absorber-backscatter pairs were calculated using the FEFF 8.0 code.[27] For Al-Al scattering in $NaAlH_4$, the reference was calculated using the input parameters as described by Rehr *et al.*.[28] The input values for FEFF are listed in Table 1. For Al-Al and Al-Na the same backscatterings amplitude and phaseshift functions were used, which is allowed since Al and Na are next nearest neighbors in the periodic table.[29] Because Na and Al have similar scattering properties and the distance and coordination number of the Na and Al in the fourth/fifth shell (3.74 Å) are the same (based on crystal structure), the refined parameters for both atoms were restrained to the same value. Due to the absence of literature to fit Al-H scattering in low Z metal hydrides, the Al-H scattering phases and amplitude were calculated without additional entries in the FEFF input file (see Table 1). The Al-O scattering phase and amplitude of a single absorber backscatterrer was calculated with the parameters listed in Table 1, ensuring that the fit of the first Al-O shell of the experimental recorded Zn-AlPO-34 had a $\Delta\sigma^2$ and E_0 of zero, with 4 Al-O atoms at 1.71 Å.[30,31]

The Fourier Transforms of the EXAFS data were fitted using “the difference file technique” in R-space [25], using a k^0 weighting with a k-range from 2.6 to 7 $Å^{-1}$. In all fits the coordination numbers from crystallographic data were used as fixed input parameters.[5-8] R, ΔE_0, and $\Delta\sigma^2$ were refined to optimal values in the fitting process. The quality of the fit was checked by means of k^0 variance and further checked by using k^0, k^1 and k^3 weightings of the difference files.[25]

Table 1. Input parameters for FEFF to create the reference files.

Absorber - backscatterer	N	R / Å	S_0^2	σ^2 / 10^{-3} Å^{-2}	V_r / eV	V_i / eV	Reference
Al-Na	1	2.86	0.78	3.28	9.0	1.0	
Al-Al	1	2.86	0.78	3.28	9.0	1.0	25
Al-H	1	1.63	1	0	0	1.0	
Al-H	1	2.93	1	0	0	1.0	
Al-O	1	1.71	0.80	5.39	7.63	1.0	Zn-AlPO-34

Hedin-Lunqvist potentials were used for the calculations.

XANES

The position of the edge position has been calculated by the maximum of the first derivative in the edge jump (inflection point). Spectra were normalized to 1570 eV. XANES spectra were simulated using FEFF 8.0.[21] The ground state potential was used for calculating μ_0 (the embedded atomic background absorption), while the Hedin-Lundqvist exchange-correlation was used for the excited state. The muffin-tin prescription with an overlap of 15% was used in the calculation of the Al and Na potentials. For the hydrogen potential, the muffin-tin prescription with –20% overlap was applied. The self consistent field calculation was performed within a radius of 4 Å, and the full multiple scattering prescription was used in a cluster comprising a number 74 of atoms.

Results and Discussion

Comparison of oxidized and non-oxidized $NaAlH_4$

Since $NaAlH_4$ is very reactive towards oxygen and water XAFS results might be easily influenced by (partial) oxidation of the sample. Therefore the XAFS of an oxidized $NaAlH_4$ will be discussed first. Oxidized $NaAlH_4$ was obtained by exposing $NaAlH_4$ to ambient air for 2 days. The EXAFS fit of the oxidized $NaAlH_4$ is shown in Figure 1. The fit parameters are listed in Table 2 and Al was surrounded with 5.9 oxygen atoms at 1.86 Å. The Al-O distance and coordination number correspond to a typical octahedral surrounding of the Al in Al-oxides/hydroxides in the ICSD crystallographic database and indicate that the sample was completely oxidized. In the next shell 3.8 Al atoms were fitted at 3.00 Å; This data is not sufficient to conclude which Al-Na-oxide/hydroxide phase was formed.

The XANES spectra of octahedral coordinated Al-oxides/hydroxides display an intense sharp whiteline.[19,20] However, the here reported whiteline of the oxidized $NaAlH_4$ did not reveal such an intense sharp whiteline (Figure 2), whereas the Al-O surrounding in the EXAFS indicated a octahedral surrounding (Table 2). This is tentatively explained by the fact that the long-range structure around Al was very disordered, therewith reducing the intensity of the whiteline.[32]

Most noticeable in the XANES of oxidized $NaAlH_4$ are the two features on the whiteline at 1569.8 and 1571.3 eV. These features are absent in the pure $NaAlH_4$. In addition the edge position for oxidized alanate was located at 1565.6 eV while for pure alanate it was 1561.1 eV (Figure 2). Thus the compounds can be easily distinguished using the XANES as a fingerprint. Therefore we have to conclude that a recently published XANES spectrum of $NaAlH_4$ by Fichtner et al. [17], which shows identical features to our air exposed $NaAlH_4$, was most likely not a XANES of $NaAlH_4$, but of an oxidized $NaAlH_4$.

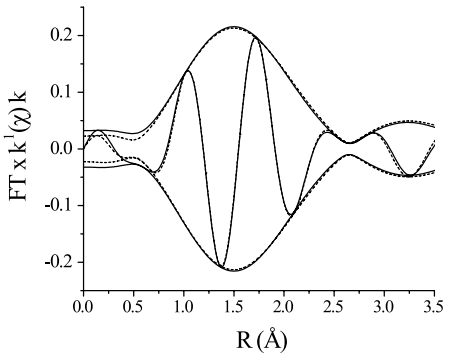

Figure 1. k^1 R-space fit of oxidized-$NaAlH_4$ (·····) (Δk: $3<k<7$ Å^{-1}, fitrange $0.5<R<3.5$ Å), and raw data (—) of an oxidized $NaAlH_4$.

Table 2. EXAFS fit parameters of oxidized $NaAlH_4$.

Sample	Absorber - backscatterer	N	$\Delta\sigma^2$ / 10^{-3} Å^{-2}	R / Å	ΔE_o / eV	k^0 –variance	
						Im.	Abs.
Oxidized $NaAlH_4$	Al-O	5.9	1.31	1.86	-1.33	0.15	0.07
	Al-Al	3.8	6.84	3.00	0.45		

Number of independent parameters was 9 and the data was fitted with 8 parameters.

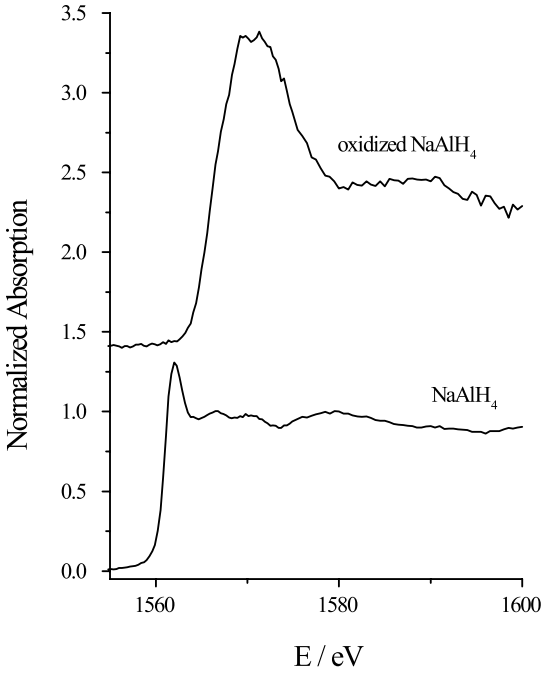

Figure 2. XANES spectra from $NaAlH_4$, and an oxidized $NaAlH_4$. Spectra are normalized to 1580 eV.

XANES analysis of $NaAlH_4$

Figure 3 shows the experimental and calculated XANES of $NaAlH_4$. The experimental XANES consisted of a narrow white line with a maximum at 1562.1 eV, followed by three resonances (a, b, c) at respectively 1566.8, 1570.5, and 1578.0 eV in the near edge structure. The FEFF calculated XANES of $NaAlH_4$ also comprised these three resonances, which is in good agreement with the experiment. The most obvious discrepancy between the calculation and the experiment is the edge position, with a shift of about 3 eV. This is most likely related to the shortcomings of the muffin tin approximation for calculating the Fermi energy in FEFF. The value of the shift is well in agreement with the discrepancies in the position of the edge found by others.[33, 34]

Figure 4 shows the influence of the full multiple scattering radius (FMS) on the FEFF calculated XANES. For full multiple scattering path length of 3 Å, *i.e.* including only the interaction with hydrogen, as well as for a length of 3.7 Å that comprised all chemical species in the nearest coordination shells, the resonances a-c were not fully developed and the rising edge displayed a shoulder that was not present in the recorded XANES (Figures 3 and 4). Whereas, when the multiple scattering path length was extended to 6 Å (that is, including also long range scattering), the experimentally detected resonances a-c appear in the simulation and the shoulder of the rising edge disappeared. From this can be concluded that that the resonances a, b, and c in $NaAlH_4$ originate from multiple scattering rather than from geometry or electronic states.

The intensity of the white line decreased when FMS-radius was lowered in the calculation from 6 to 3.7 Å; a further decrease was observed for a path length of 3 Å (Figure 4). This indicates that the intensity of the white line relates to multiple scattering paths as well. In compounds showing lattice periodicity it has been shown that full multiple scattering (multiple scattering at all orders) in a smaller cluster together with SCF calculations is adequate to describe XANES.[32] This is fully demonstrated in our case, for a rather small cluster of 74 atoms.

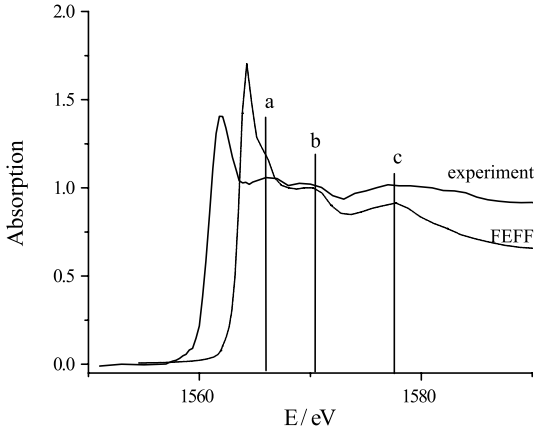

Figure 3. XANES of $NaAlH_4$ and FEFF calculated XANES.

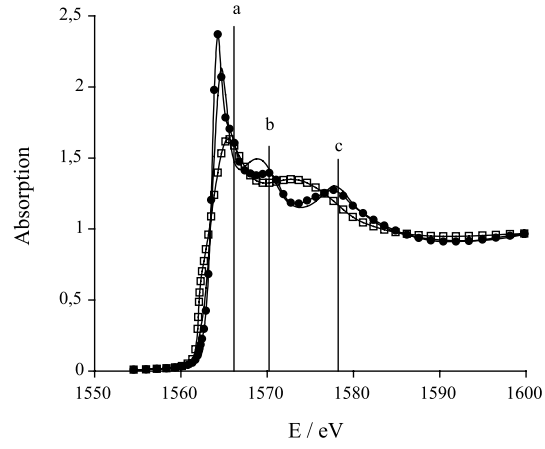

Figure 4. Calculated XANES of $NaAlH_4$ in which full multiple scattering (FMS) pathlength in FEFF calculation was varied, (● FMS=6, no symbols FMS=4, and □ FMS=3); a, b, c indicate three resonances (see text for details).

EXAFS analysis of $NaAlH_4$

The background subtracted EXAFS data of non-oxidized $NaAlH_4$ and the same $NaAlH_4$ sample after desorption are shown in Figure 5. Clearly for $NaAlH_4$ the EXAFS was featureless at $k > 5.5$ Å^{-1}. To rule out that this is the result of an experimental limitation the sample was heated to desorb hydrogen, thereby changing the local structure of Al. Figure 5 shows that after desorption of hydrogen the EXAFS oscillations are visible up to $k = 7.0$ Å^{-1}. These results were reproducible when another $NaAlH_4$ sample was prepared and desorbed, thus we concluded that the low intensity of the EXAFS oscillations for values of k higher than 5.5 Å^{-1} in the original sample are related to its structure. Please note that the sample after desorption was only included for comparison.

The data of $NaAlH_4$ were fitted using two different models. In the first model, only the Al-Al and Al-Na scattering was taken into account and the data were fitted from $R = 0.5$ to 4.5 Å. The fit describing this model is displayed in Figure 6a with a dotted line and will be referred to as 'fit without Al-H scattering'. It can be seen that the FT of the fit strongly deviates from the FT of the data for $0 < R < 2$ Å. In addition also the fit deviated slightly from the raw data for $2 < R < 4.5$ Å, *i.e.*, where Na and Al scatterers are expected and fitted. In the second model, also Al-H scattering was included in the fit. The FT of the fit is shown in Figure 6b (dotted line) and describes the data adequately in the entire fitted range (0.5 to 4.5 Å).

The EXAFS coordination parameters are given in Table 3 for the fit without hydrogen scattering and in Table 4 for the fit with hydrogen scattering. The k^0 variances for fit with hydrogen scattering (Table 4) were an order of magnitude lower than for the fit without hydrogen scattering (Table 3), thus the quality of the fit improved considerably when hydrogen was taken into account.

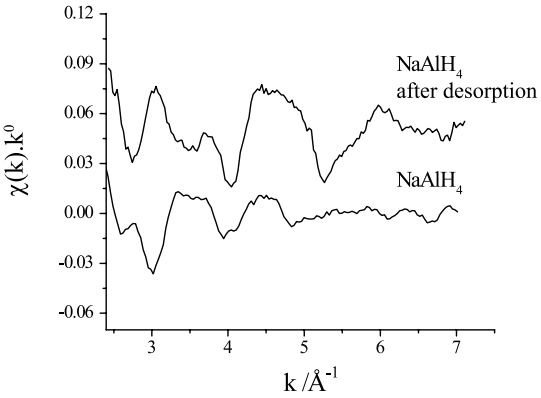

Figure 5. Background subtracted EXAFS data of $NaAlH_4$ and $NaAlH_4$ after desorption (increment 0.05)

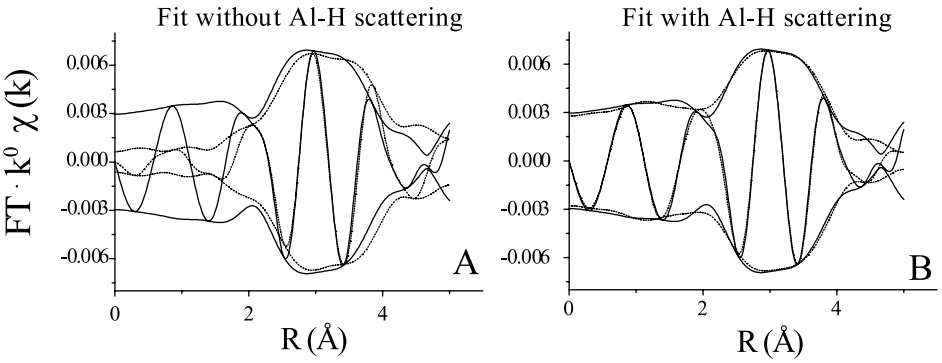

Figure 6a k^0 fits of $NaAlH_4$ without hydrogen scattering (Δk: 2.6<k<7 Å^{-1}, fit range 0.5<R<4.5 Å) and **6b** fit with hydrogen scattering (Δk: 2.6<k<7 Å^{-1}, fit range 0.5<R<4.5 Å). Raw data (—) and fit (---).

Table 3. EXAFS fit of $NaAlH_4$ without hydrogen scattering.

Sample	Absorber - backscatterer	N	$\Delta\sigma^2$ / 10^{-3} Å^{-2}	R / Å	ΔE_o / eV	k^0 –variance	
						Im.	Abs.
$NaAlH_4$	Al-Na	4	6.4 #	3.49 #	-0.18 #	2.17	9.58
	Al-Na	4	12.3 #	3.71 #	3.46 #		
	Al-Al	4	12.3 *	3.71 *	3.46 *		

Number of independent parameters was 13 and the data was fitted with 6 parameters.
* Fitted with identical parameters as the second Al-Na shell.
# Refined parameters.

Table 4. EXAFS fit of $NaAlH_4$ with hydrogen scattering.

Sample	Absorber - backscatterer	*N*	$\Delta\sigma^2$ / 10^{-3} Å^{-2}	*R* / Å	ΔE_o / eV	k^0 –variance	
						Im.	Abs.
$NaAlH_4$	Al-H	4	35 #	1.63 #	5.86 #	0.20	0.22
	Al-H	4	4.5 #	2.95 #	2.43 #		
	Al-Na	4	7.4 #	3.53 #	-2.92 #		
	Al-Na	4	11.7 #	3.74 #	1.65 #		
	Al-Al	4	11.7 *	3.74 *	1.65 *		

Number of independent parameters was 13 and the data was fitted with 12 parameters.
* Fitted with identical parameters as the second Al-Na shell.
# Refined parameters.

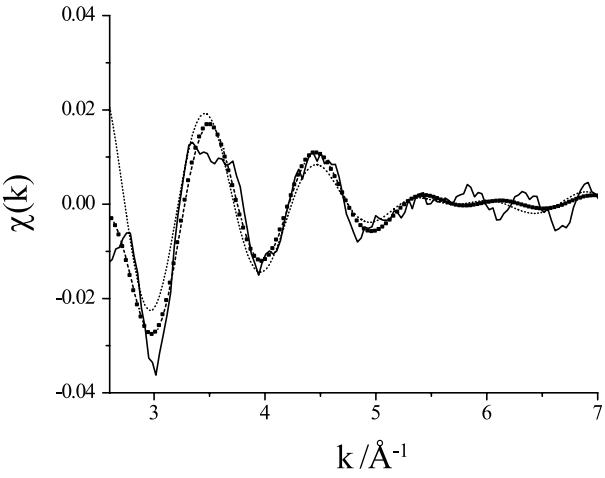

Figure 7. $\chi(k)$ of raw data (——), (—●—) fit with hydrogen scattering, (---) fit without hydrogen scattering.

The raw data in *k*-space are compared to the fits with and without hydrogen scattering in Figure 7. It can be seen that both fits describe the raw data at $k > 3.2$ Å^{-1}. However including hydrogen into the fit improved the fit at low k-values ($2.6<k<3.2$ Å^{-1}). This can be explained by the fact that the scattering power of the first hydrogen shell is strongest from 2.6 to 3.5 Å^{-1} in *k*-space (Figure 8). For these reasons, it is important to extend the *k*-range to a low value (*e.g.* 2.6 Å^{-1}) when the Al-H scattering is fitted. Extending the *k*-range to a lower value has been reported before, ensuring that contributions of a light scatterer are not removed from the data.[35,36]

The calculated contributions of the individual scatterers to the Al K-edge EXAFS of $NaAlH_4$ are visualized in Figure 8. It is noted that the third (Al-Na) and fourth shell (Al-Na and Al-Al) are out-of-phase with each other, *i.e.,* interfere destructively. This leads to a damped EXAFS signal for $NaAlH_4$ (Figure 5) while coordination numbers are high.[26]

It is seen in Table 4 that the Debye-Waller factor ($\Delta\sigma^2$) for the hydrogen atoms were considerably higher than $\Delta\sigma^2$ of Al and Na, even when we take into account that the Debye-Waller for Al-H was set to zero in the reference file. This indicates that the position of the hydrogen atoms was more disordered than that of the Na and Al atoms, which is probably caused by more thermal disorder as a hydrogen atom is significantly lighter than Na or Al.

Hydrogen scattering was previously directly detected in GdMg switchable mirrors,[37] in which the hydrogen was bonded to the Gd. Indirect hydrogen scattering was inferred from Pd-Pd lattice expansion using the lens effect in hydrides.[38] In water hydrogen has been detected on the O K-edge EXAFS.[39]

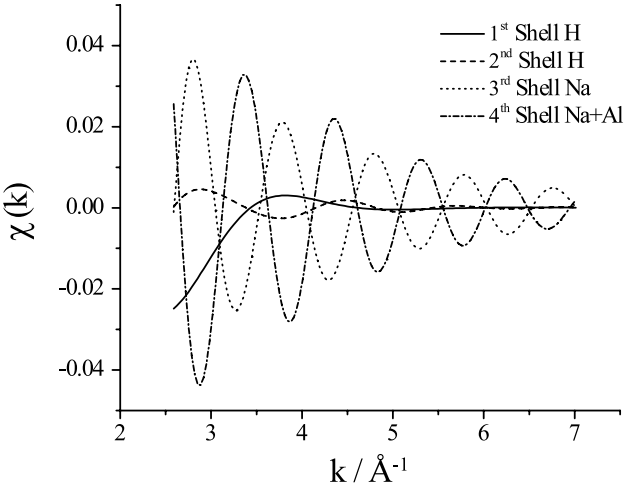

Figure 8. Calculated $\chi(k)$ of the different atomic contributions to the total fit for $NaAlH_4$

A comparison between the structural parameters of $NaAlH_4$ from literature, and from our EXAFS experiment is summarized in Table 5. The fitted distances for the hydrogen, sodium and aluminum atoms in the EXAFS fit (Tables 4 and 5) are in very good agreement with both the X-ray diffraction,[6,7] and neutron diffraction studies,[7,8] illustrating the power of the approach.

Table 5. Local distances of $NaAlH_4$ obtained from literature and from this study.

Reference	Technique	Al-H	Al-H	Al-Na	Al-Na	Al-Al
6	XRD	1.63	2.84	3.53	3.73	3.73
7	XRD and Neutron Diffraction	1.60	2.94	3.55	3.79	3.79
8	XRD and Neutron Diffraction	1.63	2.88	3.52	3.74	3.74
This study	EXAFS	1.63	2.95	3.53	3.74	3.74

Conclusions

The XANES of unoxidized $NaAlH_4$ has been recorded and it was illustrated that the 'fingerprint' of the XANES can be used as a quick quality control of the $NaAlH_4$ for *e.g.* oxidation. XANES calculations revealed that the white line intensity and the resonances have a strong contribution from the multiple scattering in a long range. The EXAFS spectrum of $NaAlH_4$ was measured and could be fitted according to the crystallographic distances data. EXAFS analysis shows that the inclusion of the Al-H scattering was essential for the refinement. These findings indicate crucial issues that should be taken into account when analyzing the structural changes in X-ray absorption spectra occurring during loading and unloading of metal-hydrides.

Acknowledgements

This work was financially supported by ACTS, project number 053.61.02 and SRS Daresbury Laboratory project number 43106. We thank Dr Gopinathan Sankar from the Royal Institution of Great Britain for providing Zn-AlPO-34. Ad van der Eerden (Utrecht University) and Andy Smith (SRS, Daresbury) are thanked for their indispensable help during the XAFS experiments. Diek Koningsberger and Ana Mijovilovich from Utrecht University are acknowledged for the help with the respective EXAFS and XANES interpretations.

References

1. Schlapbach, L.; Züttel, A.; *Nature* **2001**, *414*, 353-358
2. Schüth, F.; Bogdanovic, B.; Felderhoff, M.; *Chem. Commun.,* **2004**, *20*, 2249-2258
.3. Baldé, C.P.; Hereijgers, B.P.C.; Bitter, J.H.; de Jong, K.P.; *Angew. Chem. Int. Ed.,* **2006**, *45*, 3501-3503
4. Bodganovic, B.; Brand, R.A.; Marjanovic,A.; Schwickardi, M.; Tolle, J.; *J. Alloys Compd.* **2000**, *302***,** 36-58
5. Gross, K.J.; Guthrie, S.; Takara, S.; Thomas, G.; *J. Alloys Comp.,* **2000**, *297,* 270-281
6. Bel'skii, V.K.; Bulychev, B.M.; Golubeva, A.V.; *Zh. Neorg. Khim.,* **1983**, *28*, 2694-2696
7. Ozolins, V.; Majzoub, E.H.; Udovic, T.J.; *J. Alloys Comp.*, **2004**, *375 (1-2)*, 1-10
8. Hauback, B.C.; Brinks, H.W.; Jensen, C.M.; Murphy, K.; Maeland, A.J.; *J. Alloys Comp.*, **2003**, *358 (1-2)*, 142-145
9. Bogdanovic, B.; Felderhof, M.; Germann, M.; Pommerin, A.; Schueth, F.; Weidentaler, C.; Zibrowius, B. *J. Alloys Compd.* **2003**, *350*, 246-255
10. Majzoub, E.H.; Herberg, J.L.; Stumpf, R.; Spangler, S.; Maxwell, R.S.; *J. Alloys Comp.,***2005**, *394 (1-2),* 265-270
11. Majer, G.; Stanik, E.; Banuet, L.E.V.; Grinberg, F.; Kircher, O.; Fichtner, M.; *J. Alloys Comp.,* **2005***, 404*, 738-742
12. Felderhoff, M.; Klementiev, K.; Grünert, W.; Spliethoff, B.; Tesche, B.; Von Colbe, J.M.B.; Bogdanovic, B.; Hartel, M.; Pommerin, A.; Schüth, F.; Weidenthaler, C.; *Phys. Chem. Chem. Phys.* **2004**, *6*, 4369-4374
.13. Graetz, J.; Reilly, J. J.; Johnson, J.; Ignatov, A. Y.; Tyson, T. A.; *Appl. Phys. Lett.* **2004***,* 85 (3), 500-502
14. Léon, A.; Kircher, O.; Rothe, J.; Fichtner, M.; *J. Phys. Chem. B* **2004**, *108 (42)*, 16372-16376

15. Léon, A.; Kircher, O.; Fichtner, M.; Rothe, J.; Schild, D.; *J. Phys. Chem. B* **2006**, *110*, 1192-1200
16. Baldé, C.P.; Stil, H.A.; van der Eerden, A.M.J.; de Jong, K.P.; Bitter, J.H.; *J. Phys. Chem. C* **2007***, 111,* 2797-2802
17. Léon, A.; Balerna, A.; Cinque, G.; Frommen, C.; Fichtner, M.; J. Phys. Chem. C **2007**, *111(9)*, 3796-3798
18. van Bokhoven, J.A.; Roelofs, J.C.A.A.; de Jong, K.P.; Koningsberger, D.C.; *Chem. Eur. J.,* **2001**, *7*, 1258-1265
19. van Bokhoven, J.A.; Sambe, H.; Ramaker, D.E.; Koningsberger, D.C.; *J. Phys. Chem. B* **1999**, *103 (36),* 7557-7564
20. Beale, A.M.; van der Eerden, A.M.J.; Grandjean, D.; Petukhov, A.V.; Smith, A.D.; Weckhuysen, B.M.; *Chem Commun.*, **2006**, *42*, 4410-4412
21. van der Eerden, A.M.J.; van Bokhoven, J.A.; Smith, A.D.; Koningsberger, D.C.; *Rev. Sci. Instrum.*, **2000**, *71*, 3260
22. Vaarkamp, M.; Linders, J.C.; Koningsberger, D.C.; *Physica B* **1995**, *208/209*, 159
23. Teo, B.K.; *EXAFS: Basic Principals and data analysis;* Springer, New York, 1986
24. Cook Jr., J.W.; Sayers, D.E.; *J. Appl. Phys.* **1981,** *52*, 5024
25. Koningsberger, D.C.; Mojet, B.L.; Van Dorssen, G.E.; Ramaker, D.E.; *Topics in Catalysis* **2000**, *10 (3-4)*, 143-155
26. Tromp, M.; van Bokhoven, J.A.; Arink, A.M.; Bitter, J.H.; Van Koten, G.; Koningsberger, D.C.; *Chem. Eur. J.,* **2002**, *8(24),* 5567-5678
27. Rehr, J.J.; Albers, R.C.; *Rev. Mod. Phys*, **2000**, *72*, 621
28. Sikora, T.; Hug, G.; Jaouen, M.; Rehr, J.J.; *Phys. Rev. B: Condens. Matter Mater. Phys.*, **2000**, *62*, 1723-1732
29. Balzaroti, A.; De Crescenzi, M.; Incoccia, L.; *Phys. Rev. B: Condens. Matter Mater. Phys.*, **1982**, *25(10)*, 6349-6365
30. Gonzales, G.; Pina, C.; Jacas, A.; Hernandez, M.; Leyva, Z.; *Microporous Mesoporous Mater.* **1998,** *25,* 103-108
31. Ito, M.; Shimoyama, Y.; Saito, Y.; *Acta Cryst.* **1985**, *C41*, 1698-1700
32. Gilbert, B.; Frazer, B.H.; Zhang, H.; Huang, F.; Banfield, J.F.; Haskel, D.; Lang, J.C.; Srajer, G.; De Stasio, G.; *Phys. Rev. B: Condens. Matter Mater. Phys.*, **2002**, *66*, 245205
33. Ankudinov, A.L.; Ravel, B.; Rehr, J.J.; Conradson, S.D.; *Phys. Rev. B: Condens. Matter Mater. Phys.*, **1998**, *58(12)*, 7565-7576.

34. Mijovilovich, A.; Meyer-Klaucke, W.; *J. Synchrotron Rad*., **2003**, *10,* 64-68.
35. Ramaker, D.E.; van Dorssen, G.E.; Mojet B.L.; Koningsberger, D.C.; *Topics in Catalysis* **2000**, *10*, 157-165
36. Zhang, Y.; Toebes, M.L.; van der Eerden, A.D.; O'Grady, W.E.; de Jong, K.P.; Koningsberger, D.C.; *J. Phys. Chem. B* **2004**, *108,* 18509-18519
37. Di Vece, M.; Van der Eerden, A.M.J.; Van Bokhoven, J.A.; Lemaux, S.; Kelly, J.J.; Koningsberger, D.C.; *Phys. Rev. B: Condens. Matter Mater. Phys.*, **2003**, *67*, 035430
38. Lengeler, B.; *Phys. Rev. Lett.* **1984**, *53*, 74
39. Wilson, K.R.; Tobin, J.G.; Ankudinov, A.L.; Rehr. J.J.; Saykally, R.J.; *Phys. Rev. Lett.* **2000**, *85*, 4289

7

Summary

Summary

Hydrogen is regarded as an environmentally clean medium to store and transport energy. Many sustainable energy schemes for the future are therefore based on transport and storage of hydrogen. However, several barriers have to be crossed before the so-called hydrogen economy can be implemented. One of those is the storage of hydrogen. Promising in that respect is storage in a metal hydride. However, hydrogen absorption and desorption rates are restricted for many metal hydrides and need to be improved to make these materials suitable for application. Two solutions are envisioned, namely decreasing the particle size of the metal hydride to the nanometer size range, or the addition of a catalyst. This thesis focuses on the relation between the performance of sodium alanate and Ti-catalyzed sodium alanate and their structural properties. In particular, the effect of particle size of sodium alanate and the addition of $TiCl_3$ or $Ti(OBu)_4$ catalysts were investigated and related to the hydrogen sorption characteristics.

In **Chapter 2**, we describe a method to tune the particle size range of the sodium alanate from 2-10 nm, to 19-30 nm to 1-10 μm particles on a Carbon Nanofiber (CNF) support material. This was achieved by impregnation of $NaAlH_4$ dissolved in THF onto CNF skeins and subsequent drying. It appeared from Scanning Electron Microscopy that room-temperature drying at reduced pressure of a 9 wt% $NaAlH_4$ sample led to 1-10 μm $NaAlH_4$ particles on the outer surfaces of the CNF skeins. Drying at low-temperature (-40 to -15 °C) with a comparable $NaAlH_4$ loading reduced the particle size of the $NaAlH_4$ to 19-30 nm present on individual fibres as could be inferred from X-ray diffraction (XRD), quantitative X-ray Photoelectron Spectroscopy (XPS), and Transmission Electron Microscopy (TEM). The smallest particle size range was obtained when the $NaAlH_4$ loading was lowered to 2 wt% and a low-temperature drying step was applied. A particle size range of 2-10 nm was established from TEM and quantitative XPS.

The hydrogen desorption characteristics were verified for the three different particle size ranges and revealed that as the particle size decreased, the temperature of H_2 desorption also decreased. Moreover, a relationship has been established between the activation energy (E_{act}) for hydrogen desorption and the particle size. The E_{act} has been determined to be 116 kJ.mol^{-1} for the 1-10 μm particles, *i.e.*, close to the value for bulk $NaAlH_4$. For 19-30 nm $NaAlH_4$, the E_{act} lowered to 80 kJ.mol^{-1}. An unprecedented 58 kJ.mol^{-1} was established for the 2-10 nm $NaAlH_4$ particles.

H_2 uptake was achieved at mild conditions (20 bar H_2 pressure at 115 °C) when the particle size was reduced to the nanometer size range. During hydrogen sorption, the hydrogen storage material underwent a solid-state phase transformation. The observed improvements for hydrogen absorption and desorption attributed to the decrease of the solid-state mass transfer lengths when the particle sizes become smaller.

Chapter 3 deals with the influence of the $Ti(OBu)_4$ catalyst to ~20 nm $NaAlH_4$ particles on CNF. Dissolved $Ti(OBu)_4$ and $NaAlH_4$ were deposited to the CNF via two consecutive pore volume impregnations and drying steps. It appeared that the order of impregnation influenced the particle size of the $NaAlH_4$ and local structure of the Ti-specie. When the $NaAlH_4$ was deposited first to the CNF and secondly the $Ti(OBu)_4$, the particle size of the $NaAlH_4$ did not change compared to a similarly prepared sample without $Ti(OBu)_4$ on the CNF. The temperature at the maximum hydrogen desorption rate, however, decreased from about 160 °C (without Ti) to 132 °C. This temperature decrease for hydrogen desorption has been attributed to catalytic effects of the "Ti" specie.

In case the order of impregnation was reversed during the preparation (first the $Ti(OBu)_4$ and secondly the $NaAlH_4$), the temperature at maximum desorption rate showed a further decrease to 99 °C. Moreover, hydrogen absorption was demonstrated at mild conditions of 10 bar hydrogen pressure at 115 °C of the sample after hydrogen extraction. In contrast, 20 bar hydrogen pressure was needed for the similarly prepared sample without Ti. The improved absorption and desorption kinetics were attributed to the catalytic role of a highly dispersed Ti-Al alloy on the CNF and/or metal (hydride) as concluded from Extended X-ray Absorption Fine Structrure (EXAFS), in-situ XRD, and XPS. Besides that, the presence of Ti also decreased the particle size of the sodium alanate (from XRD), which was, in line with the conclusions of chapter 2, also beneficial for the sorption of hydrogen.

In **chapter 4**, the structure of the Ti-catalyst is studied as a function of the desorption temperature for ball milled $TiCl_3$-$NaAlH_4$ using X-ray Absorption Near Edge Structure (XANES), EXAFS, and XRD. It appeared that after ball milling ~70% of the Ti was present in the $NaAlH_4$ as triangular Ti-entities. The remaining 30% was present at the surface of Al-crystallites. After hydrogen desorption at 125 °C, the Ti mainly resided at the surface of Al-crystallites. From 125 to 225 °C, Ti migrated from the surface into the bulk and had a similar local structure to that of $TiAl_3$. These $TiAl_3$ nanoclusters sintered to crystalline $TiAl_3$ from 225 to 475 °C. The structural properties of the Ti were linked to a trend reported, on identical samples, in literature (the lower hydrogen desorption temperature, the faster the hydrogen uptake in the next step) to establish a structure-performance relationship. Thus, the activity of the Ti for hydrogen absorption could be ranked as: "Ti in the Al surface" > "$TiAl_3$ cluster" > "crystalline $TiAl_3$".

In **Chapter 5** the local structure of Ti has been investigated as a function of the desorption temperature for ball milled $Ti(OBu)_4$ with $NaAlH_4$ with EXAFS and XANES. The Ti was surrounded by the butoxide groups or decomposition products thereof (C, O atoms) after ball milling. This inhibited the performance of the Ti catalyst. Ti became surrounded by Al atoms

at the expense of the C and O atoms upon heating. The most stable specie in the Ti-Al phase diagram, $TiAl_3$, did not form in the experiment (≤ 300 °C). Besides that, the butoxide or decomposition products thereof (C, O atoms) are suspected to interfere with the hydrogen uptake of a ball milled $Ti(OBu)_4$ $NaAlH_4$ after hydrogen extraction.

Chapter 6 deals with an Al K-edge XAFS study on uncatalyzed bulk $NaAlH_4$. The XANES and EXAFS of $NaAlH_4$ were compared to those of oxidized $NaAlH_4$ and illustrated that the XANES could be used as a relatively quick qualitative check of the $NaAlH_4$ for oxidation. The self-consistent real-space multiple scattering calculations from FEFF 8.0 could reproduce the XANES features of $NaAlH_4$ using a cluster of 6 Å. The EXAFS of $NaAlH_4$ could be fitted according to crystallographic data. Although the scattering cross-section of hydrogen is low in the EXAFS experiment, its inclusion in the Al K-edge EXAFS fit for $NaAlH_4$ appeared critical in the refinement. This stresses the importance of including hydrogen scattering when analyzing structural properties with EXAFS for low Z metal hydrides.

Nederlandse Samenvatting

Samenvatting

Waterstof wordt beschouwd als een schoon opslag- en transportmiddel voor energie. Daarom zijn veel toekomstscenario's gebaseerd op het opslaan en transporteren van waterstof. Voordat deze zogenoemde waterstofeconomie op grote schaal toegepast kan worden, moeten er nog verschillende barrières genomen worden. Eén daarvan is de opslag van waterstof. Een veelbelovende methode om waterstof op te slaan, is via absorptie in een metaalhydride. Een nadeel van deze methode is dat waterstof desorptie- en absorptiesnelheden laag zijn voor metaalhydriden. Twee mogelijke oplossingen worden op het ogenblik onderzocht, namelijk het verkleinen van de deeltjesgrootte van het metaalhydride tot de nanometerschaal of het toevoegen van een katalysator. Dit proefschrift beschrijft de relatie tussen de waterstofopslagkarakteristieken van natriumalanaat en Ti-gekatalyseerd natriumalanaat en de bijbehorende structuureigenschappen. Specifiek worden de effecten van de deeltjesgrootte enerzijds en de structuur van $TiCl_3$- of $Ti(OBu)_4$-katalysatoren anderzijds beschreven en gecorreleerd aan de eigenschappen van natriumalanaat voor waterstofopslag.

Hoofdstuk 2 beschrijft een methode om de deeltjesgrootte van het natriumalanaat globaal te sturen tot 2-10 nm, 19-30 nm of 1-10 μm deeltjes. Om deze deeltjes stabiel te houden werden ze op een koolstofnanovezel dragermateriaal afgezet. Het, in tetrahyrofuran opgeloste, natriumalanaat werd geïmpregneerd op de koolstofnanovezels en vervolgens gedroogd. Wanneer 9 gewichtsprocent natriumalanaat op de koolstofnanovezels werd afgezet gevolgd door drogen bij kamertemperatuur, bleek uit Scanning Elektronen Microscopie dat het natriumalanaat als 1 tot 10 μm deeltjes op de buitenkant van de macroscopische koolstofnanovezels kluwen aanwezig was. Als echter op een lagere temperatuur (-40 tot -15 °C) werd gedroogd, was de deeltjesgrootte 19-30 nm, zoals bleek uit Röntgen diffractie (XRD), kwantitatieve Röntgen Foto-elektron Spectroscopie (XPS) en Transmissie Elektronen Microscopie (TEM). De kleinste deeltjesgrootte (2-10 nm, bepaald met TEM en kwantitatieve XPS) werd verkregen na drogen op lage temperatuur en het verlagen van de natriumalanaatbelading tot 2 gewichtsprocent.

Vervolgens werden de waterstofdesorptiekarakteristieken van deze drie monsters met de verschillende deeltjesgroottes getest, waaruit bleek dat de waterstofdesorptietemperaturen lager werden naarmate de deeltjesgrootte afnam. Bovendien werd er een correlatie gevonden tussen de activeringsenergie voor waterstofdesorptie en de deeltjesgrootte. Voor de 1-10 μm deeltjes was de activeringsenergie 116 $kJ.mol^{-1}$, dicht bij de waarde voor bulk zoals beschreven in de literatuur. Als de deeltjes kleiner werden, nam de activeringsenergie af naar 80 en 58 $kJ.mol^{-1}$ voor respectievelijk de 19-30 nm en 2-10 nm natriumalanaatdeeltjes.

Waterstofopname werd gerealiseerd bij een milde conditie van 20 bar waterstofdruk op 115 °C. Deze verbetering ten opzichte van de opnamecondities voor bulk ongekatalyseerd natriumalanaat (druk hoger dan 200 bar met een temperatuur hoger dan 300 °C) worden toegeschreven aan het verkleinen van de vastestofdiffusielengtes in de nanodeeltjes.

In **hoofdstuk 3** wordt de invloed van de $Ti(OBu)_4$-katalysator op ~20 nm natriumalanaatdeeltjes op koolstofnanovezels beschreven. $Ti(OBu)_4$ en natriumalanaat werden via twee achtereenvolgende porievolume-impregnaties en droogstappen afgezet op de koolstofnanovezels. De volgorde van de afzettingen beïnvloedde zowel de deeltjesgrootte van het natriumalanaat als de lokale structuur van het Ti-deeltje. Wanneer het natriumalanaat eerst werd afgezet en daarna de $Ti(OBu)_4$ bleef de deeltjesgrootte van het natriumalanaat onveranderd ten opzichte van alleen natriumalanaat op de koolstofnanovezels. De temperatuur waarop de maximale desorptiesnelheid bereikt werd nam echter af van boven de 160 °C (zonder Ti) naar 132 °C voor het Ti bevattende sample. Dit wordt verklaard door de katalytische werking van het Ti voor de desorptie van waterstof.

Wanneer de volgorde van afzetting werd omgedraaid, dus eerst het $Ti(OBu)_4$ en daarna het natriumalanaat, werd de temperatuur op maximale desorptie snelheid verder verlaagd tot 99 °C. Bovendien werd waterstofabsorptie gerealiseerd bij een zeer milde waterstofdruk vanaf 10 bar op 115 °C. Zonder toevoeging van Ti geschiedde dit vanaf 20 bar. De verbeterde kinetiek wordt, op basis van Extended X-ray Absorption Fine Structrure (EXAFS), in-situ XRD en XPS metingen, toegeschreven aan de katalytische werking van de aanwezige Ti-Al legering op de koolstofnanovezels. Daarnaast verkleinde de toevoeging van Ti de deeltjesgrootte van het natriumalanaat ten opzichte van alleen natriumalanaat op de koolstofnanovezels (uit XRD). Deze verkleining verklaart mede dat de waterstof ab- en desorptie snelheden toenamen, zoals ook beschreven staat in hoofdstuk 2.

Hoofdstuk 4 beschrijft de structuur van de Ti-katalysator in $TiCl_3$-gekatalyseerde natriumalanaatdeeltjes welke verkregen waren door kogelmalen. De structuur werd met behulp van XRD, EXAFS en X-ray Absorption Near Edge Structure (XANES) karakteriseringtechnieken gerelateerd aan de desorptietemperatuur. Het bleek dat 70% van het Ti aanwezig was in het rooster van het natriumalanaat als trimeren na het malen. De resterende 30% van het Ti bevond zich op het oppervlak van Al-kristallieten. Na waterstofdesorptie op 125 °C was al het Ti aanwezig in het oppervlak van de Al-kristallieten. Gedurende verdere opwarming van 125 tot 225 °C migreerde het Ti van het oppervlak in de bulk van het Al waar het dezelfde lokale structuur had als $TiAl_3$. Deze $TiAl_3$-nanoclusters kristalliseerden tot $TiAl_3$ tijdens verhitten van 225 tot 475 °C. De structurele eigenschappen van de Ti-katalysator werden gecorreleerd aan een trend bekend uit de literatuur (een lagere waterstofdesorptietemperatuur resulteert in snellere waterstofopname in de volgende

stap) om een structuur-activiteits-relatie te maken. De activiteit van de Ti-katalysator kan als volgt worden gerangschikt: “Ti in Al-oppervlak” > “$TiAl_3$-cluster” > “kristallijn $TiAl_3$”.

Hoofdstuk 5 beschrijft de structuur van de Ti-katalysator in $Ti(OBu)_4$-gekatalyseerde natriumalanaatdeeltjes welke verkregen waren door kogelmalen. De structuur werd met behulp van EXAFS en XANES karakteriseringtechnieken gerelateerd aan de desorptietemperatuur. Het Ti werd omringd door O en C atomen afkomstig van de butoxide-precursor na het kogelmalen. Dit verslechterde de presentatie van de Ti-katalysator tijdens de waterstofdesorptie. Tijdens het opwarmen tot 150 °C werden de Ti-O en Ti-C bindingen verbroken en werden Ti-Al bindingen gevormd. De meest stabiele Ti-Al legering, $TiAl_3$, werd echter niet gevormd tot en met 300 °C. Daarnaast hinderden de butoxide-groepen, of afbraakproducten daarvan, in de vastestof ook de waterstofopname in $Ti(OBu)_4$ gekatalyseerd natriumalanaat.

Hoofdstuk 6 beschrijft het onderzoek aan de structuur van ongekatalyseerd bulk natriumalanaat met Al K-edge EXAFS en XANES. De XANES en EXAFS werden vergeleken met die van geoxideerd natriumalanaat. Het bleek dat XANES gebruikt kan worden als een relatief snel uitvoerbare en interpreteerbare methode voor oxidatie. De ‘self-consistent real-time multiple scattering’ berekeningen met FEFF 8.0 konden de XANES eigenschappen van natriumalanaat goed beschrijven voor een clustergrootte van 6 Å. De EXAFS van $NaAlH_4$ kon betrouwbaar worden gefit aan de hand van de kristallografische gegevens. Ondanks dat de verstrooiings-dwarsdoorsnede van het waterstofatoom klein is, was het noodzakelijk om alle verstrooiende elementen (H, Na en Al) in de analyse mee te nemen. Dit benadrukt de relevantie van waterstofverstrooiing in de EXAFS analyse voor lichte metaalhydriden.

List of Publications and Presentations

Publications

C. P. Baldé, B.P.C. Hereijgers, J. H. Bitter, K. P. de Jong, "*Facilitated Hydrogen storage over supported $NaAlH_4$"*
Angew. Chem. Int. Ed. **2006**, *45*, 3501-3503

C.P. Baldé, H.A. Stil, A.M.J. van der Eerden, K.P. de Jong, J.H. Bitter, "*Structure of Ti in $TiCl_3$ Doped $NaAlH_4$"*
Conference Proceedings XAFS 13 **2006**

C.P. Baldé, H.A. Stil, A.M.J. van der Eerden, K.P. de Jong, J.H. Bitter, *"Active Ti species in $TiCl_3$ doped $NaAlH_4$ – Mechanism for catalyst deactivation",* Based on Chapter 4
J. Phys. Chem. C **2007**, *111*, 2797-2802

C.P. Baldé, A.E. Mijovilovich, D.C. Koningsberger, A.M.J. van der Eerden, A.D. Smith, K.P. de Jong, J.H. Bitter, *"XAFS study of the Al K-edge in $NaAlH_4$"*, Based on chapter 6
J. Phys. Chem. C **2007**, *111,* 11721-11725

C.P. Baldé, A.M.J. van der Eerden, H.A. Stil, F.M.F. de Groot, K.P. de Jong, J.H. Bitter, "*On the local structure of Ti during in-situ desorption of $Ti(OBu)_4$ and $TiCl_3$ doped $NaAlH_4$"*, Based on chapter 5
J. Alloys Comp. **2007***, 446-447,* 232-236

C.P. Baldé, B.P.C. Hereijgers, J.H. Bitter, K.P. de Jong, *"Sodium Alanate Nanoparticles – Linking Size to Hydrogen Storage Properties"* Based on chapter 2
Submitted to Journal of American Chemical Society

C.P. Baldé, O. Leynaud, P. Barnes, E. Peláez-Jiménez, J.H. Bitter, K.P. de Jong,*"Linking the Structure to Performance of Ti-catalyzed Nanosized-$NaAlH_4$"* Based on chapter 3
Submitted to Journal of American Chemical Society

A. Baldi, R. Gremaud, D. M. Borsa, C. P. Baldé, A. M. J. van der Eerden, P. E. de Jongh, B. Dam, and R. Griessen, *"Short-Range Order in $Mg_yTi_{1-y}H_x$ thin Films"*
To be submitted to Phys. Rev. B.

C.P. Baldé, O. Leynaud, P. Barnes, J.H. Bitter, K.P. de Jong, *"Thermodynamically destabilized $NaAlH_4$-Na_3AlH_6 during hydrogen desorption in nanosized $NaAlH_4$"*
Manuscript in preparation

Oral presentations

C. P. Baldé, J. H. Bitter, K. P. de Jong, *"Supported $NaAlH_4$ for hydrogen storage"*.
First Sustainable Hydrogen Conference, Hulshorst, The Netherlands, Oct 13-14 2004.

C. P. Baldé, J. H. Bitter, K. P. de Jong, *"The location and local environment of Ti in $TiCl_3$ doped $NaAlH_4$"*.
Second Sustainable Hydrogen Conference, Hulshorst, The Netherlands, Nov 2-3 2005.

C. P. Baldé, J. H. Bitter, K. P. de Jong,*"Facilitated hydrogen storage in supported $NaAlH_4$"*.
Netherlands' Catalysis and Chemistry Conference, Noordwijkerhout, The Netherlands, March 5-7 2006.

C. P. Baldé, J. H. Bitter, K. P. de Jong,*"Nanostructured $NaAlH_4$ deposited on carbon materials for hydrogen storage"*.
Third Sustainable Hydrogen Conference, Hulshorst, The Netherlands, Oct 24-25 2006.

C. P. Baldé, H. A. Stil, A. M. J. van der Eerden, K. P. de Jong, J. H. Bitter, *"Structure of Ti in Ti-doped $NaAlH_4$"*
XAFS13, Stanford, CA, USA, July 9-14 2006.

C. P. Baldé, J. H. Bitter, K. P. de Jong,*"The evolution of Ti in $TiCl_3$ doped $NaAlH_4$: Implications for hydrogen storage"*.
International Symposium on Metal-Hydrogen Systems, Maui, HI, USA, Oct 1-6 2006.

C. P. Baldé, J. H. Bitter, K. P. de Jong,*"Nanostructured $NaAlH_4$ deposited on carbon materials for hydrogen storage"*.
Netherlands' Catalysis and Chemistry Conference, Noordwijkerhout, The Netherlands, March 5-7 2007.

P.E. de Jongh, C. P. Baldé, J. H. Bitter, K. P. de Jong*,"Nanostructured Materials for Hydrogen Storage: beyond Ball-milling?"*.
Gordon conference Hydrogen-Metal Systems, Waterville, ME, USA, July 8-13 2007

C. P. Baldé, J. H. Bitter, K. P. de Jong,*"Structure-Activity Relations for Hydrogen Storage"*.
Fourth Sustainable Hydrogen Conference, Hulshorst, The Netherlands, Nov 8-10 2007.

Poster presentations

C. P. Baldé, J. H. Bitter, K. P. de Jong,*"Supported $NaAlH_4$ for hydrogen storage"*.
Netherlands' Catalysis and Chemistry Conference March, Noordwijkerhout, The Netherlands, 5-7 2005

C.P. Baldé , D.C. Koningsberger, A.M.J. van der Eerden, A.D. Smith, K.P. de Jong, J.H. Bitter*, "In-situ Al-XAFS study on NaAlH4 - Experimental evidence of Al-H scattering"*
XAFS13, Stanford, CA, USA, July 9-14 2006.

C. P. Baldé, J. H. Bitter, K. P. de Jong*,"Facilitated hydrogen storage over nanosized $NaAlH_4$"*.
International Symposium on Metal-Hydrogen Systems, Maui, HI, USA, Oct 1-6 2006.

C. P. Baldé, R.W.P. Wagemans, P.B. Radstake, J. H. Bitter, K. P. de Jong, P.E. de Jongh, *"Nanostructured materials for hydrogen storage"*.
ACTS means business, Eindhoven, The Netherlands, Dec 11 2006

C. P. Baldé, J. H. Bitter, K. P. de Jong, *"Hydrogen storage in Nanostructured $NaAlH_4$ deposited on Carbon Nanofibers"*.
IDECAT conference on catalysis, Porquerolles, France, May 12 - 17 2007

A. Baldi, D.M. Borsa, R. Gremaud, C.P. Baldé, P.E. de Jongh, A.M.J. van der Eerden, J.H. Rector, H. Schreuders, B. Dam, R. Griessen,"*The Mg-Ti-H puzzle"*.
Gordon conference Hydrogen-Metal Systems, Waterville, ME, USA, July 8-13 2007

C.P. Baldé, J.H. Bitter, K. P. de Jong, *"Hydrogen storage on Nanosized $NaAlH_4$ supported on Carbon Nanofibers - A structure-Activity Relation"*.
EuropaCat VIII, Turku, Finland, August 26-31 2007**.**

Dankwoord

Nu al het schrijf- en experimenteerwerk erop zit, is het de hoogste tijd om mensen te bedanken.

Ten eerste mijn promotor Krijn. Het doel van het onderzoek was strak geformuleerd: onderzoek kleine natriumalanaatdeeltjes. Een heuse opgave, maar na vier jaar onderzoek heeft het ontegenzeggelijk zijn vruchten afgeworpen. Ik heb tijdens de promotie je analytische denkvermogen en onze gesprekken erg inspirerend gevonden. Je wist altijd een *finishing touch* aan het onderzoek te geven door te weten waar net dat beetje extra in de data te halen viel. Daarnaast waardeer ik de ruimte die er was om een eigen richting aan het onderzoek te geven en mezelf te kunnen ontplooien. Ik kijk terug op een plezierige tijd.

Harry, jij hebt ook een grote rol gehad tijdens het onderzoek. Al dan niet MSN'end in de avonduren, of als iemand bij wie ik altijd voor een korte vraag of raad kon binnenlopen. Tijdens het schrijfproces heb je veel revisiewerk verricht waar ik veel van geleerd heb. De samenwerking heb ik zeer gewaardeerd.

Diek, als jij niet in je emiritaatdagen nog op de vakgroep was geweest, dan had ik waarschijnlijk nooit waterstof durven te fitten in EXAFS. De korte samenwerking heeft zeker mijn blik verruimd qua EXAFS-analyse.

Ad[E], jou kan ik niet onvernoemd laten. Je experimentele kennis en altijd meedenkende houding heeft een grote positieve bijdrage gehad bij het uitvoeren van goede zuurstofvrije XAFS-metingen. Met name op de lage-energie-XAFS ben je onmisbaar geweest. Ik waardeer je enthousiasme om nog extra dagen naar Daresbury te gaan, teneinde de metingen tot een goed einde te brengen. Ondanks dat de beamlijn in verre staat van ontbinding was, is het gelukt!

I have to thank Ana M. for showing me your expertise in the world of FEFF calculations. Without your help and explanations, FEFF calculations would be an even blacker box than they already are.

Petra, jij hebt altijd een pientere benadering die me regelmatig aan het denken heeft gezet over het hoe-en-waarom van mijn metingen. Ik waardeerde het dan ook dat je bereid was om suggesties te geven en hoofdstuk 2 tekstueel te stroomlijnen. Het MH-congres vond ik erg leuk, maar je moet voortaan wel eventjes al je spullen uit de hotelkamer meenemen. Veel succes toegewenst met de voortzetting van het waterstofopslagonderzoek.

Frank, jij ook bedankt voor je hulp bij het interpreteren van Ti-XANES en voor wat *mp3's* van de oerduitse *industrial electro* van Einstürzende Neubauten.

Andy Beale, you were always there for a good laugh, but also for research related questions. When I was stuck with some EXAFS or textual issues, you were always able to give some advice or directions to keep me going. See you in The Hague soon.

Tijdens de promotie heb ik het genot gehad om meerdere studenten te mogen begeleiden.

Bart, jij bent zeker de student die iedere aio zich wenst. Je goede experimentele en analytische vaardigheden maakte je zeer geschikt voor dit onderwerp en daarnaast heb ik de samenwerking als zeer prettig ervaren. Succes met je aio-schap en met Deleterious. Elena, I enjoyed working together with you. Even though sometimes you clearly lacked some sleep during the internship, you established to nanosize Ti-catalyzed alanates. I wish you luck in the future, and I hope to see you again at some point in the future. Rachid wil ik bedanken voor het inzicht dat hij middels een scriptie over de rol/structuur van de Ti-katalysator heeft gegeven. Ingmar, jij ook bedankt voor het maken en karakteriseren van de helaas te reactief gebleken mesoporeuze kolen. Nog succes met het afronden van je studie. Johnny, je breidde het initiële werk van Elena uit door meerdere Ti-precursormaterialen te testen. Je was altijd erg stipt en zeer goed in het stellen en het halen van deadlines. Ik denk dat je om die reden een goede manager zal zijn. Karin, jij hebt degelijk werk verricht. Helaas was er te weinig tijd om alles in detail uit te werken en is het niet in het proefschrift terecht gekomen. Veel succes met het behalen van je master op de universiteit.

De organisatie van NWO/ACTS wil ik bedanken voor het bijeenbrengen van het Nederlandse waterstofveld en de daaruit voortgevloeide samenwerkingen en contacten. In het bijzonder wil ik Hans Stil en Hans Geerlings van Shell Global Solutions bedanken voor de samenwerking waaruit hoofdstukken 4 en 5 voortgevloeid zijn.

Margriet, nog succes gewenst met de lastige interpretatie van de NMR-data van de nano-alanaten. Ik vertrouw erop dat je er wat mee kan. ;-)

Andy Smith, thanks a lot for the indispensable help at stn. 3.4. Without your knowledge the noise level of the typical Al-XAFS measurement would be as much as an edge-jump…

For the EXAFS measurements at HASYLAB, I have to acknowledge the Darius Zajac, Adam Webb, Mathias Herrmann, Konstantin Klementiev and Edmund Welter. My apologies to Adam and Mathias for the time I left to Utrecht without telling you. Your alertness that time is worth noting.

Furthermore, I would like to thank everybody who helped me during the lenghty day/nightshifts to collect EXAFS data. Andrea and Emiel, it is good to see that you are getting so enthusiastic about EXAFS and I wish you luck with the continuation of your PhDs.

Olivier Leynaud and Paul Barnes, thank you for the opportunity you gave me to come to Daresbury and conduct some successful in-situ XRD measurements.

Fred, jij bedankt voor je uitleg en het meedenken om goede waterstofabsorptie-metingen op de rubotherm te doen. Je kennis was onmisbaar. Eén prangende vraag heb ik alleen nog….zou je de groeten aan Jelle en Alwies willen doen van mij?

Cor, bedankt voor het TEM-werk dat een aantal zeer fraaie plaatjes in het proefschrift heeft opgeleverd. Ad^{M} wil ik graag bedanken voor de XPS en fysisorptie-metingen. Marjan, bedankt voor de XRD-training en SEM-plaatjes. Vincent, jij bedankt voor je flexibiliteit en je hulp met het bedienen van het TPD-apparaat. Verder dank ik Fouad voor de hulp tijdens de zeldzame IR/RAMAN-meting die ik gedaan heb. De glasblazerij wil ik bedanken voor het maken/repareren van het glaswerk. Rudy, ook al geloofde je niet in de BH-SAH's, toch wil ik je bedanken voor het mij wegwijs maken met Schlenken en waterstofopslag. Dymph en Moniek wil ik bedanken voor de sturing en het afhandelen van de formaliteiten en voor de gezelligheid. Zeker door jullie inzet hebben formulieren 1, 2, 3 en 4 op tijd de decaan en de pedel bereikt.

Mijn kamergenoten Jelle en Alwies wil ik vooral bedanken voor de lunchwandelingen en de goede sfeer op de kamer. Met name de discussies aangaande Radio Bergeijk en walgelijke muziek, hebben werkkast N213 tot een aangename plek gemaakt om 4 jaar te werken. Jelle, wellicht nog een keertje een concertje pakken? Alwies, ik blijf graag op de hoogte van de sketches die je in de toekomst zal gaan maken. Hoop jullie beiden in de toekomst te blijven zien!

Alle collega's wil ik verder bedanken voor gezelligheid tijdens borrels, LIIT, bbq, vakgroepsuitjes en koffiepauzes. I would like to thank all colleagues for the good moments during the drinks, LIIT, bbq, *vakgroepuitjes* and coffee breaks.

Vincent v.d. Griend, mijn steun en toeverlaat, muziektechnisch gezien dan. Ik waardeer het dat je paranimf wilt zijn. In de toekomst moeten we zeker muziek blijven maken. De rest van mijn OBL-vrienden wil ik oproepen om binnenkort weer'es te gaan *drum'n'bassen*!

Hans Peter, als een van de weinige studievrienden die ik nog regelmatig zie, leek je me een geschikte paranimf. Ga vooral door met het achterhalen van de zin van de onzin.

Mijn ouders Peter en Maatje kan ik zeker niet onvernoemd laten. Niet in het minst voor de bagage die ik van jullie heb meegekregen, maar ook door mij een jeugd te geven waarin alles kon. Het is eigenlijk niet in woorden te beschrijven, maar toch doe ik het, want wat zouden de mensen die dit lezen anders wel niet moeten denken, toch? Maatje, jij extra bedankt voor het ontwerpen van de omslag. Ook wil ik mijn oneindig veel stoerdere zus(je) Nelleke, en de lekkerst kokende Oma van de hele wereld en omstreken bedanken.

Je moet het beste altijd voor het laatst houden, dus daarom is dit stukje dankwoord voor Kaisa en Suvi gereserveerd. Bij deze wil ik Kaisa bedanken voor het begrijpen hoe het is om een thesis te schrijven en het geven van tekstuele hints. *Minä rakastan sinua aina*!! Met veel plezier en vol verwachting zie ik onze toekomst tegemoet. Suvi, ik ben benieuwd wat voor een wonderlijk persoon jij zal worden.

Kees Baldé

Curriculum Vitae

Cornelis Peter Baldé werd op 6 juni 1980 geboren te Rotterdam. In 1998 behaalde hij het VWO-diploma aan de Rijksscholen Gemeenschap te Oud-Beijerland. In september hetzelfde jaar ging hij scheikunde studeren aan de Universiteit Utrecht waar in september 1999 de propedeuse werd behaald. Na verschillende universitaire stages aan "Structuur opheldering van mandelic acid in DMAN" (Kristal en Structuurchemie, Universiteit Utrecht, onder begeleiding van Dr. H. Kooiman), "Analysis of diffusion of n-hexane in mordenite with the zero length column (ZLC) technique", University of New Brunswick, Canada, onder begeleiding van Prof. M. Eic en Prof. Dr. Ir. K.P. de Jong, studeerde Kees af bij de sectie Anorganische Chemie en Katalyse op 'Selective Catalytic Reduction of NO_x with Fe/ZSM5' onder begeleiding van Dr. A.A. Battiston, Dr. W.M. Heijboer en Prof. Dr. Ir. D.C. Koningsberger in 2003. Vanaf 2004 was Kees werkzaam als Assistent in Opleiding (AIO) in dezelfde sectie, maar nu onder begeleiding van Prof. Dr. Ir. K.P. de Jong en Dr. J.H. Bitter. Het onderzoek werd gefinancieerd door NWO/ACTS en de verkregen onderzoeksresulaten staan beschreven in dit proefschrift.